# Nonreciprocal Photon Blockade

Ran Huang,[1] Adam Miranowicz,[2,3] Jie-Qiao Liao,[1] Franco Nori,[2,4] and Hui Jing[1,*]
[1]Key Laboratory of Low-Dimensional Quantum Structures and Quantum Control of Ministry of Education, Department of Physics and Synergetic Innovation Center for Quantum Effects and Applications, Hunan Normal University, Changsha 410081, China
[2]Theoretical Quantum Physics Laboratory, RIKEN Cluster for Pioneering Research, Wako-shi, Saitama 351-0198, Japan
[3]Faculty of Physics, Adam Mickiewicz University, 61-614 Poznań, Poland
[4]Physics Department, The University of Michigan, Ann Arbor, Michigan 48109-1040, USA

(Received 25 July 2018; published 12 October 2018)

We propose how to create and manipulate one-way nonclassical light via photon blockade in rotating nonlinear devices. We refer to this effect as nonreciprocal photon blockade (PB). Specifically, we show that in a spinning Kerr resonator, PB happens when the resonator is driven in one direction but not the other. This occurs because of the Fizeau drag, leading to a full split of the resonance frequencies of the countercirculating modes. Different types of purely quantum correlations, such as single- and two-photon blockades, can emerge in different directions in a well-controlled manner, and the transition from PB to photon-induced tunneling is revealed as well. Our work opens up a new route to achieve quantum nonreciprocal devices, which are crucial elements in chiral quantum technologies or topological photonics.

DOI: 10.1103/PhysRevLett.121.153601

Nonreciprocal devices, allowing the flow of light from one side but blocking it from the other, are indispensable in a wide range of practical applications, such as invisible sensing or cloaking, and noise-free information processing [1]. To avoid the difficulties of conventional magnet-based devices (e.g., bulky and quite lossy at optical frequencies), nonreciprocal optical devices have been demonstrated in recent experiments based on nonlinear optics [2,3], optomechanics [4–6], atomic gases [7,8], and non-Hermitian optics [9–11]. Similar advances have also been achieved in making acoustic and electronic one-way devices [12–17]. However, previous studies have mainly focused on the *classical* regimes, i.e., one-way control of transmission rates instead of quantum noises. Nonreciprocal quantum devices have been explored very recently, including one-way quantum amplifiers [18–24] and routers of thermal noises [25]. Such devices can find applications for quantum control of light in chiral and topological quantum technologies [26–28].

Here we propose how to induce and control nonreciprocal *quantum* effects with rotating nonlinear devices. Specifically, we show that photon blockade (PB), which is a purely quantum effect, can emerge nonreciprocally in a spinning Kerr resonator. We note that single-photon blockade (1PB), i.e., blockade of the subsequent photons by absorbing the first one [29–32], has been demonstrated experimentally in diverse systems from cavity or circuit QED [33–40] to cavity-free devices [41]. In view of its important role in achieving single-photon devices, optomechanical PB [42–45] have also been explored, offering a way to test, e.g., the quantumness of massive objects [46–50]. In a very recent experiment [51], two-photon blockade (2PB) [31,52–59] has also been observed, opening a route for creating two-photon devices. Thus, nonreciprocal PB devices, as studied here, together with other nonreciprocal quantum devices [18–23,25], are expected to play a key role in quantum engineering [60–62], metrology [63–65], and quantum information processing [66,67] at the single- or few-photon levels.

In a very recent experiment [68], an optical diode with 99.6% isolation has been demonstrated by using a spinning resonator. Inspired by this experiment [68], here we study nonreciprocal PB in a spinning Kerr resonator. We find that light with *sub-* or *super-Poissonian* photon-number statistics can emerge when driving the resonator from its left or right side. Also, by varying the parameters of the system, different quantum correlations (i.e., 1PB or 2PB) can be achieved for the clockwise (CW) or counterclockwise (CCW) modes, for a resonator spinning along the CCW direction. We note that the main idea of nonreciprocal PB is analogous to the classical nonreciprocity induced by the Doppler effect, which has been studied extensively in various areas of physics (see, e.g., Refs. [7,8,69]). Here we focus on *quantum* nonreciprocity induced by the Fizeau light-dragging effect. This opens up the prospect of engineering nonreciprocal PB devices for applications in, e.g., unidirectional quantum sensing and quantum optical communications [28].

*Model.*—We consider a spinning optical Kerr resonator as shown in Fig. 1. As a generic PB model [30,32,53], Kerr interactions can also be experimentally achieved in cavity-atom systems [33,70], or magnon devices [71], and theoretically in optomechanical systems [42,43]. For a resonator spinning at an angular velocity $\Omega$, the light

 

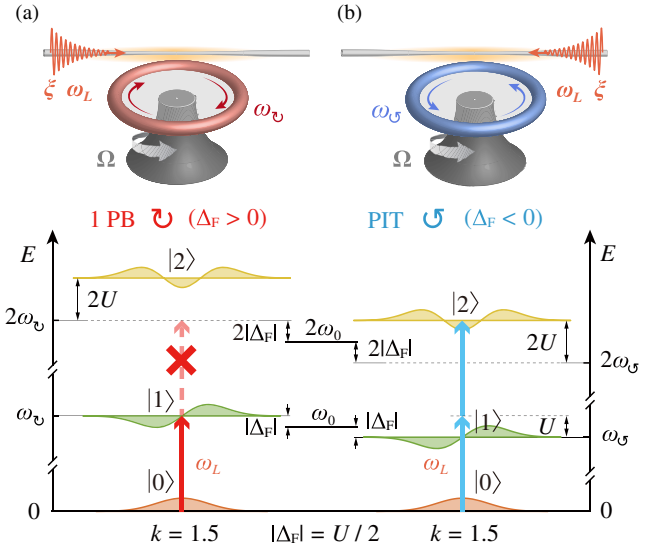


FIG. 1. Nonreciprocal 1PB in a spinning Kerr resonator. 1PB arises due to the anharmonic spacing of the energy levels $|n\rangle$. Here we take $n = 0, 1, 2$, and $\hbar = 1$, for simplicity. By fixing the CCW rotation of the resonator (the angular speed $\Omega$ fulfills the condition $\Delta_F = \pm U/2$), under the same driving power $P_{\rm in} = 2$ fW and the same detuning $\Delta_L = -U/2$, i.e., $k = 1 - \Delta_L/U = 1.5$, (a) 1PB emerges by driving the device from its left side ($\Delta_F > 0$), while (b) PIT caused by two-photon resonance occurs by driving from the right side ($\Delta_F < 0$). This PIT exhibits $g^{(\mu)}(0) > 1$ ($\mu = 2, 3, 4$) [73].

circulating in the resonator experiences a Fizeau shift, i.e., $\omega_0 \to \omega_0 + \Delta_F$, with [72]

$$\Delta_F = \pm \frac{nr\Omega\omega_0}{c}\left(1 - \frac{1}{n^2} - \frac{\lambda}{n}\frac{dn}{d\lambda}\right), \tag{1}$$

where $\omega_0$ is the resonance frequency of a nonspinning resonator, $n$ is the refractive index, $r$ is the resonator radius, and $c$ ($\lambda$) is the speed (wavelength) of light in vacuum. Usually, the dispersion term $dn/d\lambda$, characterizing the relativistic origin of the Sagnac effect, is relatively small (up to ~1%) [68,72]. We fix the CCW rotation of the resonator; hence $\Delta_F > 0$ ($\Delta_F < 0$) corresponds to the situation of driving the resonator from its left (right) side; i.e., the CW and CCW mode frequencies are $\omega_{\circlearrowright,\circlearrowleft} \equiv \omega_0 \pm |\Delta_F|$, respectively.

In a frame rotating at driving frequency $\omega_L$, the effective Hamiltonian of the system can be written at the simplest level as [73]

$$\hat{H} = \hbar(\Delta_k + \Delta_F)\hat{a}^\dagger\hat{a} + \hbar U\hat{a}^\dagger\hat{a}(\hat{a}^\dagger\hat{a} - k) + \hbar\xi(\hat{a}^\dagger + \hat{a}), \tag{2}$$

where $\Delta_k = \Delta_L + U(k-1)$, $\Delta_L = \omega_0 - \omega_L$, the tuning parameter $k$ is simply $k = 1 - \Delta_L/U$ for $\Delta_k = 0$, $\hat{a}$ ($\hat{a}^\dagger$) is the annihilation (creation) operator of the cavity field, and $\xi = \sqrt{\gamma P_{\rm in}/(\hbar\omega_L)}$, with the cavity loss rate $\gamma$ and the driving power $P_{\rm in}$. The Kerr parameter is [76] $U = \hbar\omega_0^2 c n_2/(n_0^2 V_{\rm eff})$, where $n_0$ ($n_2$) is the linear (nonlinear) refraction index, and $V_{\rm eff}$ is the effective mode volume. The Kerr coupling is also attainable by using other kinds of devices [33,42,43,70,71]. Note that the term $\Delta_F$ makes Eq. (2) fundamentally different from that used for studying conventional PB [53].

The energy eigenstates of this system are the Fock states $|n\rangle$ ($n = 0, 1, 2, \ldots$) with eigenenergies

$$E_n = n\hbar\Delta_L + (n^2 - n)\hbar U \pm n\hbar|\Delta_F|, \tag{3}$$

where $n$ is the cavity photon number. The second term, with $U$, leads to an anharmonic energy-level structure. The last term, with $\pm|\Delta_F|$, describing upper or lower shifts of energy levels with an amount being proportional to $\Omega$, is the origin of nonreciprocal implementations of PB. When $|\Delta_F| = U/2$ and the probe with frequency $\omega_0 + |\Delta_F|$ ($k = 1.5$) comes from the left side, the light is resonantly coupled to the transition $|0\rangle \to |1\rangle$. As shown in Fig. 1(a), the transition $|1\rangle \to |2\rangle$ is detuned by $2\hbar U$ and, thus, suppressed for $U > \gamma$; i.e., once a photon is coupled into the resonator, it suppresses the probability of the second photon with the same frequency going into the resonator. In contrast, by driving from the right side, there is a two-photon resonance with the transition $|0\rangle \to |2\rangle$; hence the absorption of the first photon favors also that of the second or subsequent photons, i.e., resulting in photon-induced tunneling (PIT), as defined below and shown in Fig. 1(b). This is a clear signature of nonreciprocal 1PB; i.e., *sub-Poissonian* light emerges by driving the system from one side, while *super-Poissonian* light emerges by driving from the other side.

*Analytical results.*—To confirm this intuitive picture, we study the $\mu$th-order ($\mu = 2$, 3) correlation function with zero-time delay, i.e., $g^{(\mu)}(0) \equiv \langle\hat{a}^{\dagger\mu}\hat{a}^\mu\rangle/\langle\hat{n}\rangle^\mu$, with $\hat{n} = \hat{a}^\dagger\hat{a}$. The condition $g^{(2)}(0) > 1$ [$g^{(2)}(0) < 1$] characterizes PIT [34,77] (1PB) via super-Poissonian (sub-Poissonian) photon-number statistics or photon bunching (antibunching) [78,79]. The latter terms can also refer to different (i.e., two-time) optical correlation effects [79,80], which are, however, not studied here. We stress that, although PIT has a classical-like property of super-Poissonian photon-number statistics [77,81,82], it is a purely quantum effect [34]. The analysis of higher-order correlation functions $g^{(\mu)}(0) > 1$ with $\mu > 2$ can reveal the relation of a particular PIT and multi-PB [73]. Thus, more refined criteria for PIT are sometimes applied [50,81,83], and we refer here to PIT if the conditions $g^{(\mu)}(0) > 1$ for $\mu = 2$, 3, 4 are satisfied [73]. We also note that partially coherent mixtures of the vacuum, and single- and multi-photon states, as generated here, can be described by $\mu$th-order super-Poissonian correlations, i.e., $g^{(\mu)}(0) > 1$, for specific values of $\mu$ [84]. Particularly, $g^{(3)}(0) < 1$ [$g^{(3)}(0) > 1$] is a signature of third-order sub-Poissonian

(super-Poissonian) statistics, which is also interpreted as three-photon antibunching (bunching) in recent experiments on multi-PB [51] and PIT [83]. Thus, $g^{(3)}(0)$, which is usually measured with extended Hanbury Brown–Twiss interferometers, provides a more refined test and classification of the nonclassical character of light, including 2PB (as studied below) or unconventional PB [85].

According to the quantum-trajectory method [86], the optical decay can be included in the effective Hamiltonian $\hat{H}_s = \hat{H} - (i\hbar\gamma/2)\hat{a}^\dagger\hat{a}$, where $\gamma = \omega_0/Q$ is the cavity dissipation rate and $Q$ is the quality factor. In the weak-driving regime ($\xi \ll \gamma$), by truncating the Hilbert space to $n = 2$, the state of this system is written as $|\varphi(t)\rangle = \sum_{n=0}^{2} C_n(t)|n\rangle$, with probability amplitudes $C_n$. Then we have the following equations of motion

$$\begin{aligned}
\dot{C}_0(t) &= -i\nu_0 C_0(t) - i\xi C_1(t),\\
\dot{C}_1(t) &= -i\left(\nu_1 - i\frac{\gamma}{2}\right)C_1(t) - i\xi C_0(t) - i\xi\sqrt{2}C_2(t),\\
\dot{C}_2(t) &= -i(\nu_2 - i\gamma)C_2(t) - i\xi\sqrt{2}C_1(t),
\end{aligned} \tag{4}$$

with $\hbar\nu_n = E_n$, $C_0(0) = 1$, $C_1(0) = C_2(0) = 0$. Solving these equations (and dropping higher-order terms) leads to the steady-state solutions

$$C_1(\infty) = \frac{-\xi}{(\nu_1 - \nu_0 - i\frac{\gamma}{2})}, \qquad C_2(\infty) = \frac{-\sqrt{2}\xi C_1(\infty)}{(\nu_2 - \nu_0 - i\gamma)}. \tag{5}$$

Denoting the probability of finding $m$ photons in the resonator by $P(m) = |C_m|^2$, we have

$$g^{(2)}(0) = \frac{2P_2}{(P_1 + 2P_2)^2} \simeq \frac{(\Delta_L + \Delta_F)^2 + \gamma^2/4}{(\Delta_L + \Delta_F + U)^2 + \gamma^2/4}. \tag{6}$$

1PB and PIT correspond to the minimum and the maximum of $g^{(2)}(0)$, respectively, i.e., when $U > \gamma$, $g^{(2)}_{\min}(0) = 1/[4(U/\gamma)^2 + 1] < 1$ for $\Delta_L = -\Delta_F$, and $g^{(2)}_{\max}(0) = 4(U/\gamma)^2 + 1 > 1$ for $\Delta_L = -\Delta_F - U$.

*Numerical results.*—In order to confirm our analytical results, now we numerically study the full quantum dynamics of the system. We introduce the density operator $\hat{\rho}(t)$ and then solve the master equation [87,88]:

$$\dot{\hat{\rho}} = \frac{i}{\hbar}[\hat{\rho}, \hat{H}] + \frac{\gamma}{2}(2\hat{a}\,\hat{\rho}\,\hat{a}^\dagger - \hat{a}^\dagger\hat{a}\,\hat{\rho} - \hat{\rho}\hat{a}^\dagger\hat{a}). \tag{7}$$

The photon-number probability $P(n) = \langle n|\hat{\rho}_{ss}|n\rangle$ can be obtained for the steady-state solutions $\hat{\rho}_{ss}$ of the master equation. The experimentally accessible parameters are chosen as [89–93]: $V_{\text{eff}} = 150\ \mu\text{m}^3$, $Q = 5 \times 10^9$, $n_2 = 3 \times 10^{-14}\ \text{m}^2/\text{W}$, $n_0 = 1.4$, $P_{\text{in}} = 2$ fW, $r = 30\ \mu$m, and $\lambda = 1550$ nm. $V_{\text{eff}}$ is typically $10^2$–$10^4\ \mu\text{m}^3$ [89,90], $Q$ is typically $10^9$–$10^{12}$ [91,92], and $g^{(2)}(0)$ as low as ~0.13 was achieved experimentally [33]. Moreover, in Fig. 2, we set $\Omega = 29$ kHz; a similar property of quantum nonreciprocity is also confirmed for $\Omega = 6.6$ kHz (see the Supplemental Material [73]). These values of $\Omega$ are experimentally feasible [68]. Very recently, spinning objects have reached much higher velocities, reaching the GHz regime [94,95]; such systems could also be applied to study the nonreciprocal PB via Kerr-like optomechanical interactions [96,97]. We note that the Kerr coefficient can be $n_2 \sim 10^{-14}\ \text{m}^2/\text{W}$ for materials with potassium titanyl phosphate [93], and $n_2$ can be further enhanced with various techniques [98–103], e.g., feedback control [102,103] or quadrature squeezing [100,101].

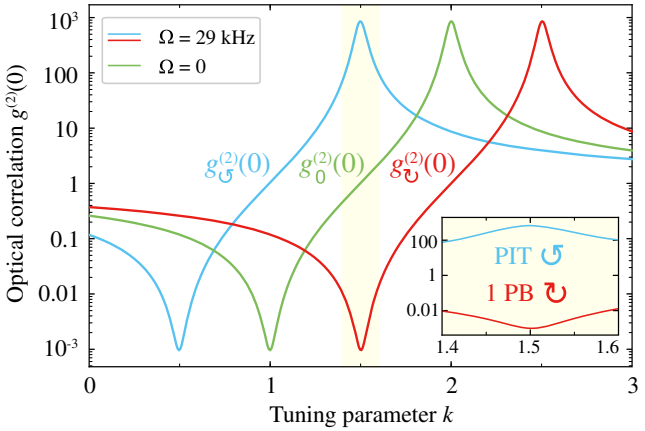


FIG. 2. The second-order correlation function $g^{(2)}(0)$ versus the tuning parameter $k$ for different input directions. At $k = 1.5$, 1PB (red curve) or PIT (blue curve) occurs by driving the device from the left or right side, with the same strength. Here $P_{\text{in}} = 2$ fW, $\Omega = 29$ kHz for the spinning resonator, and $g^{(2)}_0(0)$ corresponds to a nonspinning resonator (green). Note that $\Omega$ is related to $\Delta_F$ by Eq. (1). For the other parameter values, see the main text. On the scale of this figure, there are no differences between our numerical and (approximate) analytical results [73].

An excellent agreement between our analytical results and the exact numerical results is seen in Fig. 2. Here we use $g^{(2)}_0(0)$, $g^{(2)}_{\circlearrowleft}(0)$, and $g^{(2)}_{\circlearrowright}(0)$ to denote the cases with $\Delta_F = 0$, $\Delta_F > 0$, and $\Delta_F < 0$, respectively. For a nonspinning resonator, regardless of the driving direction, $g^{(2)}_0(0)$ always has a dip at $k = 1$ (i.e., $\Delta_L = 0$) or a peak at $k = 2$ (i.e., $\Delta_L = -U$), corresponding to 1PB or PIT, respectively. In contrast, for a spinning device, by driving from the left (right) side, we have $\Delta_F > 0$ ($\Delta_F < 0$) and, thus, a redshift (blueshift) for $g^{(2)}(0)$, leads to 1PB (PIT) at $k = 1.5$, i.e., $g^{(2)}_{\circlearrowleft}(0) \sim 0.001$, $g^{(2)}_{\circlearrowright}(0) \sim 673$. This quantum nonreciprocity, with up to 6 orders of magnitude difference of $g^{(2)}(0)$ for opposite directions, is fundamentally different from the classical transmission-rate nonreciprocity.

*Nonreciprocal 2PB.*—The absorption of 2 photons can also suppress the absorption of additional photons [53]. This 2PB effect, featuring three-photon antibunching, but with two-photon bunching, satisfies [51,73]

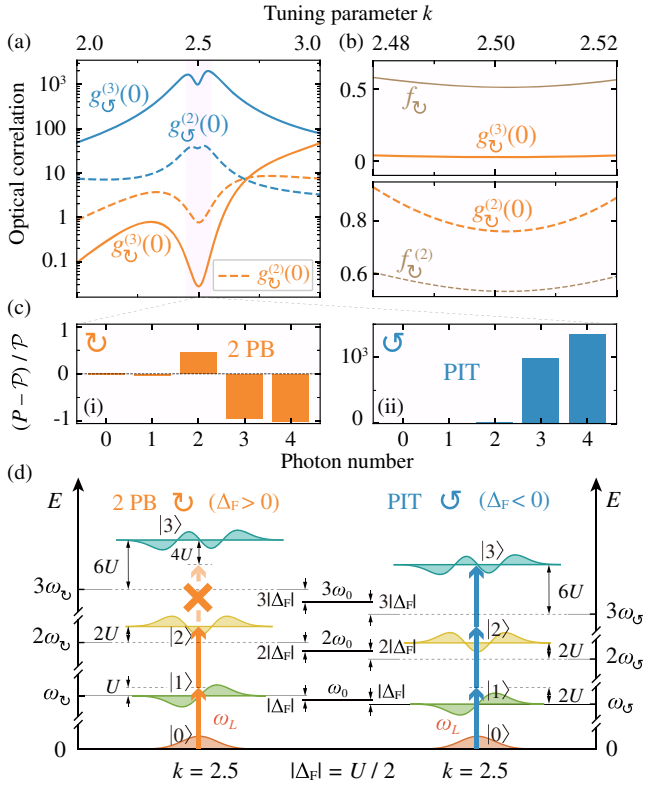


FIG. 3. (a) The correlation functions $g^{(3)}(0)$ (solid curves) and $g^{(2)}(0)$ (dashed curves) versus the tuning parameter $k$ for different driving directions. Note that at $k = 2.5$, 2PB can emerge by driving the system from the left side (orange), while PIT occurs by driving from the right side (blue). In (b), 2PB is confirmed by the criteria given in Eq. (8) for the CW mode. (c) This nonreciprocal 2PB can also be recognized from the deviations of the photon distribution to the standard Poisson distribution with the same mean photon number. (d) The energy-level diagram shows the origin of this unidirectional 2PB: with enhanced driving power $P_{\rm in} = 0.3$ pW, by choosing $\Delta_L = -3U/2$ (i.e., $k = 2.5$), 2PB emerges by driving the device from the left ($\Delta_F > 0$), while three-photon resonance-induced PIT emerges by driving from the right side ($\Delta_F < 0$). The other parameters are the same as those in Fig. 2.

$$g^{(3)}(0) < f \equiv e^{-\langle\hat{n}\rangle},$$
$$g^{(2)}(0) \geq f^{(2)} \equiv e^{-\langle\hat{n}\rangle} + \langle\hat{n}\rangle \cdot g^{(3)}(0). \quad (8)$$

The third-order correlation function can be obtained analytically as [73]

$$g^{(3)}(0) = \frac{6P_3}{(P_1 + 2P_2 + 3P_3)^3} \simeq \frac{(\Delta^2 + \gamma^2/4)g^{(2)}(0)}{(\Delta + 2U)^2 + \gamma^2/4}, \quad (9)$$

with $\Delta = \Delta_L + \Delta_F$, also agreeing well with the numerical results. Figures 3(a) and 3(b) show that 2PB emerges around $k = 2.5$ by driving from the left side, while we have PIT by driving from the right side, i.e., $g^{(2)}_{\circlearrowleft}(0) \sim 36$, $g^{(3)}_{\circlearrowleft}(0) \sim 1003$. By tuning the driving frequency to the three-photon resonance [see Fig. 3(d)], it is indeed possible to observe that $g^{(3)}(0)/g^{(2)}(0) \sim 100$, as shown in Fig. 3(a) for $\max\langle n\rangle = 0.0185$. This means that the probability of simultaneously measuring three photons can be much larger than that of two photons in this situation. Similar values of $g^{(3)}(0) \sim 10^3$, $g^{(2)}(0) \sim 10$ were also predicted in the PIT analysis in Ref. [83].

Our results can be further confirmed by comparing the photon-number distribution $P(n)$ with the Poisson distribution $\mathcal{P}(n)$. Figure 3(c) shows that $P(2)$ is enhanced while $P(n > 2)$ are suppressed by driving from the left side, which is in *sharp* contrast to the case when driving from the right side. This unidirectional 2PB effect can be intuitively understood by considering the energy-level structure of the system, as shown in Fig. 3(d). By choosing $\Delta_L = -3U/2$ or $k = 2.5$, the transition $|0\rangle \to |2\rangle$ is resonantly driven by the left input laser, but the transition $|2\rangle \to |3\rangle$ is detuned by $4\hbar U$, which features the 2PB effect; in contrast, by driving from the right side, three-photon resonance happens for the transition $|0\rangle \to |3\rangle$, leading to PIT. Hence with such a device, sub-Poissonian light can be achieved by driving it from the left side, while super-Poissonian light is observed by driving it from the right side.

*Nonreciprocity of 1PB and 2PB.*—Figure 4 shows that at $k = 1.5$, 1PB emerges by driving from the left side, due to $g^{(2)}_{\circlearrowleft}(0) \sim 0.045$, while 2PB occurs by driving from the right side since the criteria given in Eq. (8) are fulfilled for $\Delta_F < 0$. This indicates a purely quantum device with direction-dependent counting statistics, a new nonreciprocal feature, which has not been revealed previously. This 1PB-2PB nonreciprocity, as also clearly seen in Fig. 4(c) for the

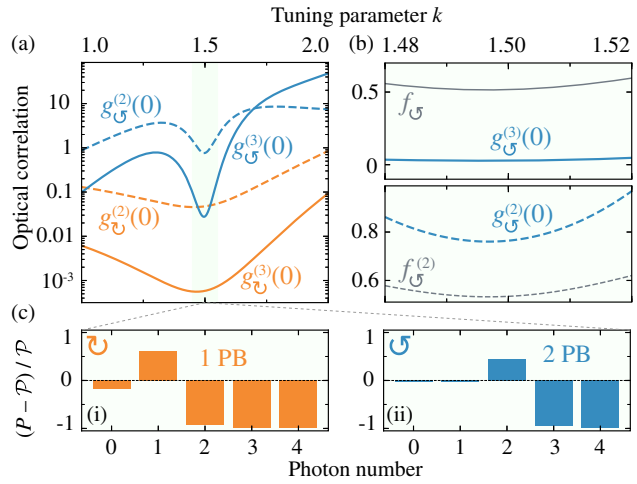


FIG. 4. (a) The correlation functions $g^{(3)}(0)$ (solid curves) and $g^{(2)}(0)$ (dashed curves) versus the tuning parameter $k$ for different driving directions. 1PB can emerge around $k = 1.5$ by driving from the left side (orange), while 2PB occurs by driving from the right side (blue). In (b), 2PB is confirmed by the criteria given in Eq. (8) for the CCW mode. (c) This 1PB-2PB nonreciprocity can also be recognized from the relative photon population numbers in the resonator. For all plots, the parameters are the same as those in Fig. 3.

populations of different Fock states, provides a route for creating or processing different quantum states in a single node of quantum networks [66,67]. Figures 3–4 present our solutions of the standard master equation, given in Eq. (7), which describes both a slow continuous nonunitary evolution and quantum jumps occurring with a small probability [104]. By contrast, our approximate analytical solutions, based on the complex Hamiltonian $H_s$ and the Schrödinger equation, were obtained by ignoring these quantum jumps following the standard approach of Ref. [105].

*Conclusions*.—We have studied nonreciprocal PB effects in a spinning Kerr resonator. By fixing the CCW rotation of the resonator, we find the following: (i) for $P_{\rm in} = 2$ fW, $\Delta_{\rm sag} = \pm U/2$ and $k = 1.5$, we have 1PB and PIT for the CW and CCW modes, respectively. (ii) For $P_{\rm in} = 0.3$ pW, $\Delta_{\rm sag} = \pm U/2$ and $k = 2.5$, we have 2PB and PIT for the CW and CCW modes, respectively. More interestingly, (iii) for $P_{\rm in} = 0.3$ pW, $\Delta_{\rm sag} = \pm U/2$ and $k = 1.5$, we have 1 and 2PB for the CW and CCW modes, respectively (for more examples, see the Supplemental Material [73]). These results can be useful in achieving, e.g., nonreciprocal few-photon sources and quantum one-way devices.

The basic mechanism of this work can be generalized to a wide range of systems, such as acoustic and electronic devices [12–17], to achieve, e.g., nonreciprocal phonon blockade [46–48] as a test of the quantumness of mechanical devices [79]. Our work can also be extended to study, e.g., nonreciprocal photon turnstiles [106], nonreciprocal photon routers [107–109], and nonreciprocal extraction of a single photon from a laser pulse [110], by considering a hybrid device with atoms [111,112], quantum dots [113], or nitrogen-vacancy centers [114].

R. H. and H. J. are supported by the National Natural Science Foundation of China (NSFC, 11474087 and 11774086). F. N. is supported by the MURI Center for Dynamic Magneto-Optics via the Air Force Office of Scientific Research (AFOSR) (FA9550-14-1-0040), Army Research Office (ARO) (Grant No. 73315PH), Asian Office of Aerospace Research and Development (AOARD) (Grant No. FA2386-18-1-4045), Japan Science and Technology Agency (JST) (the ImPACT program and CREST Grant No. JPMJCR1676), Japan Society for the Promotion of Science (JSPS) (JSPS-RFBR Grant No. 17-52-50023, and JSPS-FWO Grant No. VS.059.18N), and the RIKEN-AIST Challenge Research Fund. A. M. and F. N. are also supported by a grant from the John Templeton Foundation. J. Q. L. is supported by the NSFC (11822501 and 11774087).

*Corresponding author.
jinghui73@foxmail.com

[1] D. L. Sounas and A. Alù, Non-reciprocal photonics based on time modulation, Nat. Photonics **11**, 774 (2017).
[2] L. Fan, J. Wang, L. T. Varghese, H. Shen, B. Niu, Y. Xuan, A. M. Weiner, and M. Qi, An all-silicon passive optical diode, Science **335**, 447 (2012).
[3] Q.-T. Cao, H. Wang, C.-H. Dong, H. Jing, R.-S. Liu, X. Chen, L. Ge, Q. Gong, and Y.-F. Xiao, Experimental Demonstration of Spontaneous Chirality in a Nonlinear Microresonator, Phys. Rev. Lett. **118**, 033901 (2017).
[4] S. Manipatruni, J. T. Robinson, and M. Lipson, Optical Nonreciprocity in Optomechanical Structures, Phys. Rev. Lett. **102**, 213903 (2009).
[5] Z. Shen, Y.-L. Zhang, Y. Chen, C.-L. Zou, Y.-F. Xiao, X.-B. Zou, F.-W. Sun, G.-C. Guo, and C.-H. Dong, Experimental realization of optomechanically induced non-reciprocity, Nat. Photonics **10**, 657 (2016).
[6] N. R. Bernier, L. D. Tóth, A. Koottandavida, M. A. Ioannou, D. Malz, A. Nunnenkamp, A. K. Feofanov, and T. J. Kippenberg, Nonreciprocal reconfigurable microwave optomechanical circuit, Nat. Commun. **8**, 604 (2017).
[7] D.-W. Wang, H.-T. Zhou, M.-J. Guo, J.-X. Zhang, J. Evers, and S.-Y. Zhu, Optical Diode Made from a Moving Photonic Crystal, Phys. Rev. Lett. **110**, 093901 (2013).
[8] H. Ramezani, P. K. Jha, Y. Wang, and X. Zhang, Nonreciprocal Localization of Photons, Phys. Rev. Lett. **120**, 043901 (2018).
[9] N. Bender, S. Factor, J. D. Bodyfelt, H. Ramezani, D. N. Christodoulides, F. M. Ellis, and T. Kottos, Observation of Asymmetric Transport in Structures with Active Nonlinearities, Phys. Rev. Lett. **110**, 234101 (2013).
[10] B. Peng, Ş. K. Özdemir, F. Lei, F. Monifi, M. Gianfreda, G. L. Long, S. Fan, F. Nori, C. M. Bender, and L. Yang, Parity–time-symmetric whispering-gallery microcavities, Nat. Phys. **10**, 394 (2014).
[11] L. Chang, X. Jiang, S. Hua, C. Yang, J. Wen, L. Jiang, G. Li, G. Wang, and M. Xiao, Parity–time symmetry and variable optical isolation in active–passive-coupled microresonators, Nat. Photonics **8**, 524 (2014).
[12] B. Liang, X. S. Guo, J. Tu, D. Zhang, and J. C. Cheng, An acoustic rectifier, Nat. Mater. **9**, 989 (2010).
[13] B.-I. Popa and S. A. Cummer, Non-reciprocal and highly nonlinear active acoustic metamaterials, Nat. Commun. **5**, 3398 (2014).
[14] S. Kim, X. Xu, J. M. Taylor, and G. Bahl, Dynamically induced robust phonon transport and chiral cooling in an optomechanical system, Nat. Commun. **8**, 205 (2017).
[15] R. Fleury, D. L. Sounas, C. F. Sieck, M. R. Haberman, and A. Alù, Sound isolation and giant linear nonreciprocity in a compact acoustic circulator, Science **343**, 516 (2014).
[16] S. Barzanjeh, M. Wulf, M. Peruzzo, M. Kalaee, P. B. Dieterle, O. Painter, and J. M. Fink, Mechanical on-chip microwave circulator, Nat. Commun. **8**, 953 (2017).
[17] D. Torrent, O. Poncelet, and J.-C. Batsale, Nonreciprocal Thermal Material by Spatiotemporal Modulation, Phys. Rev. Lett. **120**, 125501 (2018).
[18] A. Metelmann and A. A. Clerk, Nonreciprocal Photon Transmission and Amplification Via Reservoir Engineering, Phys. Rev. X **5**, 021025 (2015).

[19] F. Lecocq, L. Ranzani, G. A. Peterson, K. Cicak, R. W. Simmonds, J. D. Teufel, and J. Aumentado, Nonreciprocal Microwave Signal Processing with a Field-Programmable Josephson Amplifier, Phys. Rev. Applied **7**, 024028 (2017).
[20] A. Kamal and A. Metelmann, Minimal Models for Nonreciprocal Amplification Using Biharmonic Drives, Phys. Rev. Applied **7**, 034031 (2017).
[21] G. A. Peterson, F. Lecocq, K. Cicak, R. W. Simmonds, J. Aumentado, and J. D. Teufel, Demonstration of Efficient Nonreciprocity in a Microwave Optomechanical Circuit, Phys. Rev. X **7**, 031001 (2017).
[22] D. Malz, L. D. Tóth, N. R. Bernier, A. K. Feofanov, T. J. Kippenberg, and A. Nunnenkamp, Quantum-Limited Directional Amplifiers with Optomechanics, Phys. Rev. Lett. **120**, 023601 (2018).
[23] Z. Shen, Y.-L. Zhang, Y. Chen, F.-W. Sun, X.-B. Zou, G.-C. Guo, C.-L. Zou, and C.-H. Dong, Reconfigurable optomechanical circulator and directional amplifier, Nat. Commun. **9**, 1797 (2018).
[24] X. Gu, A. F. Kockum, A. Miranowicz, Y.-X. Liu, and F. Nori, Microwave photonics with superconducting quantum circuits, Phys. Rep. **718–719**, 1 (2017).
[25] S. Barzanjeh, M. Aquilina, and A. Xuereb, Manipulating the Flow of Thermal Noise in Quantum Devices, Phys. Rev. Lett. **120**, 060601 (2018).
[26] K. Y. Bliokh, D. Smirnova, and F. Nori, Quantum spin Hall effect of light, Science **348**, 1448 (2015).
[27] K. Y. Bliokh and F. Nori, Transverse and longitudinal angular momenta of light, Phys. Rep. **592**, 1 (2015).
[28] P. Lodahl, S. Mahmoodian, S. Stobbe, A. Rauschenbeutel, P. Schneeweiss, J. Volz, H. Pichler, and P. Zoller, Chiral quantum optics, Nature (London) **541**, 473 (2017).
[29] L. Tian and H. J. Carmichael, Quantum trajectory simulations of two-state behavior in an optical cavity containing one atom, Phys. Rev. A **46**, R6801 (1992).
[30] W. Leoński and R. Tanaś, Possibility of producing the one-photon state in a kicked cavity with a nonlinear Kerr medium, Phys. Rev. A **49**, R20 (1994).
[31] A Miranowicz, W Leoński, S Dyrting, and R Tanaś, Quantum state engineering in finite-dimensional Hilbert space, Acta Phys. Slovaca **46**, 451 (1996).
[32] A. Imamoğlu, H. Schmidt, G. Woods, and M. Deutsch, Strongly Interacting Photons in a Nonlinear Cavity, Phys. Rev. Lett. **79**, 1467 (1997).
[33] K. M. Birnbaum, A. Boca, R. Miller, A. D. Boozer, T. E. Northup, and H. J. Kimble, Photon blockade in an optical cavity with one trapped atom, Nature (London) **436**, 87 (2005).
[34] A. Faraon, I. Fushman, D. Englund, N. Stoltz, P. Petroff, and J. Vučković, Coherent generation of non-classical light on a chip via photon-induced tunnelling and blockade, Nat. Phys. **4**, 859 (2008).
[35] A. Reinhard, T. Volz, M. Winger, A.o Badolato, K. J. Hennessy, E. L. Hu, and A. Imamoğlu, Strongly correlated photons on a chip, Nat. Photonics **6**, 93 (2012).
[36] K. Müller, A. Rundquist, K. A. Fischer, T. Sarmiento, K. G. Lagoudakis, Y. A. Kelaita, C. S. Muñoz, E. del Valle, F. P. Laussy, and J. Vučković, Coherent Generation of Nonclassical Light on Chip via Detuned Photon Blockade, Phys. Rev. Lett. **114**, 233601 (2015).
[37] H. J. Snijders, J. A. Frey, J. Norman, H. Flayac, V. Savona, A. C. Gossard, J. E. Bowers, M. P. van Exter, D. Bouwmeester, and W. Löffler, Observation of the Unconventional Photon Blockade, Phys. Rev. Lett. **121**, 043601 (2018).
[38] C. Lang, D. Bozyigit, C. Eichler, L. Steffen, J. M. Fink, A. A. Abdumalikov, M. Baur, S. Filipp, M. P. da Silva, A. Blais, and A. Wallraff, Observation of Resonant Photon Blockade at Microwave Frequencies Using Correlation Function Measurements, Phys. Rev. Lett. **106**, 243601 (2011).
[39] A. J. Hoffman, S. J. Srinivasan, S. Schmidt, L. Spietz, J. Aumentado, H. E. Türeci, and A. A. Houck, Dispersive Photon Blockade in a Superconducting Circuit, Phys. Rev. Lett. **107**, 053602 (2011).
[40] C. Vaneph, A. Morvan, G. Aiello, M. Féchant, M. Aprili, J. Gabelli, and J. Estève, Observation of the Unconventional Photon Blockade in the Microwave Domain, Phys. Rev. Lett. **121**, 043602 (2018).
[41] T. Peyronel, O. Firstenberg, Q.-Y. Liang, S. Hofferberth, A. V. Gorshkov, T. Pohl, M. D. Lukin, and V. Vuletić, Quantum nonlinear optics with single photons enabled by strongly interacting atoms, Nature (London) **488**, 57 (2012).
[42] P. Rabl, Photon Blockade Effect in Optomechanical Systems, Phys. Rev. Lett. **107**, 063601 (2011).
[43] A. Nunnenkamp, K. Børkje, and S. M. Girvin, Single-Photon Optomechanics, Phys. Rev. Lett. **107**, 063602 (2011).
[44] J.-Q. Liao and F. Nori, Photon blockade in quadratically coupled optomechanical systems, Phys. Rev. A **88**, 023853 (2013).
[45] J.-Q. Liao and C. K. Law, Correlated two-photon scattering in cavity optomechanics, Phys. Rev. A **87**, 043809 (2013).
[46] Y.-X. Liu, A. Miranowicz, Y. B. Gao, J. Bajer, C. P. Sun, and F. Nori, Qubit-induced phonon blockade as a signature of quantum behavior in nanomechanical resonators, Phys. Rev. A **82**, 032101 (2010).
[47] N. Didier, S. Pugnetti, Y. M. Blanter, and R. Fazio, Detecting phonon blockade with photons, Phys. Rev. B **84**, 054503 (2011).
[48] A. Miranowicz, J. Bajer, N. Lambert, Y.-X. Liu, and F. Nori, Tunable multiphonon blockade in coupled nanomechanical resonators, Phys. Rev. A **93**, 013808 (2016).
[49] X. Wang, A. Miranowicz, H.-R. Li, and F. Nori, Method for observing robust and tunable phonon blockade in a nanomechanical resonator coupled to a charge qubit, Phys. Rev. A **93**, 063861 (2016).
[50] M. Wang, X.-Y. Lü, A. Miranowicz, T.-S. Yin, Y. Wu, and F. Nori, Unconventional phonon blockade via atom-photon-phonon interaction in hybrid optomechanical systems, arXiv:1806.03754.
[51] C. Hamsen, K. N. Tolazzi, T. Wilk, and G. Rempe, Two-Photon Blockade in an Atom-Driven Cavity QED System, Phys. Rev. Lett. **118**, 133604 (2017).
[52] S. S. Shamailov, A. S. Parkins, M. J. Collett, and H. J. Carmichael, Multi-photon blockade and dressing of the dressed states, Opt. Commun. **283**, 766 (2010).

[53] A. Miranowicz, M. Paprzycka, Y.-X. Liu, J. Bajer, and F. Nori, Two-photon and three-photon blockades in driven nonlinear systems, Phys. Rev. A **87**, 023809 (2013).

[54] A. Miranowicz, J. Bajer, M. Paprzycka, Y.-X. Liu, A. M. Zagoskin, and F. Nori, State-dependent photon blockade via quantum-reservoir engineering, Phys. Rev. A **90**, 033831 (2014).

[55] H. J. Carmichael, Breakdown of Photon Blockade: A Dissipative Quantum Phase Transition in Zero Dimensions, Phys. Rev. X **5**, 031028 (2015).

[56] C. J. Zhu, Y. P. Yang, and G. S. Agarwal, Collective multiphoton blockade in cavity quantum electrodynamics, Phys. Rev. A **95**, 063842 (2017).

[57] W. Leoński, Fock states in a Kerr medium with parametric pumping, Phys. Rev. A **54**, 3369 (1996).

[58] A. Miranowicz, W. Leoński, and N. Imoto, Quantum-optical states in finite-dimensional Hilbert space. I. general formalism, Adv. Chem. Phys. **119(I)**, 155 (2001).

[59] W. Leoński and A. Miranowicz, Quantum-optical states in finite-dimensional Hilbert space. II. state generation, Adv. Chem. Phys. **119(I)**, 195 (2001).

[60] S. E. Harris and Y. Yamamoto, Photon Switching by Quantum Interference, Phys. Rev. Lett. **81**, 3611 (1998).

[61] D. E. Chang, A. S Sørensen, E. A. Demler, and M. D. Lukin, A single-photon transistor using nanoscale surface plasmons, Nat. Phys. **3**, 807 (2007).

[62] A. Kubanek, A. Ourjoumtsev, I. Schuster, M. Koch, P. W. H. Pinkse, K. Murr, and G. Rempe, Two-Photon Gateway in One-Atom Cavity Quantum Electrodynamics, Phys. Rev. Lett. **101**, 203602 (2008).

[63] D. Fattal, K. Inoue, J. Vučković, C. Santori, G. S. Solomon, and Y. Yamamoto, Entanglement Formation and Violation of Bell's Inequality with a Semiconductor Single Photon Source, Phys. Rev. Lett. **92**, 037903 (2004).

[64] I. Buluta and F. Nori, Quantum simulators, Science **326**, 108 (2009).

[65] I. M. Georgescu, S. Ashhab, and F. Nori, Quantum simulation, Rev. Mod. Phys. **86**, 153 (2014).

[66] C. H. Bennett and D. P. DiVincenzo, Quantum information and computation, Nature (London) **404**, 247 (2000).

[67] I. Buluta, S. Ashhab, and F. Nori, Natural and artificial atoms for quantum computation, Rep. Prog. Phys. **74**, 104401 (2011).

[68] S. Maayani, R. Dahan, Y. Kligerman, E. Moses, A. U. Hassan, H. Jing, F. Nori, D. N. Christodoulides, and T. Carmon, Flying couplers above spinning resonators generate irreversible refraction, Nature (London) **558**, 569 (2018).

[69] *Spin Wave Confinement: Propagating Waves*, edited by S. O. Demokritov (CRC Press, Singapore, 2017).

[70] H. Schmidt and A. Imamoğlu, Giant Kerr nonlinearities obtained by electromagnetically induced transparency, Opt. Lett. **21**, 1936 (1996).

[71] Y.-P. Wang, G.-Q. Zhang, D. Zhang, T.-F. Li, C.-M. Hu, and J. Q. You, Bistability of Cavity Magnon Polaritons, Phys. Rev. Lett. **120**, 057202 (2018).

[72] G. B. Malykin, The Sagnac effect: Correct and incorrect explanations, Phys. Usp. **43**, 1229 (2000).

[73] See Supplementary Material at http://link.aps.org/supplemental/10.1103/PhysRevLett.121.153601 for detailed derivations of our main results, which includes Refs. [74,75].

[74] G. J. Milburn, Quantum and classical Liouville dynamics of the anharmonic oscillator, Phys. Rev. A **33**, 674 (1986).

[75] R. J. Glayber, *Quantum Theory of Optical Coherence* (Wiley-VCH, Weinheim, 2007).

[76] P. Marin-Palomo, J. N. Kemal, M. Karpov, A. Kordts, J. Pfeifle, M. H. P. Pfeiffer, P. Trocha, S. Wolf, V. Brasch, M. H. Anderson, R. Rosenberger, K. Vijayan, W. Freude, T. J. Kippenberg, and C. Koos, Microresonator-based solitons for massively parallel coherent optical communications, Nature (London) **546**, 274 (2017).

[77] A. Majumdar, M. Bajcsy, A. Rundquist, and J. Vučković, Loss-Enabled Sub-Poissonian Light Generation in a Bimodal Nanocavity, Phys. Rev. Lett. **108**, 183601 (2012).

[78] M. O. Scully and M. S. Zubairy, *Quantum Optics* (Cambridge University Press, Cambridge, England, 1997).

[79] A. Miranowicz, M. Bartkowiak, X. Wang, Y.-X. Liu, and F. Nori, Testing nonclassicality in multimode fields: A unified derivation of classical inequalities, Phys. Rev. A **82**, 013824 (2010).

[80] X. T. Zou and L. Mandel, Photon-antibunching and sub-Poissonian photon statistics, Phys. Rev. A **41**, 475 (1990).

[81] X.-W. Xu, Y.-J. Li, and Y.-X. Liu, Photon-induced tunneling in optomechanical systems, Phys. Rev. A **87**, 025803 (2013).

[82] A. Majumdar, M. Bajcsy, and J. Vućković, Probing the ladder of dressed states and nonclassical light generation in quantum-dot–cavity QED, Phys. Rev. A **85**, 041801 (2012).

[83] A. Rundquist, M. Bajcsy, A. Majumdar, T. Sarmiento, K. Fischer, K. G. Lagoudakis, S. Buckley, A. Y. Piggott, and J. Vućković, Nonclassical higher-order photon correlations with a quantum dot strongly coupled to a photonic-crystal nanocavity, Phys. Rev. A **90**, 023846 (2014).

[84] W. Vogel and D. Welsch, *Quantum Optics* (Wiley-VCH, Weinheim, 2006).

[85] M. Radulaski, K. A. Fischer, K. G. Lagoudakis, J. L. Zhang, and J. Vučković, Photon blockade in two-emitter-cavity systems, Phys. Rev. A **96**, 011801 (2017).

[86] M. B. Plenio and P. L. Knight, The quantum-jump approach to dissipative dynamics in quantum optics, Rev. Mod. Phys. **70**, 101 (1998).

[87] J. R. Johansson, P. D. Nation, and F. Nori, Qutip: An open-source Python framework for the dynamics of open quantum systems, Comput. Phys. Commun. **183**, 1760 (2012).

[88] J. R. Johansson, P. D. Nation, and F. Nori, Qutip 2: A Python framework for the dynamics of open quantum systems, Comput. Phys. Commun. **184**, 1234 (2013).

[89] K. J. Vahala, Optical microcavities, Nature (London) **424**, 839 (2003).

[90] S. M. Spillane, T. J. Kippenberg, K. J. Vahala, K. W. Goh, E. Wilcut, and H. J. Kimble, Ultrahigh-$Q$ toroidal microresonators for cavity quantum electrodynamics, Phys. Rev. A **71**, 013817 (2005).

[91] N. G. Pavlov, G. Lihachev, S. Koptyaev, E. Lucas, M. Karpov, N. M. Kondratiev, I. A. Bilenko, T. J. Kippenberg, and M. L. Gorodetsky, Soliton dual frequency combs in crystalline microresonators, Opt. Lett. **42**, 514 (2017).

[92] V. Huet, A. Rasoloniaina, P. Guillemé, P. Rochard, P. Féron, M. Mortier, A. Levenson, K. Bencheikh, A. Yacomotti, and Y. Dumeige, Millisecond Photon Lifetime in a Slow-Light Microcavity, Phys. Rev. Lett. **116**, 133902 (2016).

[93] J. A. Zielińska and M. W. Mitchell, Self-tuning optical resonator, Opt. Lett. **42**, 5298 (2017).

[94] R. Reimann, M. Doderer, E. Hebestreit, R. Diehl, M. Frimmer, D. Windey, F. Tebbenjohanns, and L. Novotny, GHz Rotation of an Optically Trapped Nanoparticle in Vacuum, Phys. Rev. Lett. **121**, 033602 (2018).

[95] J. Ahn, Z. Xu, J. Bang, Y.-H. Deng, T. M. Hoang, Q. Han, R.-M. Ma, and T. Li, Optically Levitated Nanodumbbell Torsion Balance and GHz Nanomechanical Rotor, Phys. Rev. Lett. **121**, 033603 (2018).

[96] D. E. Chang, C. A. Regal, S. B. Papp, D. J. Wilson, J. Ye, O. Painter, H. J. Kimble, and P. Zoller, Cavity opto-mechanics using an optically levitated nanosphere, Proc. Natl. Acad. Sci. U.S.A. **107**, 1005 (2010).

[97] P. Z. G. Fonseca, E. B. Aranas, J. Millen, T. S. Monteiro, and P. F. Barker, Nonlinear Dynamics and Strong Cavity Cooling of Levitated Nanoparticles, Phys. Rev. Lett. **117**, 173602 (2016).

[98] T. Higo, H. Man, D. B. Gopman, L. Wu, T. Koretsune, O. M. J. van't Erve, Y. P. Kabanov, D. Rees, Y. Li, M.-T. Suzuki, S. Patankar, M. Ikhlas, C. L. Chien, R. Arita, R. D. Shull, J. Orenstein, and S. Nakatsuji, Large magneto-optical Kerr effect and imaging of magnetic octupole domains in an antiferromagnetic metal, Nat. Photonics **12**, 73 (2018).

[99] X.-Y. Lü, W.-M. Zhang, S. Ashhab, Y. Wu, and F. Nori, Quantum-criticality-induced strong Kerr nonlinearities in optomechanical systems, Sci. Rep. **3**, 2943 (2013).

[100] M. Bartkowiak, L.-A. Wu, and A. Miranowicz, Quantum circuits for amplification of Kerr nonlinearity via quadrature squeezing, J. Phys. B **47**, 145501 (2014).

[101] X.-Y. Lü, Y. Wu, J. R. Johansson, H. Jing, J. Zhang, and F. Nori, Squeezed Optomechanics with Phase-Matched Amplification and Dissipation, Phys. Rev. Lett. **114**, 093602 (2015).

[102] J. Zhang, Y.-X. Liu, R.-B. Wu, K. Jacobs, and F. Nori, Quantum feedback: Theory, experiments, and applications, Phys. Rep. **679**, 1 (2017).

[103] M. Rossi, N. Kralj, S. Zippilli, R. Natali, A. Borrielli, G. Pandraud, E. Serra, G. Di Giuseppe, and D. Vitali, Normal-Mode Splitting in a Weakly Coupled Optomechanical System, Phys. Rev. Lett. **120**, 073601 (2018).

[104] S. Haroche and J.-M. Raimond, *Exploring the Quantum: Atoms, Cavities, and Photons* (Oxford University, New York, 2006).

[105] H. J. Carmichael, R. J. Brecha, and P. R. Rice, Quantum interference and collapse of the wave function in cavity QED, Opt. Commun. **82**, 73 (1991).

[106] B. Dayan, A. S. Parkins, T. Aoki, E. P. Ostby, K. J. Vahala, and H. J. Kimble, A photon turnstile dynamically regulated by one atom, Science **319**, 1062 (2008).

[107] T. Aoki, A. S. Parkins, D. J. Alton, C. A. Regal, B. Dayan, E. Ostby, K. J. Vahala, and H. J. Kimble, Efficient Routing of Single Photons by One Atom and a Microtoroidal Cavity, Phys. Rev. Lett. **102**, 083601 (2009).

[108] I. Shomroni, S. Rosenblum, Y. Lovsky, O. Bechler, G. Guendelman, and B. Dayan, All-optical routing of single photons by a one-atom switch controlled by a single photon, Science **345**, 903 (2014).

[109] Y.-X. Liu, X.-W. Xu, A. Miranowicz, and F. Nori, From blockade to transparency: Controllable photon transmission through a circuit-QED system, Phys. Rev. A **89**, 043818 (2014).

[110] S. Rosenblum, O. Bechler, I. Shomroni, Y. Lovsky, G. Guendelman, and B. Dayan, Extraction of a single photon from an optical pulse, Nat. Photonics **10**, 19 (2016).

[111] T. Aoki, B. Dayan, E. Wilcut, W. P. Bowen, A. S. Parkins, T. J. Kippenberg, K. J. Vahala, and H. J. Kimble, Observation of strong coupling between one atom and a monolithic microresonator, Nature (London) **443**, 671 (2006).

[112] C. Junge, D. O'Shea, J. Volz, and A. Rauschenbeutel, Strong Coupling between Single Atoms and Nontransversal Photons, Phys. Rev. Lett. **110**, 213604 (2013).

[113] P. Michler, A. Kiraz, C. Becher, W. V. Schoenfeld, P. M. Petroff, L. Zhang, E. Hu, and A. Imamoğlu, A quantum dot single-photon turnstile device, Science **290**, 2282 (2000).

[114] A. Faraon, P. E. Barclay, C. Santori, K.-M. C. Fu, and R. Beausoleil, Resonant enhancement of the zero-phonon emission from a colour centre in a diamond cavity, Nat. Photonics **5**, 301 (2011).

# Supplementary Material for "Nonreciprocal Photon Blockade"

Ran Huang[1], Adam Miranowicz[2,3], Jie-Qiao Liao[1], Franco Nori[2,4], and Hui Jing[1,*]

[1] *Key Laboratory of Low-Dimensional Quantum Structures and Quantum Control of Ministry of Education, Department of Physics and Synergetic Innovation Center for Quantum Effects and Applications, Hunan Normal University, Changsha 410081, China*
[2] *Theoretical Quantum Physics Laboratory, RIKEN Cluster for Pioneering Research, Wako-shi, Saitama 351-0198, Japan*
[3] *Faculty of Physics, Adam Mickiewicz University, 61-614 Poznań, Poland*
[4] *Physics Department, The University of Michigan, Ann Arbor, Michigan 48109-1040, USA*

Here, we present technical details on nonreciprocal photon blockade (PB) in a driven Kerr-type model with a Fizeau drag. Our discussion includes: (1) single- (1PB) and two-photon blockade (2PB) effects; (2) our analytical solutions for the steady-state optical-intensity correlation functions; and (3) rotation-induced quantum nonreciprocity.

## S1. KERR-TYPE INTERACTION WITH THE FIZEAU DRAG

To realize nonreciprocal photon blockade, we consider a rotating optical resonator with a nonlinear Kerr medium which can be described by a Kerr-type interaction with a Fizeau drag term,

$$\hat{H}_{\rm R} = \hbar(\omega_0 + \Delta_{\rm F})\hat{a}^\dagger\hat{a} + \hbar U\hat{a}^\dagger\hat{a}^\dagger\hat{a}\hat{a}. \tag{S1}$$

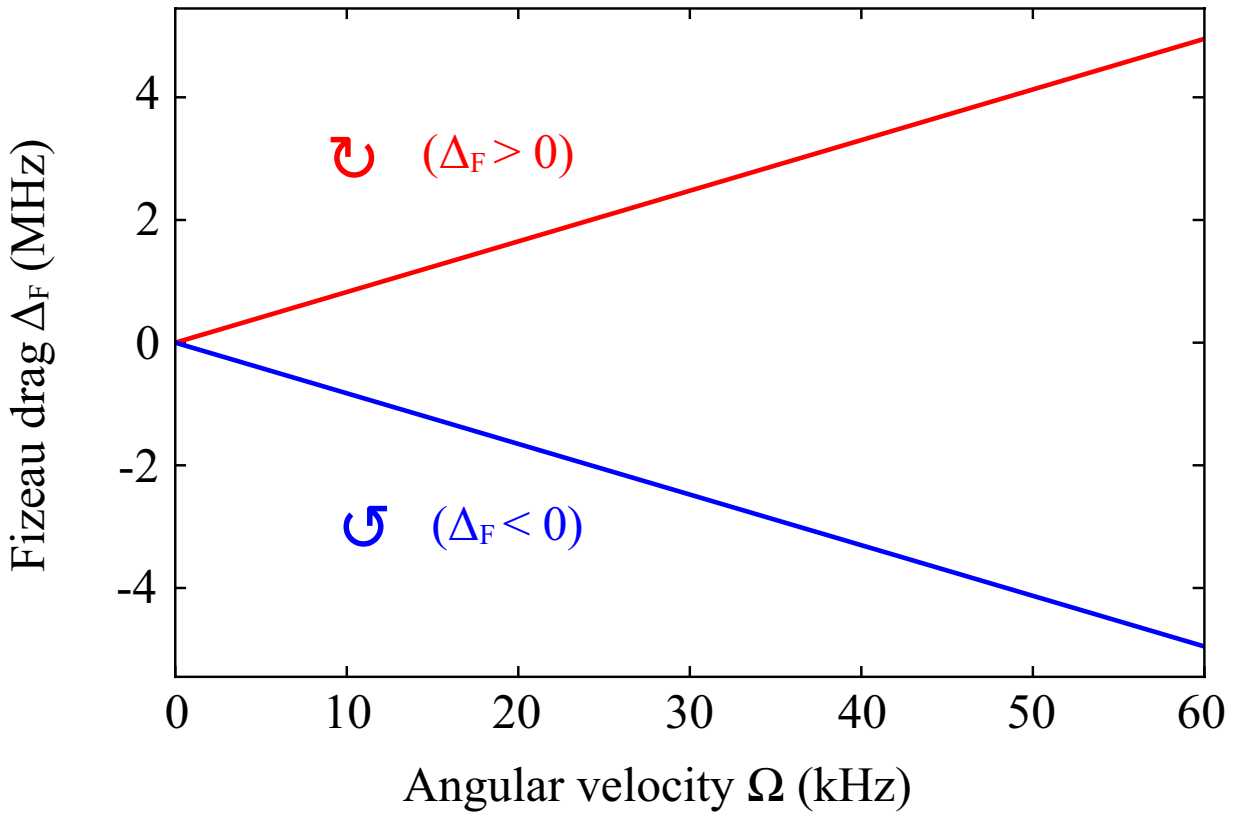


FIG. S1. Fizeau drag $\Delta_{\rm F}$ versus angular velocity of the resonator for $\Delta_{\rm F} > 0$ (red line) and $\Delta_{\rm F} < 0$ (blue line) cases. The optical wavelength is $\lambda = 1550$ nm, the radius of the resonator is $R = 30$ $\mu$m, and the linear refractive index of the resonator is $n = 1.4$.

Here, $U\hat{a}^\dagger\hat{a}^\dagger\hat{a}\hat{a}$ is the standard Kerr interaction term [S1–S4], $\hat{a}$ ($\hat{a}^\dagger$) is the annihilation (creation) operator for the cavity field, while $U = \hbar\omega_0^2 c n_2/(n_0^2 V_{\rm eff})$ is the strength of the nonlinear interaction with the nonlinear (linear) refraction index $n_2$ ($n_0$), an effective cavity-mode volume $V_{\rm eff}$, and the speed of light in vacuum $c$ . Moreover, $\omega_0$ is the resonance frequency of the non-spinning resonator, and the rotation leads to a Fizeau shift [S5]:

$$\omega_0 \to \omega_\pm = \omega_0 + \Delta_{\rm F}, \tag{S2}$$

with

$$\Delta_{\rm F} = \pm\frac{nr\Omega\omega_0}{c}\left(1 - \frac{1}{n^2} - \frac{\lambda}{n}\frac{dn}{d\lambda}\right) = \pm\eta\Omega, \tag{S3}$$

where $\Delta_{\rm F} > 0$ ($\Delta_{\rm F} < 0$) denotes the light propagating against (along) the direction of the spinning resonator, $\lambda$ is the optical wavelength, $n$ is the refractive index of the resonator, and $r$ is the radius of the cavity. The dispersion term $dn/d\lambda$, characterizing the relativistic origin of the Sagnac effect, is relatively small ($\sim 1\%$) [S5, S6].

When the resonator is not spinning, the Fizeau drag is equal to zero, owing to the same resonance frequency of light coming from the left or right side. As implied by Eq. (S3), increasing the rotation frequency $\Omega$ results in an opposing frequency linear shift of $\eta\Omega$ (see Fig. S1) for light coming from opposite directions [S6].

## S2. PHOTON BLOCKADE EFFECTS

### A. Origin of photon blockade

In order to study conventional photon blockade (PB), we consider the Hamiltonian (S1) including the driving term

$$\hat{H} = \hat{H}_{\rm R} + \hbar\xi(\hat{a}^\dagger e^{-i\omega_L t} + \hat{a}e^{i\omega_L t}), \tag{S4}$$

where $\xi = \sqrt{\gamma P_{\rm in}/(\hbar\omega_L)}$ is the driving amplitude with the cavity loss rate $\gamma$, the driving power $P_{\rm in}$, and the driving frequency $\omega_L$ [S7]. In a frame rotating with the driving frequency $\omega_L$, the Hamiltonian is transformed to

$$\hat{H}_{\rm eff} = i\hbar\frac{d\hat{D}^\dagger}{dt}\hat{D} + \hat{D}^\dagger\hat{H}\hat{D},$$

with $\hat{D} = \exp\left(-i\omega_L\hat{a}^\dagger\hat{a}t\right)$, which leads to

$$\begin{aligned}\hat{H}_{\rm eff} &= -\hbar\omega_L\hat{a}^\dagger\hat{a} + \hbar\omega_\pm\hat{a}^\dagger\hat{a} + \hbar U\hat{a}^\dagger\hat{a}^\dagger\hat{a}\hat{a} + \hbar\xi(\hat{a}^\dagger + \hat{a}) \\ &= \hbar(\omega_0 + \Delta_{\rm F} - \omega_L)\hat{a}^\dagger\hat{a} + \hbar U\hat{a}^\dagger\hat{a}^\dagger\hat{a}\hat{a} + \hbar\xi(\hat{a}^\dagger + \hat{a}).\end{aligned}$$

Thus, the effective Hamiltonian of this system becomes

$$\hat{H}_{\rm eff} = \hbar(\Delta_L + \Delta_{\rm F})\hat{a}^\dagger\hat{a} + \hbar U\hat{a}^\dagger\hat{a}^\dagger\hat{a}\hat{a} + \hbar\xi(\hat{a}^\dagger + \hat{a}), \tag{S5}$$

where $\Delta_L = \omega_0 - \omega_L$ is the detuning between the driving field and the cavity field for the non-spinning resonator. The Hamiltonian of the isolated spinning system, i.e.,

$$H_0 = \hbar(\Delta_L + \Delta_{\rm F})\hat{a}^\dagger\hat{a} + \hbar U\hat{a}^\dagger\hat{a}^\dagger\hat{a}\hat{a},$$

can be expressed as

$$\begin{aligned}\hat{H}_0|n\rangle &= [\hbar\Delta_L\hat{a}^\dagger\hat{a} + \hbar\Delta_{\rm F}\hat{a}^\dagger\hat{a} + \hbar U a^\dagger(\hat{a}\hat{a}^\dagger - 1)\hat{a}]|n\rangle \\ &= [\hbar\Delta_L\hat{a}^\dagger\hat{a} + \hbar\Delta_{\rm F}\hat{a}^\dagger\hat{a} + \hbar U\hat{a}^\dagger\hat{a}\hat{a}^\dagger\hat{a} - \hbar U\hat{a}^\dagger\hat{a}]|n\rangle \\ &= [\hbar\Delta_L\hat{a}^\dagger\hat{a} + \hbar(\Delta_{\rm F} - U)\hat{a}^\dagger\hat{a} + \hbar U(\hat{a}^\dagger\hat{a})^2]|n\rangle \\ &= [n\hbar\Delta_L + n\hbar(\Delta_{\rm F} - U) + n^2\hbar U]|n\rangle \\ &= E_n|n\rangle.\end{aligned}$$

Thus, we obtain the eigensystem for the weak-driving case,

$$\hat{H}_0|n\rangle = E_n|n\rangle, \tag{S6}$$

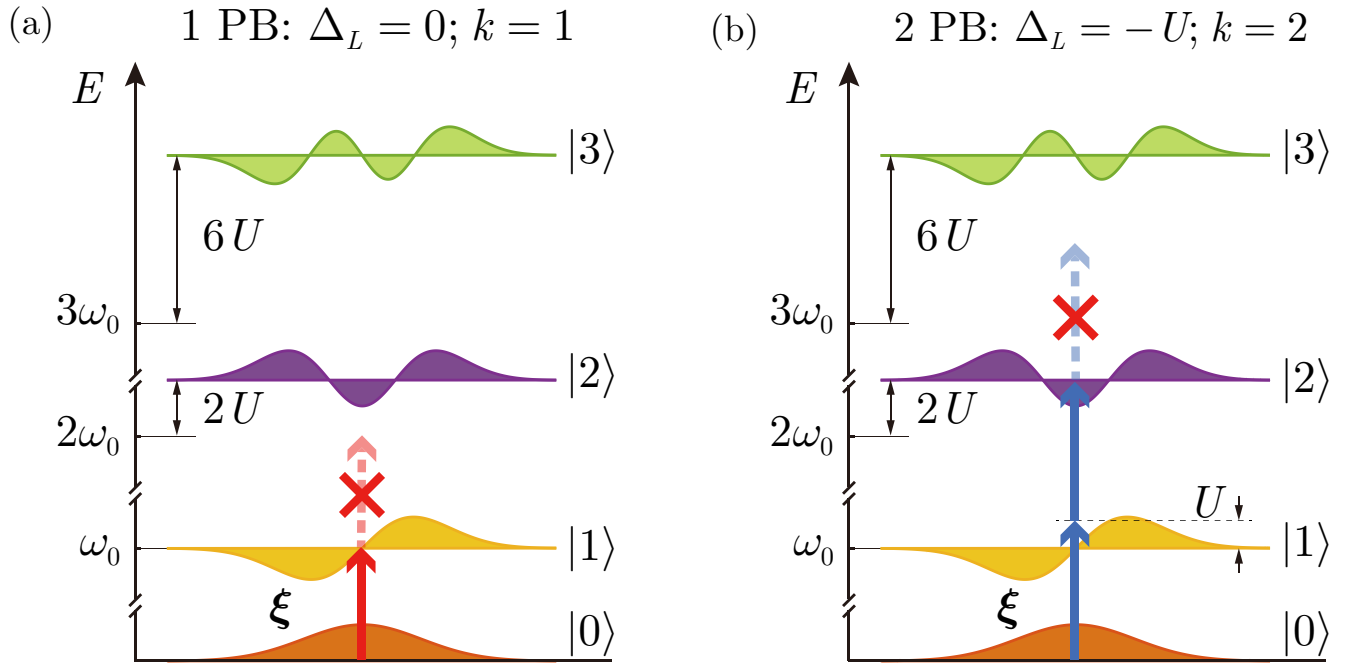


FIG. S2. Schematic energy-level diagram of the non-spinning resonator. This explains the occurrence of $k$-photon blockade for $\Delta_F = 0$ in terms of $k$-photon transitions induced by the driving field satisfying the resonance condition $\Delta_k = 0$, which corresponds to the driving-field frequency $\omega_L = \omega_0 + U(k-1)$. Here $\hbar = 1$.

with eigenvalues

$$E_n = n\hbar\Delta_L + n\hbar\Delta_F + (n^2 - n)\hbar U = n\hbar\Delta_L + (n^2 - n)\hbar U \pm n\hbar|\Delta_F|, \tag{S7}$$

where $+n\hbar|\Delta_F|$ and $-n\hbar|\Delta_F|$ denote the light propagating against ($\Delta_F > 0$) and along ($\Delta_F < 0$) the direction of the spinning resonator, respectively.

The origin of conventional $n$-photon blockade can be understood from the fact that due to the anharmonicity of the energy structure, i.e., the energy difference between consecutive manifolds is not constant, the Hilbert space of the system is restricted to the states containing at most $n$ quanta. For example, when the optical resonator is non-spinning ($|\Delta_F|$=0), single-photon blockade (1PB) is illustrated in Fig. S2(a). If a coherent probe beam, tuned to $\omega_0$ ($\Delta_L = 0$), is coupled to the system, the probe is on resonance with the $|0\rangle \to |1\rangle$ transition, but the $|1\rangle \to |2\rangle$ transition is detuned by $2\hbar U$ and is suppressed for $U > \gamma$ (where $\gamma$ denotes the optical loss of the resonator). Consequently, once a photon is coupled to the system, it suppresses the probability of coupling a second photon with the same frequency. Similarly, two-photon blockade (2PB) corresponds to a two-photon resonance (2PR) for a non-spinning case, as shown in Fig. S2(b). Morever, multi-PB corresponds to a multi-photon resonance [S4, S8–S12]. In addition to multi-PB, the energy-level diagrams of multi-photon resonances in a Kerr-type system [S4] also correspond to photon-induced tunneling (PIT) [S7, S13–S16]. This indicates that the absorption of the first photon enhances the absorption of subsequent photons [S13]. The distinction of 1PB, multi-PB, and PIT can be found by analysing higher-order correlation functions $g^{(\mu)}(0)$ with $\mu \geq 2$, as discussed below.

Due to the rotation of the resonator, different cases of nonreciprocal PB effects can be achieved. For example, Table II and Fig. S3 summarize the main results for $P_{\rm in} = 0.3$ pW, and these are elaborated in detail later on in this Supplementary Material.

We observe that the Hamiltonian, given in Eq. (S5), can be rewritten as follows

$$\hat{H}_k = \hbar(\Delta_k + \Delta_F)\hat{a}^\dagger\hat{a} + \hbar U\hat{a}^\dagger\hat{a}(\hat{a}^\dagger\hat{a} - k) + \hbar\xi(\hat{a}^\dagger + \hat{a}), \tag{S8}$$

where $\Delta_k = \Delta_L + U(k-1)$ is the frequency mismatch for the non-spinning resonator. For convenience, we refer to $k$ as a tuning parameter, as in Ref. [S4]. Hereafter, we analyze the resonant case of $\Delta_k = 0$, which is related to the resonant $k$-photon transitions in the non-spinning resonator, as shown in Fig. S2. This condition implies that the tuning parameter $k$ is related to the Kerr nonlinearity and the driving-field and cavity frequencies as follows

$$k = -\Delta_L/U + 1. \tag{S9}$$

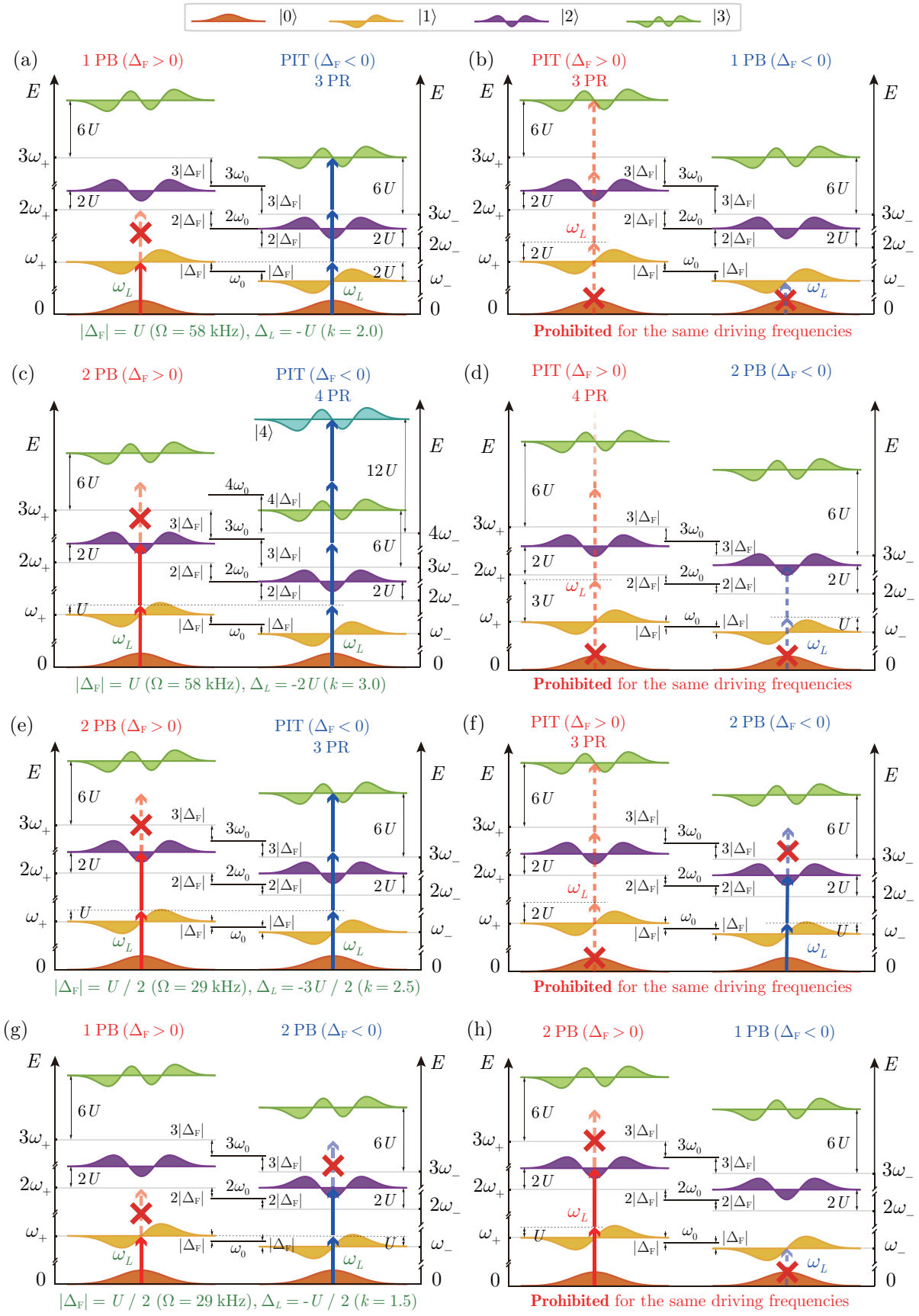


FIG. S3. Energy-level diagrams of the spinning resonator for different cases of nonreciprocal PB effects. Here, photon-induced tunneling (PIT) corresponds to an $n$-photon resonance ($n$ PR), and $\hbar = 1$. All of these diagrams correspond to the cases given in Table II.

### B. Criteria of photon blockade

We have studied the origin of conventional PB via the anharmonic energy-level structure. In order to describe this picture quantitatively, we apply two approaches. One is based on studying the photon-number distribution of the system [S4, S12], and the other is based on investigating the optical intensity correlations [S12, S13, S17]. Both can be experimentally measured [S12, S13, S17].

Concerning the first method, in the case of an ideal $n$-photon blockade, the cavity field shows the following photon-number distribution [S4]:

$$(i) \quad P(m) = 0 \qquad \text{for } m > n, \tag{S10a}$$

$$(ii) \quad P(n) \neq 0. \tag{S10b}$$

with normalization $\sum_{m=0}^{\infty} P(m) = 1$. While the first $n$ photons are resonantly absorbed in the system, the generation of more photons is blockaded in the cavity. However, these photon-number distribution conditions are hard to achieve in an experiment, where $P(m) \neq 0$ even for $m > n$. Thus, a comparison with the Poissonian distribution was proposed by Hamsen *et al* [S12]:

$$(i) \quad P(m) < \mathcal{P}(m) \qquad \text{for } m > n, \tag{S11a}$$

$$(ii) \quad P(n) \geq \mathcal{P}(n). \tag{S11b}$$

where $\mathcal{P}(m)$ is the Poissonian distribution

$$\mathcal{P}(m) = \frac{\langle \hat{m} \rangle^m}{m!} \exp\left(-\langle \hat{m} \rangle\right), \tag{S12}$$

with the same average photon number $\langle \hat{m} \rangle$ as the cavity field. The condition, given in Eq. (S11a), indicates that the first $n$ photons are effectively impenetrable to the following photons; while the condition, given in Eq. (S11b), indicates that the coupling of an initial photon to the system favors the coupling of the subsequent photons within the first $n$ photons. This leads to the sub-Poissonian photon-number statistics for $(n+1)$ photons with the simultaneous super-Poissonian statistics of the first $n$ photons. To show a relative deviation of a given photon-number distribution from the corresponding Poissonian distribution, we use the formula [S12]:

$$[P(n) - \mathcal{P}(n)]/\mathcal{P}(n). \tag{S13}$$

For the second approach, correlation function $G^{(n)}(t_1, t_2, \cdots, t_n)$ is the quantity measured at moments $t_1, t_2, \cdots, t_n$ in extended Hanbury Brown-Twiss experiments with $n$ detectors. Note that $g^{(n)}$ is $G^{(n)}$ normalized by the $n$th power of the mean photon number. Thus, $g^{(n)}(0) \equiv \lim_{t\to\infty}(t, t, \cdots, t)$ is related to the probability of simultaneously measuring $n$ photons in their steady state assuming photon detections at the same time $t = t_1 = t_2 = \cdots = t_n$. The larger value of $g^{(n)}(0) > 1$, the higher probability of $n$-photon bunching (photon coalescence). And the smaller value of $g^{(n)}(0) < 1$, the lower probability of $n$-photon bunching, which corresponds to the higher probability of $n$-photon antibunching (photon anticoalescence). The case of $g^{(n)}(0) = 1$ is called photon unbunching, which is a typical feature of coherent light for any $n$. These correlation functions $G^{(n)}$ and $g^{(n)}$ are basic elements of the quantum coherence theory of Glauber [S18]."

The normalized equal-time $\mu$th-order photon correlation is given by

$$g^{(\mu)}(0) = \sum_{m=\mu}^{\infty} \frac{m!}{(m-\mu)!} \frac{P(m)}{\langle \hat{m} \rangle^{\mu}} = \langle \hat{m} \rangle^{-\mu} \sum_{m=\mu}^{\infty} m(m-1)\cdots(m-\mu+1)P(m) = \frac{\langle \hat{a}^{\dagger\mu}\hat{a}^{\mu} \rangle}{\langle \hat{a}^{\dagger}\hat{a} \rangle^{\mu}}. \tag{S14}$$

In particular, the second-order photon correlation function is

$$g^{(2)}(0) = \sum_{m=2}^{\infty} m(m-1)\frac{P(m)}{\langle \hat{m} \rangle^2} = \frac{\langle \hat{m}(\hat{m}-1) \rangle}{\langle \hat{m} \rangle^2} = \frac{\langle \hat{a}^{\dagger 2}\hat{a}^2 \rangle}{\langle \hat{a}^{\dagger}\hat{a} \rangle^2}, \tag{S15}$$

and the third-order photon correlation function is

$$g^{(3)}(0) = \sum_{m=3}^{\infty} m(m-1)(m-2)\frac{P(m)}{\langle \hat{m} \rangle^3} = \frac{\langle \hat{m}(\hat{m}-1)(\hat{m}-2) \rangle}{\langle \hat{m} \rangle^3} = \frac{\langle \hat{a}^{\dagger 3}\hat{a}^3 \rangle}{\langle \hat{a}^{\dagger}\hat{a} \rangle^3}. \tag{S16}$$

The photon-number distribution conditions for $n$-photon blockade, given in Eqs. (S10a) and (S10b), can be translated into the following conditions:

$$(i) \quad g^{(n+1)}(0) = 0, \tag{S17a}$$

$$(ii) \quad g^{(n)}(0) \neq 0. \tag{S17b}$$

As aforementioned, these strict conditions can only be fulfilled for an ideal case. The experimentally-realizable conditions can be obtained based on Eqs. (S11a) and (S11b). Since in the weak-driving regime, the photon-number distribution fulfills the condition $P(m) \gg P(m+1)$, it is sufficient to satisfy $P(n+1) < \mathcal{P}(n+1)$ according to the condition in Eq. (S11a). Meanwhile, we can approximately express $P(n+1)$ with $g^{(n+1)}(0)$ as follows:

$$\begin{aligned} g^{(n+1)}(0) &= \sum_{m=n+1}^{\infty} \frac{m!}{(m-n-1)!} \frac{P(m)}{\langle \hat{m} \rangle^{n+1}} \approx \frac{(n+1)!}{\langle \hat{m} \rangle^{n+1}} P(n+1), \\ P(n+1) &\approx \frac{\langle \hat{m} \rangle^{n+1}}{(n+1)!} \cdot g^{(n+1)}, \end{aligned} \tag{S18}$$

as the $P(m)$ have been neglected for all $m > (n+1)$. Thus, the condition, given in Eq. (S11a), reads [S12]:

$$\begin{aligned} P(n+1) &< \mathcal{P}(n+1), \\ \frac{\langle \hat{m} \rangle^{n+1}}{(n+1)!} \cdot g^{(n+1)}(0) &< \frac{\langle \hat{m} \rangle^{n+1}}{(n+1)!} \exp\left(-\langle \hat{m} \rangle\right), \\ g^{(n+1)}(0) &< \exp\left(-\langle \hat{m} \rangle\right). \end{aligned} \tag{S19}$$

We can also obtain an approximate $P(n)$ using a similar method as follows:

$$\begin{aligned} g^{(n)}(0) &= \sum_{m=n}^{\infty} \frac{m!}{(m-n)!} \frac{P(m)}{\langle \hat{m} \rangle^{n}} \approx \frac{n!}{\langle \hat{m} \rangle^{n}} P(n) + \frac{(n+1)!}{\langle \hat{m} \rangle^{n}} P(n+1), \\ P(n) &\approx \frac{\langle \hat{m} \rangle^{n}}{n!} \cdot g^{(n)}(0) - (n+1) P(n+1), \\ P(n) &\approx \frac{\langle \hat{m} \rangle^{n}}{n!} \cdot g^{(n)}(0) - \frac{\langle \hat{m} \rangle^{n+1}}{n!} \cdot g^{(n+1)}(0). \end{aligned} \tag{S20}$$

Moreover, the condition, given in Eq. (S11b), then reads:

$$\begin{aligned} P(n) &\geq \mathcal{P}(n), \\ \frac{\langle \hat{m} \rangle^{n}}{n!} \cdot g^{(n)}(0) - \frac{\langle \hat{m} \rangle^{n+1}}{n!} \cdot g^{(n+1)}(0) &\geq \frac{\langle \hat{m} \rangle^{n}}{n!} \exp\left(-\langle \hat{m} \rangle\right), \\ g^{(n)}(0) - \langle \hat{m} \rangle \cdot g^{(n+1)}(0) &\geq \exp\left(-\langle \hat{m} \rangle\right), \\ g^{(n)}(0) &\geq \exp\left(-\langle \hat{m} \rangle\right) + \langle \hat{m} \rangle \cdot g^{(n+1)}(0), \end{aligned} \tag{S21}$$

i.e., the experimentally-realizable conditions, given in Eqs. (S11a) and (S11b), can be translated into the following conditions [S12]:

$$(i) \quad g^{(n+1)}(0) < \exp\left(-\langle \hat{m} \rangle\right), \tag{S22a}$$

$$(ii) \quad g^{(n)}(0) \geq \exp\left(-\langle \hat{m} \rangle\right) + \langle \hat{m} \rangle \cdot g^{(n+1)}(0), \tag{S22b}$$

indicating a higher-order sub-Poissonian photon-number statistics.

Moreover, PIT can be quantified by photon-number correlation functions. Table I shows that more refined criteria for PIT are sometimes applied based on higher-order correlation functions $g^{(\mu)}(0)$ with $\mu > 2$ [S16, S19]. Here, we refer to PIT if the following conditions are satisfied for $\mu \geq 2$:

$$g^{(\mu)}(0) > \exp\left(-\langle \hat{m} \rangle\right). \tag{S23}$$

For simplicity, in this work, we consider these conditions only for $2 \leq \mu \leq 4$. This indicates light with higher-order super-Poissonian photon-number statistics, i.e., once, a photon is coupled in a resonator, it enhances the probabilities of more photons entering the resonator. In the few-photon regime ($\langle \hat{m} \rangle \ll 1$), these criteria become

$$g^{(\mu)}(0) > 1 \quad \text{for} \quad \mu = 2, 3, 4. \tag{S24}$$

We provide a more basic criteria to identify multi-PB and PIT by using $\mu$th-order correlation functions $g^{(\mu)}(0)$. These criteria lead to the same conclusions as those based on Eq. (S13).

TABLE I. Criteria of photon-induced tunneling (PIT) used in literature.

| Reference | Criteria of PIT |
|---|---|
| Faraon *et al.* (2008) [S13] | $g^{(2)}(0)$ is a local maximum |
| Majumdar *et al.* (2012) [S7, S14] | $g^{(2)}(0) > 1$ |
| Xu *et al.* (2013) [S15] | $g^{(2)}(0) > 1$ (two-photon tunneling); $g^{(3)}(0) > g^{(2)}(0) > 1$ (three-photon tunneling) |
| Rundquist *et al.* (2014) [S16] | $g^{(3)}(0) > g^{(2)}(0)$ |
| Wang *et al.* (2018) [S19] | $g^{(4)}(0) > g^{(3)}(0) > g^{(2)}(0) > 1$ (phonon-induced tunneling, an analogue of PIT) |

### C. Single- and Multi-photon blockade

In this section, we only consider the non-spinning case ($\Delta_{\rm F}$=0), while the spinning case is discussed in Sec. S4. According to criteria, given in Eqs. (S22a) and (S22b), 1PB has to fulfill the following conditions for $n = 1$:

$$(i) \quad g^{(2)}(0) < \exp\left(-\langle\hat{m}\rangle\right) \equiv f, \tag{S25a}$$

$$(ii) \quad g^{(1)}(0) \geq \exp\left(-\langle\hat{m}\rangle\right) + \langle\hat{m}\rangle \cdot g^{(2)}(0) \equiv f^{(1)}. \tag{S25b}$$

As expected from the intuitive picture discussed in Sec. S2 A, the strongest 1PB occurs at $\Delta_L = 0$ ($k = 1$), since the correlation functions fulfill the criteria of 1PB given in Eqs. (S25a) and (S25b) [see Fig. S4(a)]. In the weak-driving regime, $\langle\hat{m}\rangle \ll 1$ implies that $f \to 1$ and $f^{(1)} \to 1$. Then we obtain $g^{(2)}(0) < 1$, which corresponds to the usual criterion of 1PB, as known in the published literature.

As aforementioned in 1PB, the first photon blocks the entrance of a second photon, which indicates the enhancement of the single-photon probability, and also the suppression of the two- or more-photon probabilities. We can clearly see that $P(1) > \mathcal{P}(1)$, while $P(2) < \mathcal{P}(2)$ and $P(3) < \mathcal{P}(3)$ at $k = 1$ in Fig. S4(b). Moreover, 1PB can be recognized from the the deviations of the photon distribution from the standard Poissonian distribution with the same mean photon number [i.e., Eq. (S13)], as shown in Fig. S4(c-i).

At $k = 2$, we find the correlation functions fulfill $g^{(2)}(0) > g^{(3)}(0) > g^{(4)}(0) > 1$, as shown in the inset in Fig. S4(a). This shows that PIT corresponding to super-Poissonian photon-number behavior of light, which occurs at $k = 2$, since the correlation functions satisfy the conditions given in Eq. (S24). PIT can also be recognized from the photon-number distributions and the deviations given in Eq. (S13). As shown in Figs. S4(b) and S4(c-ii), we find that $P(1) < \mathcal{P}(1)$, $P(2) > \mathcal{P}(2)$, $P(3) > \mathcal{P}(3)$, and $P(4) > \mathcal{P}(4)$ at $k = 2$. This is a clear signature of PIT. Since the case for $k = 2$ corresponds to a two-photon resonance, we refer to this PIT as two-photon resonance-induced PIT.

Similarly, the 2PB has to fulfill the criteria in Eqs. (S22a) and (S22b) for $n = 2$:

$$(i) \quad g^{(3)}(0) < \exp\left(-\langle\hat{m}\rangle\right) \equiv f, \tag{S26a}$$

$$(ii) \quad g^{(2)}(0) \geq \exp\left(-\langle\hat{m}\rangle\right) + \langle\hat{m}\rangle \cdot g^{(3)}(0) \equiv f^{(2)}. \tag{S26b}$$

As expected from the intuitive picture discussed in Sec. S2 A, 2PB occurs at $\Delta_L = -U$ ($k = 2$), since the correlation functions fulfill the conditions of 2PB given in Eqs. (S26a) and (S26b) [see Fig. S5(a)]. We find that, at $k = 2$, $g^{(3)}(0)$ is smaller than $f$ defined in the criterion given in Eq. (S26a), while $g^{(2)}(0)$ is greater than $f^{(2)}$ defined in the criterion given in Eq. (S26b). Here, 2PB indicates that the two-photon probability is enhanced as $P(2) > \mathcal{P}(2)$, while the other photon-number probabilities are suppressed, as shown in Figs. S5(b) and S5(c-ii). In Fig. S4, there is PIT at $k = 2$. However, in Fig. S5, there is 2PB at $k = 2$ with an enhanced input power. We note that it is necessary to properly increase the driving power to obtain a good-quality 2PB, since we need a larger average photon number. Thus, we enhance the input power from $P_{\rm in} = 2\,{\rm fW}$ (Fig. S4) to $P_{\rm in} = 0.3\,{\rm pW}$ (Fig. S5). Also, the 1PB still emerges at $k = 1$, since the second-order correlation function fulfills $g^{(2)}(0) < 1$ [see Fig. S5(a)], or only the single-photon probability is enhanced at $k = 1$ [see Figs. S5(b) and S5(c-i)].

At $k = 3$, we find the correlation functions fulfill $g^{(4)}(0) > g^{(3)}(0) > g^{(2)}(0) > 1$, as shown in the inset in Fig. S4(a). It shows PIT occurs at $k = 3$, since the correlation functions satisfy the conditions given in Eq. (S24). PIT can also be recognized from the photon-number distributions and the deviations given in Eq. (S13). As shown in Figs. S5(b) and S5(c-iii), we find that $P(1) < \mathcal{P}(1)$, $P(2) > \mathcal{P}(2)$, $P(3) > \mathcal{P}(3)$, and $P(4) > \mathcal{P}(4)$ at $k = 3$. This is a clear signature of PIT. Since the case for $k = 3$ corresponds to a three-photon resonance, we refer to this PIT as three-photon resonance-induced PIT.

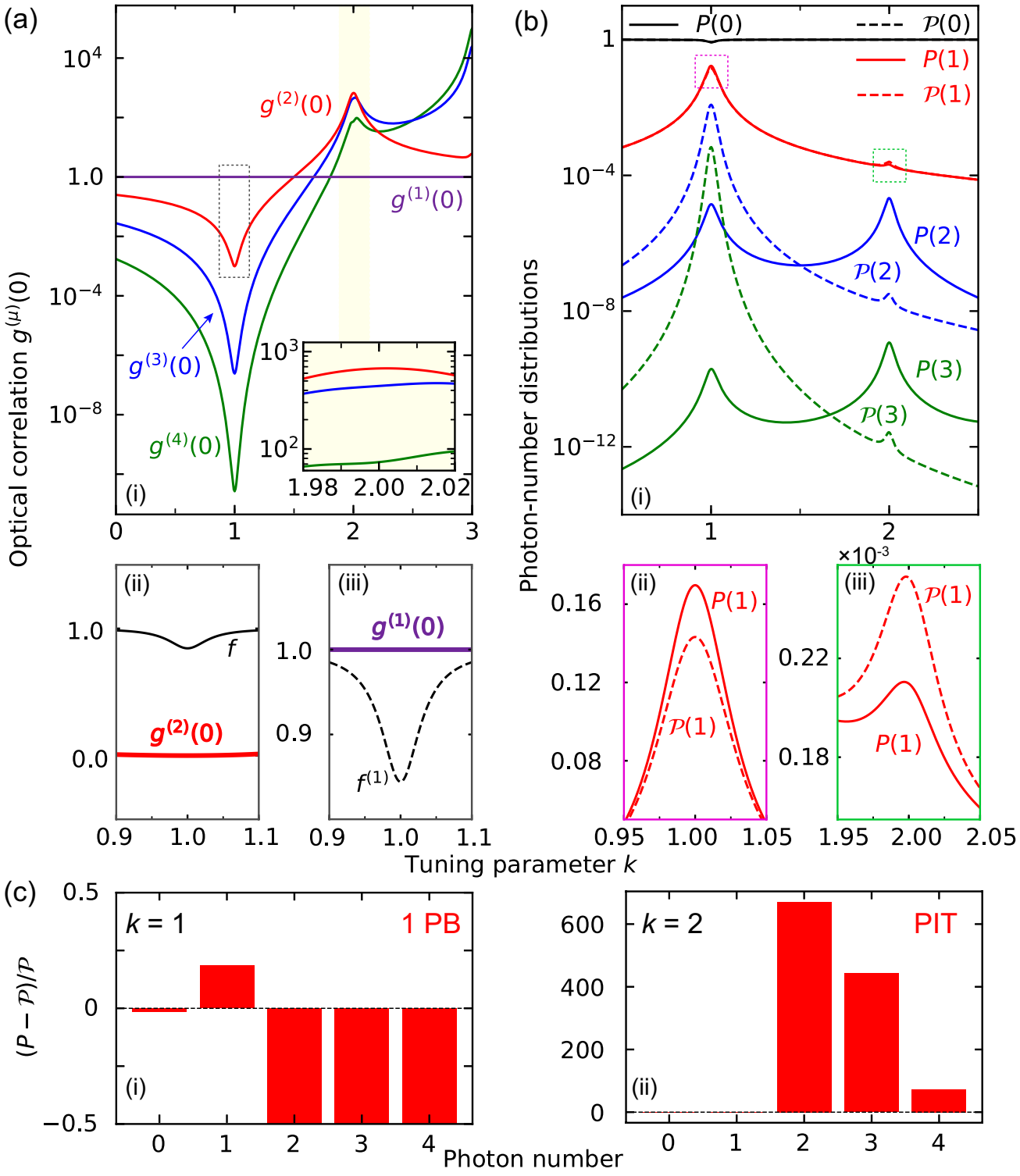


FIG. S4. (a) Correlation functions $g^{(\mu)}(0)$ versus the tuning parameter $k$ for the non-spinning resonator ($\Delta_{\rm F} = 0$). Note that 1PB emerges at $k = 1$, since (a-ii) $g^{(2)}(0) < f$ and (a-iii) $g^{(1)}(0) > f^{(1)}$ fulfill the criteria given in Eqs. (S25a) and (S25b), respectively. PIT occurs at $k = 2$, since $g^{(2)}(0) > g^{(3)}(0) > g^{(4)}(0) > 1$ [see the inset in panel (a-i)] fulfills the condition given in Eq. (S24). These 1PB and PIT can also be recognized from (b) the photon-number distributions and (c) the deviations given in Eq. (S13). At $k = 1$, (b-ii) single-photon probability is enhanced as $P(1) > \mathcal{P}(1)$, while $m$-photon ($m > 1$) probabilities are suppressed as $P(m) < \mathcal{P}(m)$ [see panels (b-i) and (c-i)]. These photon-number distributions fulfill the conditions given in Eqs. (S11a) and (S11b) for $n = 1$, i.e., resulting in 1PB. At $k = 2$, (b-iii) single-photon probability is suppressed as $P(1) < \mathcal{P}(1)$, while $m$-photon ($m > 1$) probabilities are enhanced as $P(m) > \mathcal{P}(m)$ [see panels (b-i) and (c-ii)], i.e., resulting in PIT. The parameters used here are: $\Omega = 0$, $n_2 = 3 \times 10^{-14}\,\mathrm{m^2/W}$, $n_0 = 1.4$, $V_{\rm eff} = 150\,\mu\mathrm{m}^3$, $Q = 5 \times 10^9$, $\lambda = 1550\,\mathrm{nm}$, $P_{\rm in} = 2\,\mathrm{fW}$, and $r = 30\,\mu\mathrm{m}$.

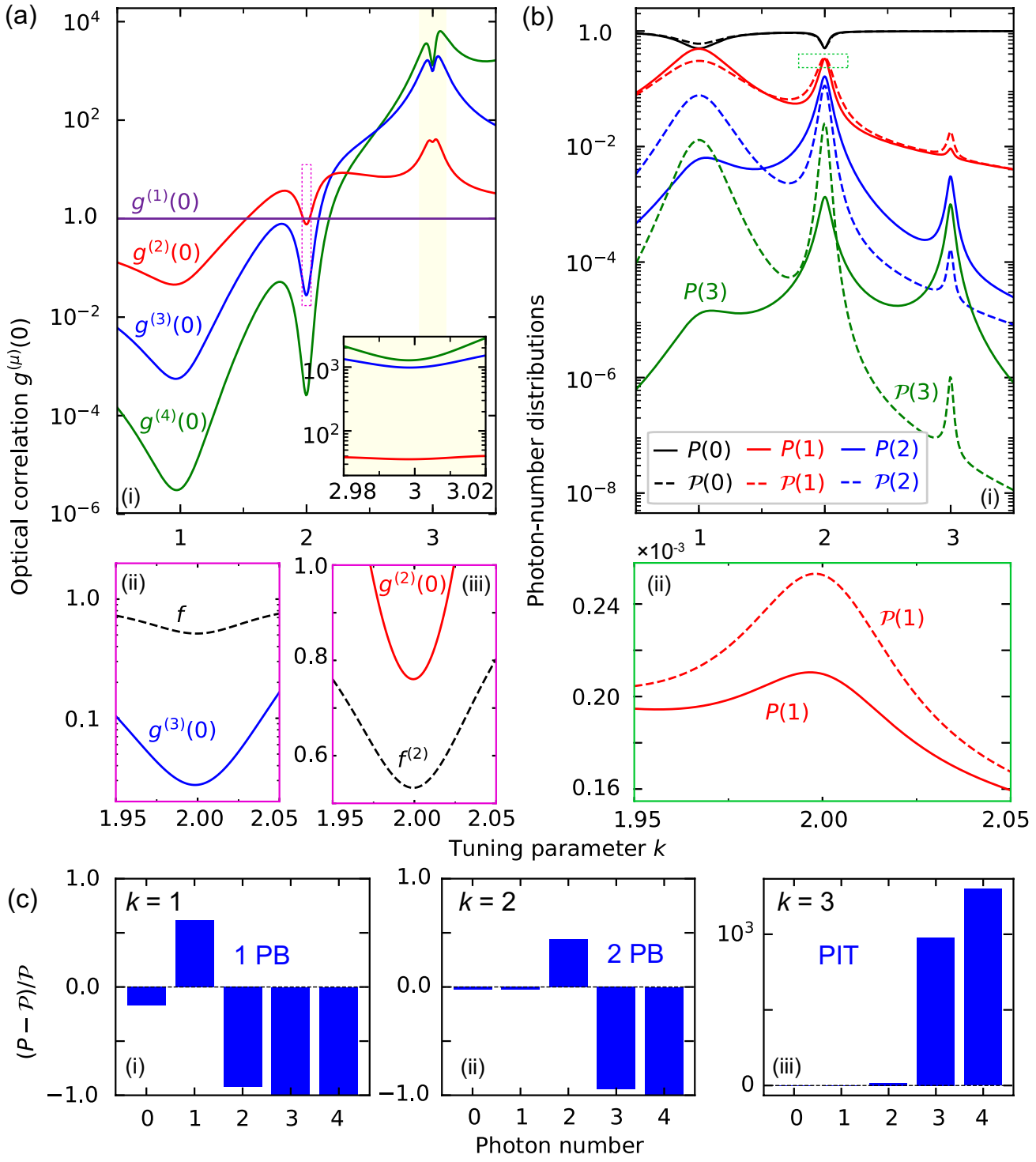


FIG. S5. (a) Correlation functions $g^{(\mu)}(0)$ versus the tuning parameter $k$ for the non-spinning resonator ($\Delta_{\rm F} = 0$). Note that 2PB occurs at $k = 2$, since (a-ii) $g^{(3)}(0) < f$ and (a-iii) $g^{(2)}(0) > f^{(2)}$ fulfill the criteria given in Eqs. (S26a) and (S26b), respectively. Also, 1PB emerges at $k = 1$, since $g^{(2)}(0) < 1$. PIT occurs at $k = 3$, since $g^{(4)}(0) > g^{(3)}(0) > g^{(2)}(0) > 1$ fulfills the conditions given in Eq. (S24) [see the inset in panel (a-i)]. These 1PB, 2PB, and PIT can also be recognized from (b) the photon-number distributions and (c) the deviations given in Eq. (S13). At $k = 1$, single-photon probability is enhanced as $P(1) > \mathcal{P}(1)$, while $m$-photon ($m > 1$) probabilities are suppressed as $P(m) < \mathcal{P}(m)$ [see panels (b-i) and (c-i)]. These photon-number distributions fulfill the conditions given in Eqs. (S11a) and (S11b) for $n = 1$, i.e., resulting in 1PB. At $k = 2$, only two-photon probability $P(2)$ is enhanced [see panels (b-i), (b-ii) and (c-ii)]. These photon-number distributions fulfill the conditions given in Eqs. (S11a) and (S11b) for $n = 2$, i.e., resulting in 2PB. At $k = 3$, single-photon probability is suppressed as $P(1) < \mathcal{P}(1)$, while $m$-photon ($m > 1$) probabilities are enhanced as $P(m) > \mathcal{P}(m)$ [see panels (b-i) and (c-ii)], i.e., resulting in PIT. Here, $P_{\rm in} = 0.3\,{\rm pW}$, and the other parameters are the same as those in Fig. S4.

In a sense, light with $g^{(3)}(0) \sim 1000$ has three-photon correlations 1000 stronger than those for coherent light. We note that the ratio of $g^{(3)}(0)/g^{(2)}(0)$ can be quite large. For example, $g^{(3)}(0)/g^{(2)}(0) \sim 100$ can be seen in Fig. S5(a). A similar prediction $g^{(3)}(0)/g^{(2)}(0) \sim 100$ has been reported in [S16]. This is possible since the mean photon number is $\langle \hat{n} \rangle \ll 1$. For example, if additionally $\langle \hat{a}^{\dagger 3}\hat{a}^3 \rangle \approx \langle \hat{a}^{\dagger 2}\hat{a}^2 \rangle$, then $g^{(3)}(0)/g^{(2)}(0) \approx 1/\langle \hat{n} \rangle \gg 1$.

## S3. ANALYTIC SOLUTION OF THE OPTICAL INTENSITY CORRELATION FUNCTIONS

### A. Second-order correlation function

According to the quantum trajectory method [S20], we introduce an anti-Hermitian term to the Hamiltonian in Eq. (S5) to describe the dissipation of the cavity photons. The effective non-Hermitian Hamiltonian is, thus, given by

$$\hat{H}_{\rm t} = \hbar(\Delta_L + \Delta_{\rm F})\hat{a}^\dagger\hat{a} + \hbar U\hat{a}^\dagger\hat{a}^\dagger\hat{a}\hat{a} + \hbar\xi(\hat{a}^\dagger + \hat{a}) - i\hbar\frac{\gamma}{2}\hat{a}^\dagger\hat{a}, \tag{S27}$$

where $\gamma$ is the rate of the cavity dissipation. Then the Hamiltonian (S27) can be expressed in a *spectral representation* as

$$\begin{aligned}
\hat{H}_{\rm t} &= \sum_{n=0}^{\infty}\left(E_n - i\hbar\frac{\gamma}{2}n\right)|n\rangle\langle n| + \hbar\xi\sum_{n=0}^{\infty}|n\rangle\langle n|(\hat{a}^\dagger + \hat{a})\sum_{n'=0}^{\infty}|n'\rangle\langle n'| \\
&= \sum_{n=0}^{\infty}\left(E_n - i\hbar\frac{\gamma}{2}n\right)|n\rangle\langle n| + \hbar\xi\sum_{n=0}^{\infty}\sum_{n'=0}^{\infty}|n\rangle(\langle n|\hat{a}^\dagger|n'\rangle + \langle n|\hat{a}|n'\rangle)\langle n'| \\
&= \sum_{n=0}^{\infty}\left(E_n - i\hbar\frac{\gamma}{2}n\right)|n\rangle\langle n| + \hbar\xi\sum_{n=0}^{\infty}\sum_{n'=0}^{\infty}|n\rangle(\sqrt{n'+1}\langle n|n'+1\rangle + \sqrt{n'}\langle n|n'-1\rangle)\langle n'| \\
&= \sum_{n=0}^{\infty}\left(E_n - i\hbar\frac{\gamma}{2}n\right)|n\rangle\langle n| + \hbar\xi\sum_{n=0}^{\infty}\sum_{n'=0}^{\infty}|n\rangle(\sqrt{n'+1}\delta_{n,n'+1} + \sqrt{n'}\delta_{n,n'-1})\langle n'| \\
&= \sum_{n=0}^{\infty}\left(E_n - i\hbar\frac{\gamma}{2}n\right)|n\rangle\langle n| + \hbar\xi\sum_{n=0}^{\infty}\sum_{n'=0}^{\infty}|n\rangle(\sqrt{n'+1}\delta_{n,n'+1} + \sqrt{n'}\delta_{n',n+1})\langle n'| \qquad \text{(i)} \\
&= \sum_{n=0}^{\infty}\left(E_n - i\hbar\frac{\gamma}{2}n\right)|n\rangle\langle n| + \hbar\xi\sum_{n'=0}^{\infty}\sqrt{n'+1}|n'+1\rangle\langle n'| + \hbar\xi\sum_{n=0}^{\infty}\sqrt{n+1}|n\rangle\langle n+1| \\
&= \sum_{n=0}^{\infty}\left(E_n - i\hbar\frac{\gamma}{2}n\right)|n\rangle\langle n| + \hbar\xi\sum_{n=0}^{\infty}\sqrt{n+1}|n+1\rangle\langle n| + \hbar\xi\sum_{n=0}^{\infty}\sqrt{n+1}|n\rangle\langle n+1|\,, \qquad \text{(ii)}
\end{aligned}$$

(i) To avoid negative $n$, we changed the subscript of the second $\delta$; Also, (ii) we substituted $n$ for $n'$, for convenience. Therefore, we obtain the Hamiltonian of the whole system as

$$\hat{H}_{\rm t} = \sum_{n=0}^{\infty}\left(E_n - i\hbar\frac{\gamma}{2}n\right)|n\rangle\langle n| + \hbar\xi\sum_{n=0}^{\infty}\sqrt{n+1}|n+1\rangle\langle n| + \hbar\xi\sum_{n=0}^{\infty}\sqrt{n+1}|n\rangle\langle n+1|\,, \tag{S28}$$

with eigenenergies

$$E_n = n\hbar\Delta_L + n\hbar\Delta_{\rm F} + (n^2 - n)\hbar U, \tag{S29}$$

where $\Delta_{\rm F} > 0$ ($\Delta_{\rm F} < 0$) denotes the light propagating against (along) the direction of the spinning resonator.

For the weak-driving case, we restrict to a subspace spanned by the basis states $\{|0\rangle, |1\rangle, |2\rangle\}$. Then, the Hamiltonian in Eq. (S28) becomes

$$\begin{aligned}
\hat{H}_{\rm t} = E_0|0\rangle\langle 0| &+ \left(E_1 - i\hbar\frac{\gamma}{2}\right)|1\rangle\langle 1| + (E_2 - i\hbar\gamma)|2\rangle\langle 2| \\
&+ \hbar\xi\sqrt{1}|1\rangle\langle 0| + \hbar\xi\sqrt{2}|2\rangle\langle 1| + \hbar\xi\sqrt{3}|3\rangle\langle 2| \\
&+ \hbar\xi\sqrt{1}|0\rangle\langle 1| + \hbar\xi\sqrt{2}|1\rangle\langle 2| + \hbar\xi\sqrt{3}|2\rangle\langle 3|\,.
\end{aligned}$$

Due to the limits of the basis states, the terms including $|3\rangle$ can be neglected. Then we have

$$\hat{H}_{\mathrm{t}} = E_0|0\rangle\langle 0| + \left(E_1 - i\hbar\frac{\gamma}{2}\right)|1\rangle\langle 1| + (E_2 - i\hbar\gamma)|2\rangle\langle 2| + \hbar\xi|1\rangle\langle 0| + \hbar\xi\sqrt{2}|2\rangle\langle 1| + \hbar\xi|0\rangle\langle 1| + \hbar\xi\sqrt{2}|1\rangle\langle 2|, \tag{S30}$$

where:

$$\begin{aligned} E_0 &= 0, \\ E_1 &= \hbar\Delta_L + \hbar\Delta_{\mathrm{F}}, \\ E_2 &= 2\hbar\Delta_L + 2\hbar\Delta_{\mathrm{F}} + 2\hbar U. \end{aligned} \tag{S31}$$

In this subspace, a general state can be written as

$$|\varphi(t)\rangle = \sum_{n=0}^{2} C_n(t)|n\rangle = C_0(t)|0\rangle + C_1(t)|1\rangle + C_2(t)|2\rangle. \tag{S32}$$

where $C_n$ are probability amplitudes. We substitute the Hamiltonian (S30) and the general state (S32) into the Schrödinger equation

$$i\hbar|\dot{\varphi}(t)\rangle = \hat{H}_{\mathrm{t}}|\varphi(t)\rangle. \tag{S33}$$

Then we have

$$i\hbar|\dot{\varphi}(t)\rangle = i\hbar\dot{C}_0(t)|0\rangle + i\hbar\dot{C}_1(t)|1\rangle + i\hbar\dot{C}_2(t)|2\rangle, \tag{S34}$$

and

$$\hat{H}_{\mathrm{t}}|\varphi(t)\rangle = \hat{H}_{\mathrm{t}}C_0(t)|0\rangle + \hat{H}_{\mathrm{t}}C_1(t)|1\rangle + \hat{H}_{\mathrm{t}}C_2(t)|2\rangle, \tag{S35}$$

where:

$$\hat{H}_{\mathrm{t}}C_0(t)|0\rangle = (E_0|0\rangle\langle 0| + \hbar\xi|1\rangle\langle 0|)C_0(t)|0\rangle = E_0C_0(t)|0\rangle + \hbar\xi C_0(t)|1\rangle,$$

$$\begin{aligned} \hat{H}_{\mathrm{t}}C_1(t)|1\rangle &= \left[\left(E_1 - i\hbar\frac{\gamma}{2}\right)|1\rangle\langle 1| + \hbar\xi\sqrt{2}|2\rangle\langle 1| + \hbar\xi|0\rangle\langle 1|\right]C_1(t)|1\rangle \\ &= \hbar\xi C_1(t)|0\rangle + \left(E_1 - i\hbar\frac{\gamma}{2}\right)C_1(t)|1\rangle + \hbar\xi\sqrt{2}C_1(t)|2\rangle, \end{aligned}$$

$$\hat{H}_{\mathrm{t}}C_2(t)|2\rangle = [(E_2 - i\hbar\gamma)|2\rangle\langle 2| + \hbar\xi\sqrt{2}|1\rangle\langle 2|]C_2(t)|2\rangle = \hbar\xi\sqrt{2}C_2(t)|1\rangle + (E_2 - i\hbar\gamma)C_2(t)|2\rangle,$$

i.e.,

$$\begin{aligned} \hat{H}_{\mathrm{t}}|\varphi(t)\rangle = {} & [E_0C_0(t) + \hbar\xi C_1(t)]|0\rangle + \left[\left(E_1 - i\hbar\frac{\gamma}{2}\right)C_1(t) + \hbar\xi C_0(t) + \hbar\xi\sqrt{2}C_2(t)\right]|1\rangle \\ & + [(E_2 - i\hbar\gamma)C_2(t) + \hbar\xi\sqrt{2}C_1(t)]|2\rangle. \end{aligned} \tag{S36}$$

By comparing the coefficients of the same basis states in Eqs. (S34) and (S36), we have:

$$\begin{aligned} i\hbar\dot{C}_0(t)|0\rangle &= [E_0C_0(t) + \hbar\xi C_1(t)]|0\rangle, \\ i\hbar\dot{C}_1(t)|1\rangle &= \left[\left(E_1 - i\hbar\frac{\gamma}{2}\right)C_1(t) + \hbar\xi C_0(t) + \hbar\xi\sqrt{2}C_2(t)\right]|1\rangle, \\ i\hbar\dot{C}_2(t)|2\rangle &= [(E_2 - i\hbar\gamma)C_2(t) + \hbar\xi\sqrt{2}C_1(t)]|2\rangle, \end{aligned}$$

with $\nu_n = E_n/\hbar$. Then we obtain the following equations of motion for the probability amplitudes $C_n(t)$:

$$\begin{aligned} \dot{C}_0(t) &= -i\nu_0C_0(t) - i\xi C_1(t), \\ \dot{C}_1(t) &= -i\left(\nu_1 - i\frac{\gamma}{2}\right)C_1(t) - i\xi C_0(t) - i\xi\sqrt{2}C_2(t), \\ \dot{C}_2(t) &= -i(\nu_2 - i\gamma)C_2(t) - i\xi\sqrt{2}C_1(t), \end{aligned} \tag{S37}$$

where $\nu_n = E_n/\hbar$.

Weak driving means the driving strength is smaller than the cavity damping rate $\xi < \gamma$. If there is no driving field, the cavity field remains in the vacuum. When a weak-driving field is applied to the cavity, it may excite a single photon or two photons in the cavity. Thus, we have the following approximate expressions: $C_0 \sim 1$, $C_1 \sim \xi/\gamma$, and $C_2 \sim \xi^2/\gamma^2$. Then we can approximately solve the equations in Eq. (S37) using a perturbation method by discarding higher-order terms in each equation for lower-order variables. Thus, the Eq. (S37) becomes:

$$\begin{aligned}
\dot{C}_0(t) &= -i\nu_0 C_0(t), \\
\dot{C}_1(t) &= -i\left(\nu_1 - i\frac{\gamma}{2}\right) C_1(t) - i\xi C_0(t), \\
\dot{C}_2(t) &= -i(\nu_2 - i\gamma) C_2(t) - i\xi\sqrt{2} C_1(t),
\end{aligned} \tag{S38}$$

where $\nu_n = E_n/\hbar$.

For the initially empty cavity, the initial conditions read as: $C_0(0) = C_0(0)$, and $C_1(0) = C_2(0) = 0$. Accordingly, the solution of the zero-photon amplitude can be obtained as

$$C_0(t) = C_0(0)\exp\left(-i\nu_0 t\right). \tag{S39}$$

Hence, the equation for the single-photon amplitude in Eq. (S38) becomes

$$\dot{C}_1(t) = -i\left(\nu_1 - i\frac{\gamma}{2}\right) C_1(t) - i\xi C_0(t)\exp\left(-i\nu_0 t\right). \tag{S40}$$

To solve this equation, we introduce a slowly-varying amplitude:

$$\begin{aligned}
C_1(t) &= c_1(t)\exp\left[-i\left(\nu_1 - i\frac{\gamma}{2}\right) t\right], \\
C_1(0) &= c_1(0).
\end{aligned} \tag{S41}$$

Then we obtain

$$\dot{C}_1(t) = \dot{c}_1(t)\exp\left[-i\left(\nu_1 - i\frac{\gamma}{2}\right) t\right] - i\left(\nu_1 - i\frac{\gamma}{2}\right) c_1(t)\exp\left[-i\left(\nu_1 - i\frac{\gamma}{2}\right) t\right], \tag{S42}$$

and Eq. (S40) becomes:

$$\begin{aligned}
\dot{c}_1(t)e^{-i\left(\nu_1 - i\frac{\gamma}{2}\right)t} - i\left(\nu_1 - i\frac{\gamma}{2}\right) c_1(t)e^{-i\left(\nu_1 - i\frac{\gamma}{2}\right)t} &= -i\left(\nu_1 - i\frac{\gamma}{2}\right) c_1(t)e^{-i\left(\nu_1 - i\frac{\gamma}{2}\right)t} - i\xi C_0(t)e^{-i\nu_0 t}, \\
\dot{c}_1(t) &= -i\xi C_0(t)\exp\left[i\left(\nu_1 - \nu_0 - i\frac{\gamma}{2}\right) t\right].
\end{aligned} \tag{S43}$$

The solution can be obtained by integrating both sides of Eq. (S43), as follows:

$$\begin{aligned}
c_1(t) - c_1(0) &= -i\xi C_0(t)\int_0^t \exp\left[i\left(\nu_1 - \nu_0 - i\frac{\gamma}{2}\right) t'\right]\, dt', \\
c_1(t) - c_1(0) &= -i\xi\frac{C_0(t)}{i\left(\nu_1 - \nu_0 - i\frac{\gamma}{2}\right)}\left\{\exp\left[i\left(\nu_1 - \nu_0 - i\frac{\gamma}{2}\right) t\right] - 1\right\}, \\
c_1(t)\exp\left[-i\left(\nu_1 - i\frac{\gamma}{2}\right) t\right] &= c_1(0)\exp\left[-i\left(\nu_1 - i\frac{\gamma}{2}\right) t\right] - i\xi\frac{C_0(t)}{i\left(\nu_1 - \nu_0 - i\frac{\gamma}{2}\right)}\left\{\exp\left(-i\nu_0 t\right) - \exp\left[-i\left(\nu_1 - i\frac{\gamma}{2}\right) t\right]\right\}, \\
C_1(t) &= C_1(0)\exp\left[-i\left(\nu_1 - i\frac{\gamma}{2}\right) t\right] - i\xi\frac{C_0(t)}{i\left(\nu_1 - \nu_0 - i\frac{\gamma}{2}\right)}\left\{\exp\left(-i\nu_0 t\right) - \exp\left[-i\left(\nu_1 - i\frac{\gamma}{2}\right) t\right]\right\}.
\end{aligned}$$

With the initial condition $C_1(0) = 0$, we have the solution for the single-photon amplitude given by

$$C_1(t) = -i\xi\frac{C_0(t)}{i\left(\nu_1 - \nu_0 - i\frac{\gamma}{2}\right)}\left\{\exp\left(-i\nu_0 t\right) - \exp\left[-i\left(\nu_1 - i\frac{\gamma}{2}\right) t\right]\right\}. \tag{S44}$$

Consider the solution of the single-photon amplitude in Eq. (S44), the equation for the two-photon amplitude in Eq. (S38) becomes

$$\dot{C}_2(t) = -i(\nu_2 - i\gamma) C_2(t) - \sqrt{2}\xi^2\frac{C_0(t)}{i\left(\nu_1 - \nu_0 - i\frac{\gamma}{2}\right)}\left\{\exp\left(-i\nu_0 t\right) - \exp\left[-i\left(\nu_1 - i\frac{\gamma}{2}\right) t\right]\right\}. \tag{S45}$$

To solve this equation, we introduce another slowly-varying amplitude:

$$\begin{aligned} C_2(t) &= c_2(t)\exp\left[-i(\nu_2 - i\gamma)t\right], \\ C_2(0) &= c_2(0), \end{aligned} \tag{S46}$$

and obtain

$$\dot{C}_2(t) = \dot{c}_2(t)\exp\left[-i(\nu_2 - i\gamma)t\right] - i(\nu_2 - i\gamma)c_2(t)\exp\left[-i(\nu_2 - i\gamma)t\right], \tag{S47}$$

then Eq. (S45) becomes:

$$\begin{aligned} &\dot{c}_2(t)e^{-i(\nu_2 - i\gamma)t} - i(\nu_2 - i\gamma)c_2(t)e^{-i(\nu_2 - i\gamma)t} = -i(\nu_2 - i\gamma)c_2(t)e^{-i(\nu_2 - i\gamma)t} - \sqrt{2}\xi^2 \frac{C_0(t)}{i\left(\nu_1 - \nu_0 - i\frac{\gamma}{2}\right)}\left[e^{-i\nu_0 t} - e^{-i\left(\nu_1 - i\frac{\gamma}{2}\right)t}\right], \\ &\dot{c}_2(t) = -\sqrt{2}\xi^2 \frac{C_0(t)}{i\left(\nu_1 - \nu_0 - i\frac{\gamma}{2}\right)}\left\{\exp\left[i(\nu_2 - \nu_0 - i\gamma)t\right] - \exp\left[i\left(\nu_2 - \nu_1 - i\frac{\gamma}{2}\right)t\right]\right\}. \end{aligned} \tag{S48}$$

The solution can also be obtained by integrating both sides of Eq. (S48), as follows:

$$\begin{aligned} c_2(t) - c_2(0) =& -\sqrt{2}\xi^2 \frac{C_0(t)}{i\left(\nu_1 - \nu_0 - i\frac{\gamma}{2}\right)} \int_0^t \left\{\exp[i(\nu_2 - \nu_0 - i\gamma)t'] - \exp\left[i\left(\nu_2 - \nu_1 - i\frac{\gamma}{2}\right)t'\right]\right\} dt', \\ c_2(t) - c_2(0) =& -\sqrt{2}\xi^2 \frac{C_0(t)}{i\left(\nu_1 - \nu_0 - i\frac{\gamma}{2}\right)} \left\{\frac{\exp\left[i(\nu_2 - \nu_0 - i\gamma)t\right] - 1}{i(\nu_2 - \nu_0 - i\gamma)} - \frac{\exp\left[i\left(\nu_2 - \nu_1 - i\frac{\gamma}{2}\right)t\right] - 1}{i\left(\nu_2 - \nu_1 - i\frac{\gamma}{2}\right)}\right\}, \\ c_2(t)\exp\left[-i(\nu_2 - i\gamma)t\right] =& c_2(0)\exp\left[-i(\nu_2 - i\gamma)t\right] - \sqrt{2}\xi^2 \frac{C_0(t)}{i\left(\nu_1 - \nu_0 - i\frac{\gamma}{2}\right)} \cdot \frac{\exp\left(-i\nu_0 t\right) - \exp\left[-i(\nu_2 - i\gamma)t\right]}{i(\nu_2 - \nu_0 - i\gamma)} \\ &+ \sqrt{2}\xi^2 \frac{C_0(t)}{i\left(\nu_1 - \nu_0 - i\frac{\gamma}{2}\right)} \cdot \frac{\exp\left[-i\left(\nu_1 - i\frac{\gamma}{2}\right)t\right] - \exp\left[-i(\nu_2 - i\gamma)t\right]}{i\left(\nu_2 - \nu_1 - i\frac{\gamma}{2}\right)}, \\ C_2(t) =& C_2(0)\exp\left[-i(\nu_2 - i\gamma)t\right] - \sqrt{2}\xi^2 \frac{C_0(t)}{i\left(\nu_1 - \nu_0 - i\frac{\gamma}{2}\right)} \cdot \frac{\exp\left(-i\nu_0 t\right) - \exp\left[-i(\nu_2 - i\gamma)t\right]}{i(\nu_2 - \nu_0 - i\gamma)} \\ &+ \sqrt{2}\xi^2 \frac{C_0(t)}{i\left(\nu_1 - \nu_0 - i\frac{\gamma}{2}\right)} \cdot \frac{\exp\left[-i\left(\nu_1 - i\frac{\gamma}{2}\right)t\right] - \exp\left[-i(\nu_2 - i\gamma)t\right]}{i\left(\nu_2 - \nu_1 - i\frac{\gamma}{2}\right)}. \end{aligned}$$

With the initial condition $C_2(0) = 0$, we have the following solution of the two-photon amplitude

$$C_2(t) = \sqrt{2}\xi^2 \frac{C_0(t)}{\left(\nu_1 - \nu_0 - i\frac{\gamma}{2}\right)} \left\{\frac{\exp\left(-i\nu_0 t\right) - \exp\left[-i(\nu_2 - i\gamma)t\right]}{(\nu_2 - \nu_0 - i\gamma)} - \frac{\exp\left[-i\left(\nu_1 - i\frac{\gamma}{2}\right)t\right] - \exp\left[-i(\nu_2 - i\gamma)t\right]}{\left(\nu_2 - \nu_1 - i\frac{\gamma}{2}\right)}\right\}. \tag{S49}$$

Thus, for the initially empty resonator, the solutions of the equations of motion for the probability amplitudes in the equations in Eq. (S38) can be obtained as:

$$\begin{aligned} C_0(t) &= C_0(0)\exp\left(-i\nu_0 t\right), \\ C_1(t) &= -\xi \frac{C_0(t)}{\left(\nu_1 - \nu_0 - i\frac{\gamma}{2}\right)} \left\{\exp\left(-i\nu_0 t\right) - \exp\left[-i\left(\nu_1 - i\frac{\gamma}{2}\right)t\right]\right\}, \\ C_2(t) &= \sqrt{2}\xi^2 \frac{C_0(t)}{\left(\nu_1 - \nu_0 - i\frac{\gamma}{2}\right)} \left\{\frac{\exp\left(-i\nu_0 t\right) - \exp\left[-i(\nu_2 - i\gamma)t\right]}{(\nu_2 - \nu_0 - i\gamma)} - \frac{\exp\left[-i\left(\nu_1 - i\frac{\gamma}{2}\right)t\right] - \exp\left[-i(\nu_2 - i\gamma)t\right]}{\left(\nu_2 - \nu_1 - i\frac{\gamma}{2}\right)}\right\}, \end{aligned} \tag{S50}$$

where

$$\nu_0 = 0, \quad \nu_1 = \Delta_L + \Delta_{\mathrm{F}}, \quad \nu_2 = 2\Delta_L + 2\Delta_{\mathrm{F}} + 2U.$$

When the initial state of the system is the vacuum state $|0\rangle$, i.e., the initial condition $C_0(0) = 1$, then the solutions

in Eq. (S50) are reduced to:

$$\begin{aligned}
C_0(t) =& 1, \\
C_1(t) =& -i\xi \frac{1}{i\left(\Delta_L+\Delta_{\mathrm{F}}-i\frac{\gamma}{2}\right)}\left\{1-\exp\left[-i\left(\Delta_L+\Delta_{\mathrm{F}}-i\frac{\gamma}{2}\right)t\right]\right\}, \\
C_2(t) =& \frac{\sqrt{2}\xi^2}{\left(\Delta_L+\Delta_{\mathrm{F}}-i\frac{\gamma}{2}\right)}\left\{\frac{1-\exp[-i(2\Delta_L+2\Delta_{\mathrm{F}}+2U-i\gamma)t]}{(2\Delta_L+2\Delta_{\mathrm{F}}+2U-i\gamma)}-\frac{\exp\left[-i\left(\Delta_L+\Delta_{\mathrm{F}}-i\frac{\gamma}{2}\right)t\right]}{\left(\Delta_L+\Delta_{\mathrm{F}}+2U-i\frac{\gamma}{2}\right)}\right\} \\
&+\sqrt{2}\xi^2\cdot\frac{-\exp[i(2\Delta_L+2\Delta_{\mathrm{F}}+2U-i\gamma)t]}{\left(\Delta_L+\Delta_{\mathrm{F}}-i\frac{\gamma}{2}\right)\left(\Delta_L+\Delta_{\mathrm{F}}+2U-i\frac{\gamma}{2}\right)},
\end{aligned} \tag{S51}$$

and for the infinite-time limit $\exp(-At)\to 0$ $(t\to\infty)$, we have:

$$\begin{aligned}
C_0(\infty)\equiv C_0 &= 1, \\
C_1(\infty)\equiv C_1 &= \frac{-\xi}{\left(\Delta_L+\Delta_{\mathrm{F}}-i\frac{\gamma}{2}\right)}, \\
C_2(\infty)\equiv C_2 &= \frac{-\sqrt{2}\xi C_1}{(2\Delta_L+2\Delta_{\mathrm{F}}+2U-i\gamma)}.
\end{aligned} \tag{S52}$$

For the state given in Eq. (S32), the infinite-time state (steady state) of the system reads as

$$|\varphi(t\to\infty)\rangle = |0\rangle+\frac{-\xi}{\left(\Delta_L+\Delta_{\mathrm{F}}-i\frac{\gamma}{2}\right)}|1\rangle+\frac{\sqrt{2}\xi^2}{\left(\Delta_L+\Delta_{\mathrm{F}}-i\frac{\gamma}{2}\right)(2\Delta_L+2\Delta_{\mathrm{F}}+2U-i\gamma)}|2\rangle, \tag{S53}$$

and the normalization coefficient of the state is given by

$$N = 1+|C_1|^2+|C_2|^2, \tag{S54}$$

where:

$$|C_1|^2 = \left|\frac{\xi}{\left(\Delta_L+\Delta_{\mathrm{F}}-i\frac{\gamma}{2}\right)}\right|^2 = \frac{\xi^2}{\left(\Delta_L+\Delta_{\mathrm{F}}-i\frac{\gamma}{2}\right)\left(\Delta_L+\Delta_{\mathrm{F}}+i\frac{\gamma}{2}\right)} = \frac{\xi^2}{\left[(\Delta_L+\Delta_{\mathrm{F}})^2+\frac{\gamma^2}{4}\right]}, \tag{S55}$$

$$\begin{aligned}
|C_2|^2 &= \left|\frac{\sqrt{2}\xi^2}{\left(\Delta_L+\Delta_{\mathrm{F}}-i\frac{\gamma}{2}\right)(2\Delta_L+2\Delta_{\mathrm{F}}+2U-i\gamma)}\right|^2 \\
&= \frac{2\xi^4}{\left(\Delta_L+\Delta_{\mathrm{F}}-i\frac{\gamma}{2}\right)\left(\Delta_L+\Delta_{\mathrm{F}}+i\frac{\gamma}{2}\right)(2\Delta_L+2\Delta_{\mathrm{F}}+2U-i\gamma)(2\Delta_L+2\Delta_{\mathrm{F}}+2U+i\gamma)} \\
&= \frac{2\xi^4}{\left[(\Delta_L+\Delta_{\mathrm{F}})^2+\frac{\gamma^2}{4}\right][4(\Delta_L+\Delta_{\mathrm{F}}+U)^2+\gamma^2]}.
\end{aligned} \tag{S56}$$

The probabilities of finding single and two photons in the cavity are, respectively, given by:

$$P_1 = \frac{|C_1|^2}{N}, \tag{S57}$$

$$P_2 = \frac{|C_2|^2}{N}. \tag{S58}$$

As mentioned in Sec. S2 B, the equal-time (namely zero-time-delay) second-order correlation function can be written as

$$g^{(2)}(0)\equiv\frac{\langle\hat{a}^{\dagger 2}\hat{a}^2\rangle}{\langle\hat{a}^\dagger\hat{a}\rangle^2} = \frac{\langle\hat{a}^\dagger\hat{a}\hat{a}^\dagger\hat{a}\rangle-\langle\hat{a}^\dagger\hat{a}\rangle}{\langle\hat{a}^\dagger\hat{a}\rangle^2}.$$

When the cavity field is in the state given in (S32), we have

$$\begin{aligned} g^{(2)}(0) &= \frac{\sum_{n,n'=0}^{2} C_n^* C_n \langle n|\,\hat{a}^\dagger\hat{a}\hat{a}^\dagger\hat{a}|n'\rangle - \sum_{n,n'=0}^{2} C_n^* C_n \langle n|\,\hat{a}^\dagger\hat{a}|n'\rangle}{(\sum_{n,n'=0}^{2} C_n^* C_n \langle n|\,\hat{a}^\dagger\hat{a}|n'\rangle)^2} \\ &= \frac{0+|C_1|^2+4\,|C_2|^2-(0+|C_1|^2+2\,|C_2|^2)}{(0+|C_1|^2+2\,|C_2|^2)^2} \\ &= \frac{N(P_1+4P_2-P_1-2P_2)}{N^2(P_1+2P_2)^2} \\ &= \frac{2P_2}{N(P_1+2P_2)^2}. \end{aligned}$$

In the weak-driving regime, we have the following approximate formulas: $C_0 \sim 1$, $C_1 \sim \xi/\gamma$, and $C_2 \sim \xi^2/\gamma^2$, i.e., $N \sim 1$ with $|C_2|^2 \ll |C_1|^2 \ll 1$. Hence, the second-order correlation function can be written as

$$g^{(2)}(0) \approx \frac{2P_2}{(P_1+2P_2)^2}. \tag{S59}$$

Because $P_1 \gg P_2$, we have

$$g^{(2)}(0) \approx \frac{2P_2}{P_1^2}. \tag{S60}$$

Substituting Eqs. (S57) and (S58) into Eq. (S60), we can easily obtain

$$\begin{aligned} g^{(2)}(0) &\approx \frac{4\xi^4}{\left[(\Delta_L+\Delta_\mathrm{F})^2+\frac{\gamma^2}{4}\right]\left[4(\Delta_L+\Delta_\mathrm{F}+U)^2+\gamma^2\right]} \cdot \frac{\left[(\Delta_L+\Delta_\mathrm{F})^2+\frac{\gamma^2}{4}\right]^2}{\xi^4} \\ &= \frac{(\Delta_L+\Delta_\mathrm{F})^2+\gamma^2/4}{(\Delta_L+\Delta_\mathrm{F}+U)^2+\gamma^2/4}, \end{aligned} \tag{S61}$$

where $\Delta_\mathrm{F} > 0$ ($\Delta_\mathrm{F} < 0$) denotes the light propagating against (along) the direction of the spinning resonator.

Here, we focus on the non-spinning case ($\Delta_\mathrm{F} = 0$), the rotating case is discussed in Sec. S4. Then, the second-order correlation function becomes

$$g_0^{(2)}(0) = \frac{\Delta_L^2+\gamma^2/4}{(\Delta_L+U)^2+\gamma^2/4}. \tag{S62}$$

When the driving laser tuned to a single-photon resonance, $\Delta_L = 0$ ($k = 1$), the minimum of $g_0^{(2)}(0)$ is $g_{0\mathrm{min}}^{(2)} = (\gamma^2/4)/(U^2+\gamma^2/4) = [4(U/\gamma)^2+1]^{-1}$. We have $g_{0\mathrm{min}}^{(2)} < 1$, when $U \neq 0$. The larger $U/\gamma$, the smaller is the correlation function $g_{0\mathrm{min}}^{(2)}$. This indicates that 1PB can be achieved. On the other hand, for the driving laser tuning to the two-photon resonance, $\Delta_L = -U$ ($k = 2$), there is $g_{0\mathrm{max}}^{(2)} = (U^2+\gamma^2/4)/(\gamma^2/4) = 4(U/\gamma)^2+1$. We have $g_{0\mathrm{max}}^{(2)} > 1$ when $U \neq 0$. The larger $U/\gamma$, the larger is the correlation function $g_{0\mathrm{max}}^{(2)}$, which indicates a strong photon-induced tunneling caused by two-photon resonance. In Sec. S3 B, we find that this conclusion is completely confirmed by our numerical results.

### B. Third-order correlation function

Using a method similar to that in Sec. S3 A, we calculate the third-order photon-number correlation function. For the weak-driving case, we restrict to a subspace spanned by the basis states $\{|0\rangle, |1\rangle, |2\rangle, |3\rangle\}$. Then, the Hamiltonian in Eq. (S28) becomes

$$\begin{aligned} \hat{H}_\mathrm{t} = {} & E_0|0\rangle\langle 0| + \left(E_1 - i\hbar\frac{\gamma}{2}\right)|1\rangle\langle 1| + (E_2 - i\hbar\gamma)|2\rangle\langle 2| + \left(E_3 - i\hbar\frac{3\gamma}{2}\right)|3\rangle\langle 3| \\ & + \hbar\xi\sqrt{1}|1\rangle\langle 0| + \hbar\xi\sqrt{2}|2\rangle\langle 1| + \hbar\xi\sqrt{3}|3\rangle\langle 2| + \hbar\xi\sqrt{4}|4\rangle\langle 3| \\ & + \hbar\xi\sqrt{1}|0\rangle\langle 1| + \hbar\xi\sqrt{2}|1\rangle\langle 2| + \hbar\xi\sqrt{3}|2\rangle\langle 3| + \hbar\xi\sqrt{4}|3\rangle\langle 4|\,. \end{aligned}$$

Due to the limits of the basis states, the terms including $|4\rangle$ can be neglected. Then we have

$$\begin{aligned}\hat{H}_{\mathrm{t}} = E_0|0\rangle\langle 0| + \left(E_1 - i\hbar\frac{\gamma}{2}\right)|1\rangle\langle 1| + (E_2 - i\hbar\gamma)|2\rangle\langle 2| + \left(E_3 - i\hbar\frac{3\gamma}{2}\right)|3\rangle\langle 3| \\ + +\hbar\xi|1\rangle\langle 0| + \hbar\xi\sqrt{2}|2\rangle\langle 1| + \hbar\xi\sqrt{3}|3\rangle\langle 2| + \hbar\xi|0\rangle\langle 1| + \hbar\xi\sqrt{2}|1\rangle\langle 2| + \hbar\xi\sqrt{3}|2\rangle\langle 3|\,,\end{aligned} \tag{S63}$$

where:

$$\begin{aligned}E_0 &= 0,\\ E_1 &= \hbar\Delta_L + \hbar\Delta_{\mathrm{F}},\\ E_2 &= 2\hbar\Delta_L + 2\hbar\Delta_{\mathrm{F}} + 2\hbar U,\\ E_3 &= 3\hbar\Delta_L + 3\hbar\Delta_{\mathrm{F}} + 6\hbar U.\end{aligned} \tag{S64}$$

In this subspace, a general state can be written as

$$|\varphi(t)\rangle = \sum_{n=0}^{3} C_n(t)|n\rangle = C_0(t)|0\rangle + C_1(t)|1\rangle + C_2(t)|2\rangle + C_3(t)|3\rangle. \tag{S65}$$

where $C_n$ are probability amplitudes. We substitute Hamiltonian (S63) and the general state (S65) into the Schrödinger equation (S33) to obtain

$$i\hbar|\dot{\varphi}(t)\rangle = i\hbar\dot{C}_0(t)|0\rangle + i\hbar\dot{C}_1(t)|1\rangle + i\hbar\dot{C}_2(t)|2\rangle + i\hbar\dot{C}_3(t)|3\rangle; \tag{S66}$$

and

$$\hat{H}_{\mathrm{t}}|\varphi(t)\rangle = \hat{H}_{\mathrm{t}}C_0(t)|0\rangle + \hat{H}_{\mathrm{t}}C_1(t)|1\rangle + \hat{H}_{\mathrm{t}}C_2(t)|2\rangle + \hat{H}_{\mathrm{t}}C_3(t)|3\rangle, \tag{S67}$$

where:

$$\hat{H}_{\mathrm{t}}C_0(t)|0\rangle = [E_0|0\rangle\langle 0| + \hbar\xi|1\rangle\langle 0|]C_0(t)|0\rangle = E_0C_0(t)|0\rangle + \hbar\xi C_0(t)|1\rangle,$$

$$\begin{aligned}\hat{H}_{\mathrm{t}}C_1(t)|1\rangle &= \left[\left(E_1 - i\hbar\frac{\gamma}{2}\right)|1\rangle\langle 1| + \hbar\xi\sqrt{2}|2\rangle\langle 1| + \hbar\xi|0\rangle\langle 1|\right]C_1(t)|1\rangle\\ &= \hbar\xi C_1(t)|0\rangle + \left(E_1 - i\hbar\frac{\gamma}{2}\right)C_1(t)|1\rangle + \hbar\xi\sqrt{2}C_1(t)|2\rangle,\end{aligned}$$

$$\begin{aligned}\hat{H}_{\mathrm{t}}C_2(t)|2\rangle &= [(E_2 - i\hbar\gamma)|2\rangle\langle 2| + \hbar\xi\sqrt{2}|1\rangle\langle 2| + \hbar\xi\sqrt{3}|3\rangle\langle 2|]C_2(t)|2\rangle\\ &= \hbar\xi\sqrt{2}C_2(t)|1\rangle + (E_2 - i\hbar\gamma)C_2(t)|2\rangle + \hbar\xi\sqrt{3}C_2(t)|3\rangle,\end{aligned}$$

$$\hat{H}_{\mathrm{t}}C_3(t)|0\rangle = \left[\left(E_3 - i\hbar\frac{3\gamma}{2}\right)|3\rangle\langle 3| + \hbar\xi\sqrt{3}|2\rangle\langle 3|\right]C_3(t)|3\rangle = \hbar\xi\sqrt{3}C_3(t)|2\rangle + \left(E_3 - i\hbar\frac{3\gamma}{2}\right)C_3(t)|3\rangle,$$

i.e.,

$$\begin{aligned}\hat{H}_{\mathrm{t}}|\varphi(t)\rangle = [E_0C_0(t) + \hbar\xi C_1(t)]|0\rangle + \left[\hbar\xi C_0(t) + \left(E_1 - i\hbar\frac{\gamma}{2}\right)C_1(t) + \hbar\xi\sqrt{2}C_2(t)\right]|1\rangle \\ + [\hbar\xi\sqrt{2}C_1(t) + (E_2 - i\hbar\gamma)C_2(t) + \hbar\xi\sqrt{3}C_3(t)]|2\rangle + \left[\hbar\xi\sqrt{3}C_2(t) + \left(E_3 - i\hbar\frac{3\gamma}{2}\right)C_3(t)\right]|3\rangle.\end{aligned} \tag{S68}$$

By comparing the coefficients of the same basis states in Eqs. (S66) and (S68), we have:

$$\begin{aligned}i\hbar\dot{C}_0(t)|0\rangle &= [E_0C_0(t) + \hbar\xi C_1(t)]|0\rangle,\\ i\hbar\dot{C}_1(t)|1\rangle &= \left[\hbar\xi C_0(t) + \left(E_1 - i\hbar\frac{\gamma}{2}\right)C_1(t) + \hbar\xi\sqrt{2}C_2(t)\right]|1\rangle,\\ i\hbar\dot{C}_2(t)|2\rangle &= [\hbar\xi\sqrt{2}C_1(t) + (E_2 - i\hbar\gamma)C_2(t) + \hbar\xi\sqrt{3}C_3(t)]|2\rangle,\\ i\hbar\dot{C}_3(t)|3\rangle &= \left[\hbar\xi\sqrt{3}C_2(t) + \left(E_3 - i\hbar\frac{3\gamma}{2}\right)C_3(t)\right]|3\rangle,\end{aligned}$$

with $\nu_n = E_n/\hbar$. Then we obtain the following equations of motion for the probability amplitudes $C_n(t)$:

$$\begin{aligned}
\dot{C}_0(t) &= -i\nu_0 C_0(t) - i\xi C_1(t),\\
\dot{C}_1(t) &= -i\xi C_0(t) - i\left(\nu_1 - i\frac{\gamma}{2}\right) C_1(t) - i\xi\sqrt{2} C_2(t),\\
\dot{C}_2(t) &= -i\xi\sqrt{2} C_1(t) - i(\nu_2 - i\gamma) C_2(t) - i\xi\sqrt{3} C_3(t),\\
\dot{C}_3(t) &= -i\xi\sqrt{3} C_2(t) - i\left(\nu_3 - i\frac{3\gamma}{2}\right) C_3(t),
\end{aligned} \tag{S69}$$

where $\nu_n = E_n/\hbar$.

Similarly, due to the weak-driving case, we have the following approximate formulas: $C_0 \sim 1$, $C_1 \sim \xi/\gamma$, $C_2 \sim \xi^2/\gamma^2$, and $C_3 \sim \xi^3/\gamma^3$. Then we can approximately solve the equations in Eq. (S69) using a perturbation method by discarding higher-order terms in each equation for lower-order variables. Thus, the Eq. (S69) becomes:

$$\begin{aligned}
\dot{C}_0(t) &= -i\nu_0 C_0(t),\\
\dot{C}_1(t) &= -i\left(\nu_1 - i\frac{\gamma}{2}\right) C_1(t) - i\xi C_0(t),\\
\dot{C}_2(t) &= -i(\nu_2 - i\gamma) C_2(t) - i\xi\sqrt{2} C_1(t),\\
\dot{C}_3(t) &= -i\left(\nu_3 - i\frac{3\gamma}{2}\right) C_3(t) - i\xi\sqrt{3} C_2(t),
\end{aligned} \tag{S70}$$

where $\nu_n = E_n/\hbar$.

For an initially empty cavity, the initial conditions read as: $C_0(0) = C_0(0)$, and $C_1(0) = C_2(0) = C_3(0) = 0$. Then, the solution of the zero-photon amplitude can be obtained as

$$C_0(t) = C_0(0)\exp\left(-i\nu_0 t\right). \tag{S71}$$

Hence, the equation for the single-photon amplitude in Eq. (S70) becomes

$$\dot{C}_1(t) = -i\left(\nu_1 - i\frac{\gamma}{2}\right) C_1(t) - i\xi C_0(0)\exp\left(-i\nu_0 t\right). \tag{S72}$$

To solve this equation, we introduce a slowly-varying amplitude:

$$\begin{aligned}
C_1(t) &= c_1(t)\exp\left[-i\left(\nu_1 - i\frac{\gamma}{2}\right) t\right],\\
C_1(0) &= c_1(0),
\end{aligned} \tag{S73}$$

then we obtain

$$\dot{C}_1(t) = \dot{c}_1(t)\exp\left[-i\left(\nu_1 - i\frac{\gamma}{2}\right) t\right] - i\left(\nu_1 - i\frac{\gamma}{2}\right) c_1(t)\exp\left[-i\left(\nu_1 - i\frac{\gamma}{2}\right) t\right], \tag{S74}$$

and Eq. (S72) becomes:

$$\begin{aligned}
\dot{c}_1(t)e^{-i\left(\nu_1 - i\frac{\gamma}{2}\right)t} - i\left(\nu_1 - i\frac{\gamma}{2}\right) c_1(t)e^{-i\left(\nu_1 - i\frac{\gamma}{2}\right)t} &= -i\left(\nu_1 - i\frac{\gamma}{2}\right) c_1(t)e^{-i\left(\nu_1 - i\frac{\gamma}{2}\right)t} - i\xi C_0(0)e^{-i\nu_0 t},\\
\dot{c}_1(t) &= -i\xi C_0(0)\exp\left[i\left(\nu_1 - \nu_0 - i\frac{\gamma}{2}\right) t\right].
\end{aligned} \tag{S75}$$

The solution can be obtained by integrating both sides of Eq. (S75), as follows:

$$\begin{aligned}
c_1(t) - c_1(0) &= -i\xi C_0(0)\int_0^t \exp\left[i\left(\nu_1 - \nu_0 - i\frac{\gamma}{2}\right) t'\right]\, dt',\\
c_1(t) - c_1(0) &= -i\xi\frac{C_0(0)}{i\left(\nu_1 - \nu_0 - i\frac{\gamma}{2}\right)}\left\{\exp\left[i\left(\nu_1 - \nu_0 - i\frac{\gamma}{2}\right) t\right] - 1\right\},\\
c_1(t)\exp\left[-i\left(\nu_1 - i\frac{\gamma}{2}\right) t\right] &= c_1(0)\exp\left[-i\left(\nu_1 - i\frac{\gamma}{2}\right) t\right] - i\xi\frac{C_0(0)}{i\left(\nu_1 - \nu_0 - i\frac{\gamma}{2}\right)}\left\{\exp\left(-i\nu_0 t\right) - \exp\left[-i\left(\nu_1 - i\frac{\gamma}{2}\right) t\right]\right\},\\
C_1(t) &= C_1(0)\exp\left[-i\left(\nu_1 - i\frac{\gamma}{2}\right) t\right] - i\xi\frac{C_0(0)}{i\left(\nu_1 - \nu_0 - i\frac{\gamma}{2}\right)}\left\{\exp\left(-i\nu_0 t\right) - \exp\left[-i\left(\nu_1 - i\frac{\gamma}{2}\right) t\right]\right\}.
\end{aligned}$$

With the initial condition $C_1(0) = 0$, we have the solution for the single-photon amplitude given by

$$C_1(t) = -i\xi \frac{C_0(0)}{i\left(\nu_1 - \nu_0 - i\frac{\gamma}{2}\right)} \left\{ \exp\left(-i\nu_0 t\right) - \exp\left[-i\left(\nu_1 - i\frac{\gamma}{2}\right)t\right] \right\}. \tag{S76}$$

Consider the solution of the single-photon amplitude in Eq. (S76), the equation for the two-photon amplitude in Eq. (S70) becomes

$$\dot{C}_2(t) = -i(\nu_2 - i\gamma)C_2(t) - \sqrt{2}\xi^2 \frac{C_0(0)}{i\left(\nu_1 - \nu_0 - i\frac{\gamma}{2}\right)} \left\{ \exp\left(-i\nu_0 t\right) - \exp\left[-i\left(\nu_1 - i\frac{\gamma}{2}\right)t\right] \right\}. \tag{S77}$$

To solve this equation, we introduce another slowly-varying amplitude:

$$\begin{aligned} C_2(t) &= c_2(t)\exp\left[-i(\nu_2 - i\gamma)t\right], \\ C_2(0) &= c_2(0), \end{aligned} \tag{S78}$$

and obtain

$$\dot{C}_2(t) = \dot{c}_2(t)\exp\left[-i(\nu_2 - i\gamma)t\right] - i(\nu_2 - i\gamma)c_2(t)\exp\left[-i(\nu_2 - i\gamma)t\right], \tag{S79}$$

then Eq. (S77) becomes:

$$\begin{aligned} &\dot{c}_2(t)e^{-i(\nu_2 - i\gamma)t} - i(\nu_2 - i\gamma)c_2(t)e^{-i(\nu_2 - i\gamma)t} = -i(\nu_2 - i\gamma)c_2(t)e^{-i(\nu_2 - i\gamma)t} - \sqrt{2}\xi^2 \frac{C_0(0)}{i\left(\nu_1 - \nu_0 - i\frac{\gamma}{2}\right)} \left[ e^{-i\nu_0 t} - e^{-i\left(\nu_1 - i\frac{\gamma}{2}\right)t} \right], \\ &\dot{c}_2(t) = -\sqrt{2}\xi^2 \frac{C_0(0)}{i\left(\nu_1 - \nu_0 - i\frac{\gamma}{2}\right)} \left\{ \exp\left[i(\nu_2 - \nu_0 - i\gamma)t\right] - \exp\left[i\left(\nu_2 - \nu_1 - i\frac{\gamma}{2}\right)t\right] \right\}. \end{aligned} \tag{S80}$$

The solution can also be obtained by integrating both sides of Eq. (S80), as follows:

$$\begin{aligned} c_2(t) - c_2(0) =& -\sqrt{2}\xi^2 \frac{C_0(0)}{i\left(\nu_1 - \nu_0 - i\frac{\gamma}{2}\right)} \int_0^t \left\{ \exp[i(\nu_2 - \nu_0 - i\gamma)t'] - \exp\left[i\left(\nu_2 - \nu_1 - i\frac{\gamma}{2}\right)t'\right] \right\} dt', \\ c_2(t) - c_2(0) =& -\sqrt{2}\xi^2 \frac{C_0(0)}{i\left(\nu_1 - \nu_0 - i\frac{\gamma}{2}\right)} \left\{ \frac{\exp\left[i(\nu_2 - \nu_0 - i\gamma)t\right] - 1}{i(\nu_2 - \nu_0 - i\gamma)} - \frac{\exp\left[i\left(\nu_2 - \nu_1 - i\frac{\gamma}{2}\right)t\right] - 1}{i\left(\nu_2 - \nu_1 - i\frac{\gamma}{2}\right)} \right\}, \\ c_2(t)\exp\left[-i(\nu_2 - i\gamma)t\right] =& c_2(0)\exp\left[-i(\nu_2 - i\gamma)t\right] - \sqrt{2}\xi^2 \frac{C_0(0)}{i\left(\nu_1 - \nu_0 - i\frac{\gamma}{2}\right)} \cdot \frac{\exp\left(-i\nu_0 t\right) - \exp\left[-i(\nu_2 - i\gamma)t\right]}{i(\nu_2 - \nu_0 - i\gamma)} \\ &+ \sqrt{2}\xi^2 \frac{C_0(0)}{i\left(\nu_1 - \nu_0 - i\frac{\gamma}{2}\right)} \cdot \frac{\exp\left[-i\left(\nu_1 - i\frac{\gamma}{2}\right)t\right] - \exp\left[-i(\nu_2 - i\gamma)t\right]}{i\left(\nu_2 - \nu_1 - i\frac{\gamma}{2}\right)}, \\ C_2(t) =& C_2(0)\exp\left[-i(\nu_2 - i\gamma)t\right] - \sqrt{2}\xi^2 \frac{C_0(0)}{i\left(\nu_1 - \nu_0 - i\frac{\gamma}{2}\right)} \cdot \frac{\exp\left(-i\nu_0 t\right) - \exp\left[-i(\nu_2 - i\gamma)t\right]}{i(\nu_2 - \nu_0 - i\gamma)} \\ &+ \sqrt{2}\xi^2 \frac{C_0(0)}{i\left(\nu_1 - \nu_0 - i\frac{\gamma}{2}\right)} \cdot \frac{\exp\left[-i\left(\nu_1 - i\frac{\gamma}{2}\right)t\right] - \exp\left[-i(\nu_2 - i\gamma)t\right]}{i\left(\nu_2 - \nu_1 - i\frac{\gamma}{2}\right)}. \end{aligned}$$

With the initial condition $C_2(0) = 0$, we have the following solution of the two-photon amplitude

$$C_2(t) = \sqrt{2}\xi^2 \frac{C_0(0)}{\left(\nu_1 - \nu_0 - i\frac{\gamma}{2}\right)} \left\{ \frac{\exp\left(-i\nu_0 t\right) - \exp\left[-i(\nu_2 - i\gamma)t\right]}{(\nu_2 - \nu_0 - i\gamma)} - \frac{\exp\left[-i\left(\nu_1 - i\frac{\gamma}{2}\right)t\right] - \exp\left[-i(\nu_2 - i\gamma)t\right]}{\left(\nu_2 - \nu_1 - i\frac{\gamma}{2}\right)} \right\}. \tag{S81}$$

Consider the solution of the two-photon amplitude in Eq. (S81), the equation for the three-photon amplitude in Eq. (S70) becomes

$$\begin{aligned} \dot{C}_3(t) =& -i\left(\nu_3 - i\frac{3\gamma}{2}\right)C_3(t) + \sqrt{6}\xi^3 C_0(0) \frac{\exp\left(-i\nu_0 t\right) - \exp\left[-i(\nu_2 - i\gamma)t\right]}{i\left(\nu_1 - \nu_0 - i\frac{\gamma}{2}\right)(\nu_2 - \nu_0 - i\gamma)} \\ &- \sqrt{6}\xi^3 C_0(0) \frac{\exp\left[-i\left(\nu_1 - i\frac{\gamma}{2}\right)t\right] - \exp\left[-i(\nu_2 - i\gamma)t\right]}{i\left(\nu_1 - \nu_0 - i\frac{\gamma}{2}\right)\left(\nu_2 - \nu_1 - i\frac{\gamma}{2}\right)}. \end{aligned} \tag{S82}$$

To solve this equation, we introduce the slowly-varying amplitude:

$$C_3(t) = c_3(t)\exp\left[-i\left(\nu_3 - i\frac{3\gamma}{2}\right)t\right],$$
$$C_3(0) = c_3(0), \tag{S83}$$

and obtain

$$\dot{C}_3(t) = \dot{c}_3(t)\exp\left[-i\left(\nu_3 - i\frac{3\gamma}{2}\right)t\right] - i\left(\nu_3 - i\frac{3\gamma}{2}\right)c_3(t)\exp\left[-i\left(\nu_3 - i\frac{3\gamma}{2}\right)t\right], \tag{S84}$$

then Eq. (S82) becomes:

$$\begin{aligned}\dot{c}_3(t)e^{-i\left(\nu_3 - i\frac{3\gamma}{2}\right)t} - i\left(\nu_3 - i\frac{3\gamma}{2}\right)c_3(t)e^{-i\left(\nu_3 - i\frac{3\gamma}{2}\right)t} =& -i\left(\nu_3 - i\frac{3\gamma}{2}\right)C_3(t) + \sqrt{6}\xi^3 C_0(0)\frac{e^{-i\nu_0 t} - e^{-i(\nu_2 - i\gamma)t}}{i\left(\nu_1 - \nu_0 - i\frac{\gamma}{2}\right)(\nu_2 - \nu_0 - i\gamma)} \\ &- \sqrt{6}\xi^3 C_0(0)\frac{e^{-i\left(\nu_1 - i\frac{\gamma}{2}\right)t} - e^{-i(\nu_2 - i\gamma)t}}{i\left(\nu_1 - \nu_0 - i\frac{\gamma}{2}\right)\left(\nu_2 - \nu_1 - i\frac{\gamma}{2}\right)},\end{aligned}$$

$$\begin{aligned}\dot{c}_3(t) =& \sqrt{6}\xi^3 C_0(0)\frac{\exp\left[i(\nu_3 - \nu_0 - i\frac{3\gamma}{2})t\right] - \exp\left[i(\nu_3 - \nu_2 - i\frac{\gamma}{2})t\right]}{i\left(\nu_1 - \nu_0 - i\frac{\gamma}{2}\right)(\nu_2 - \nu_0 - i\gamma)} \\ &- \sqrt{6}\xi^3 C_0(0)\frac{\exp[i(\nu_3 - \nu_1 - i\gamma)t] - \exp\left[-i(\nu_3 - \nu_2 - i\frac{\gamma}{2})t\right]}{i\left(\nu_1 - \nu_0 - i\frac{\gamma}{2}\right)\left(\nu_2 - \nu_1 - i\frac{\gamma}{2}\right)}.\end{aligned} \tag{S85}$$

The solution can also be obtained by integrating both sides of Eq. (S85), as follows:

$$\begin{aligned}c_3(t) - c_3(0) =& \sqrt{6}\xi^3\frac{C_0(0)}{i\left(\nu_1 - \nu_0 - i\frac{\gamma}{2}\right)(\nu_2 - \nu_0 - i\gamma)}\int_0^t\left\{\exp\left[i(\nu_3 - \nu_0 - i\frac{3\gamma}{2})t'\right] - \exp\left[i(\nu_3 - \nu_2 - i\frac{\gamma}{2})t'\right]\right\}dt' \\ &- \sqrt{6}\xi^3\frac{C_0(0)}{i\left(\nu_1 - \nu_0 - i\frac{\gamma}{2}\right)\left(\nu_2 - \nu_1 - i\frac{\gamma}{2}\right)}\int_0^t\left\{\exp[i(\nu_3 - \nu_1 - i\gamma)t'] - \exp\left[-i(\nu_3 - \nu_2 - i\frac{\gamma}{2})t'\right]\right\}dt' \\ =& \sqrt{6}\xi^3\frac{C_0(0)}{i\left(\nu_1 - \nu_0 - i\frac{\gamma}{2}\right)(\nu_2 - \nu_0 - i\gamma)}\left\{\frac{\exp\left[i(\nu_3 - \nu_0 - i\frac{3\gamma}{2})t\right] - 1}{i(\nu_3 - \nu_0 - i\frac{3\gamma}{2})} - \frac{\exp\left[i(\nu_3 - \nu_2 - i\frac{\gamma}{2})t\right] - 1}{i(\nu_3 - \nu_2 - i\frac{\gamma}{2})}\right\} \\ &- \sqrt{6}\xi^3\frac{C_0(0)}{i\left(\nu_1 - \nu_0 - i\frac{\gamma}{2}\right)\left(\nu_2 - \nu_1 - i\frac{\gamma}{2}\right)}\left\{\frac{\exp[i(\nu_3 - \nu_1 - i\gamma)t] - 1}{i(\nu_3 - \nu_1 - i\gamma)} - \frac{\exp\left[i(\nu_3 - \nu_2 - i\frac{\gamma}{2})t\right] - 1}{i(\nu_3 - \nu_2 - i\frac{\gamma}{2})}\right\},\end{aligned}$$

$$\begin{aligned}c_3(t)\exp\left[-i\left(\nu_3 - i\frac{3\gamma}{2}\right)t\right] =& c_3(0)\exp\left[-i\left(\nu_3 - i\frac{3\gamma}{2}\right)t\right] - \sqrt{6}\xi^3\frac{C_0(0)\left\{\exp\left(-i\nu_0 t\right) - \exp\left[-i\left(\nu_3 - i\frac{3\gamma}{2}\right)t\right]\right\}}{\left(\nu_1 - \nu_0 - i\frac{\gamma}{2}\right)(\nu_2 - \nu_0 - i\gamma)(\nu_3 - \nu_0 - i\frac{3\gamma}{2})} \\ &+ \sqrt{6}\xi^3\frac{C_0(0)\left\{\exp\left[-i(\nu_2 - i\gamma)t\right] - \exp\left[-i\left(\nu_3 - i\frac{3\gamma}{2}\right)t\right]\right\}}{\left(\nu_1 - \nu_0 - i\frac{\gamma}{2}\right)(\nu_2 - \nu_0 - i\gamma)(\nu_3 - \nu_2 - i\frac{\gamma}{2})} \\ &+ \sqrt{6}\xi^3\frac{C_0(0)\left\{\exp\left[-i\left(\nu_1 - i\frac{\gamma}{2}\right)t\right] - \exp\left[-i\left(\nu_3 - i\frac{3\gamma}{2}\right)t\right]\right\}}{\left(\nu_1 - \nu_0 - i\frac{\gamma}{2}\right)\left(\nu_2 - \nu_1 - i\frac{\gamma}{2}\right)(\nu_3 - \nu_1 - i\gamma)} \\ &- \sqrt{6}\xi^3\frac{C_0(0)\left\{\exp\left[-i(\nu_2 - i\gamma)t\right] - \exp\left[-i\left(\nu_3 - i\frac{3\gamma}{2}\right)t\right]\right\}}{\left(\nu_1 - \nu_0 - i\frac{\gamma}{2}\right)\left(\nu_2 - \nu_1 - i\frac{\gamma}{2}\right)(\nu_3 - \nu_2 - i\frac{\gamma}{2})},\end{aligned}$$

$$\begin{aligned}C_3(t) =& C_3(0)\exp\left[-i\left(\nu_3 - i\frac{3\gamma}{2}\right)t\right] - \sqrt{6}\xi^3\frac{C_0(0)\left\{\exp\left(-i\nu_0 t\right) - \exp\left[-i\left(\nu_3 - i\frac{3\gamma}{2}\right)t\right]\right\}}{\left(\nu_1 - \nu_0 - i\frac{\gamma}{2}\right)(\nu_2 - \nu_0 - i\gamma)(\nu_3 - \nu_0 - i\frac{3\gamma}{2})} \\ &+ \sqrt{6}\xi^3\frac{C_0(0)\left\{\exp\left[-i(\nu_2 - i\gamma)t\right] - \exp\left[-i\left(\nu_3 - i\frac{3\gamma}{2}\right)t\right]\right\}}{\left(\nu_1 - \nu_0 - i\frac{\gamma}{2}\right)(\nu_2 - \nu_0 - i\gamma)(\nu_3 - \nu_2 - i\frac{\gamma}{2})} \\ &+ \sqrt{6}\xi^3\frac{C_0(0)\left\{\exp\left[-i\left(\nu_1 - i\frac{\gamma}{2}\right)t\right] - \exp\left[-i\left(\nu_3 - i\frac{3\gamma}{2}\right)t\right]\right\}}{\left(\nu_1 - \nu_0 - i\frac{\gamma}{2}\right)\left(\nu_2 - \nu_1 - i\frac{\gamma}{2}\right)(\nu_3 - \nu_1 - i\gamma)} \\ &- \sqrt{6}\xi^3\frac{C_0(0)\left\{\exp\left[-i(\nu_2 - i\gamma)t\right] - \exp\left[-i\left(\nu_3 - i\frac{3\gamma}{2}\right)t\right]\right\}}{\left(\nu_1 - \nu_0 - i\frac{\gamma}{2}\right)\left(\nu_2 - \nu_1 - i\frac{\gamma}{2}\right)(\nu_3 - \nu_2 - i\frac{\gamma}{2})}.\end{aligned}$$

With the initial condition $C_3(0)=0$, we have the following solution of the three-photon amplitude

$$\begin{aligned}
C_3(t) = &-\sqrt{6}\xi^3 \frac{C_0(0)\left\{\exp\left(-i\nu_0 t\right)-\exp\left[-i\left(\nu_3-i\frac{3\gamma}{2}\right)t\right]\right\}}{\left(\nu_1-\nu_0-i\frac{\gamma}{2}\right)\left(\nu_2-\nu_0-i\gamma\right)\left(\nu_3-\nu_0-i\frac{3\gamma}{2}\right)} \\
&+\sqrt{6}\xi^3 \frac{C_0(0)\left\{\exp\left[-i(\nu_2-i\gamma)t\right]-\exp\left[-i\left(\nu_3-i\frac{3\gamma}{2}\right)t\right]\right\}}{\left(\nu_1-\nu_0-i\frac{\gamma}{2}\right)\left(\nu_2-\nu_0-i\gamma\right)\left(\nu_3-\nu_2-i\frac{\gamma}{2}\right)} \\
&+\sqrt{6}\xi^3 \frac{C_0(0)\left\{\exp\left[-i\left(\nu_1-i\frac{\gamma}{2}\right)t\right]-\exp\left[-i\left(\nu_3-i\frac{3\gamma}{2}\right)t\right]\right\}}{\left(\nu_1-\nu_0-i\frac{\gamma}{2}\right)\left(\nu_2-\nu_1-i\frac{\gamma}{2}\right)\left(\nu_3-\nu_1-i\gamma\right)} \\
&-\sqrt{6}\xi^3 \frac{C_0(0)\left\{\exp\left[-i(\nu_2-i\gamma)t\right]-\exp\left[-i\left(\nu_3-i\frac{3\gamma}{2}\right)t\right]\right\}}{\left(\nu_1-\nu_0-i\frac{\gamma}{2}\right)\left(\nu_2-\nu_1-i\frac{\gamma}{2}\right)\left(\nu_3-\nu_2-i\frac{\gamma}{2}\right)}.
\end{aligned} \tag{S86}$$

Thus, for the initially empty resonator, the solutions of the equations of motion for the probability amplitudes in the equations in Eq. (S70) can be obtained as:

$$\begin{aligned}
C_0(t) &= C_0(0)\exp\left(-i\nu_0 t\right), \\
C_1(t) &= -\xi\frac{C_0(0)}{\left(\nu_1-\nu_0-i\frac{\gamma}{2}\right)}\left\{\exp\left(-i\nu_0 t\right)-\exp\left[-i\left(\nu_1-i\frac{\gamma}{2}\right)t\right]\right\}, \\
C_2(t) &= \sqrt{2}\xi^2\frac{C_0(0)}{\left(\nu_1-\nu_0-i\frac{\gamma}{2}\right)}\left\{\frac{\exp\left(-i\nu_0 t\right)-\exp\left[-i(\nu_2-i\gamma)t\right]}{\left(\nu_2-\nu_0-i\gamma\right)}-\frac{\exp\left[-i\left(\nu_1-i\frac{\gamma}{2}\right)t\right]-\exp\left[-i(\nu_2-i\gamma)t\right]}{\left(\nu_2-\nu_1-i\frac{\gamma}{2}\right)}\right\}, \\
C_3(t) &= -\sqrt{6}\xi^3 \frac{C_0(0)\left\{\exp\left(-i\nu_0 t\right)-\exp\left[-i\left(\nu_3-i\frac{3\gamma}{2}\right)t\right]\right\}}{\left(\nu_1-\nu_0-i\frac{\gamma}{2}\right)\left(\nu_2-\nu_0-i\gamma\right)\left(\nu_3-\nu_0-i\frac{3\gamma}{2}\right)} \\
&\quad+\sqrt{6}\xi^3 \frac{C_0(0)\left\{\exp\left[-i(\nu_2-i\gamma)t\right]-\exp\left[-i\left(\nu_3-i\frac{3\gamma}{2}\right)t\right]\right\}}{\left(\nu_1-\nu_0-i\frac{\gamma}{2}\right)\left(\nu_2-\nu_0-i\gamma\right)\left(\nu_3-\nu_2-i\frac{\gamma}{2}\right)} \\
&\quad+\sqrt{6}\xi^3 \frac{C_0(0)\left\{\exp\left[-i\left(\nu_1-i\frac{\gamma}{2}\right)t\right]-\exp\left[-i\left(\nu_3-i\frac{3\gamma}{2}\right)t\right]\right\}}{\left(\nu_1-\nu_0-i\frac{\gamma}{2}\right)\left(\nu_2-\nu_1-i\frac{\gamma}{2}\right)\left(\nu_3-\nu_1-i\gamma\right)} \\
&\quad-\sqrt{6}\xi^3 \frac{C_0(0)\left\{\exp\left[-i(\nu_2-i\gamma)t\right]-\exp\left[-i\left(\nu_3-i\frac{3\gamma}{2}\right)t\right]\right\}}{\left(\nu_1-\nu_0-i\frac{\gamma}{2}\right)\left(\nu_2-\nu_1-i\frac{\gamma}{2}\right)\left(\nu_3-\nu_2-i\frac{\gamma}{2}\right)},
\end{aligned} \tag{S87}$$

where

$$\nu_0=0, \quad \nu_1=\Delta_L+\Delta_{\mathrm{F}}, \quad \nu_2=2\Delta_L+2\Delta_{\mathrm{F}}+2U, \quad \nu_3=3\Delta_L+3\Delta_{\mathrm{F}}+6U.$$

When the initial state of the system is the vacuum state $|0\rangle$, i.e., the initial condition $C_0(0)=1$, the solutions in Eq. (S87) are reduced to:

$$\begin{aligned}
C_0(t) =& 1, \\
C_1(t) =& -\xi\frac{1}{\left(\Delta_L+\Delta_{\mathrm{F}}-i\frac{\gamma}{2}\right)}\left\{1-\exp\left[-i\left(\Delta_L+\Delta_{\mathrm{F}}-i\frac{\gamma}{2}\right)t\right]\right\}, \\
C_2(t) =& \frac{\sqrt{2}\xi^2}{\left(\Delta_L+\Delta_{\mathrm{F}}-i\frac{\gamma}{2}\right)}\left\{\frac{1-\exp[-i(2\Delta_L+2\Delta_{\mathrm{F}}+2U-i\gamma)t]}{(2\Delta_L+2\Delta_{\mathrm{F}}+2U-i\gamma)}-\frac{\exp\left[-i\left(\Delta_L+\Delta_{\mathrm{F}}-i\frac{\gamma}{2}\right)t\right]}{\left(\Delta_L+\Delta_{\mathrm{F}}+2U-i\frac{\gamma}{2}\right)}\right\} \\
&+\sqrt{2}\xi^2\frac{\exp[-i(2\Delta_L+2\Delta_{\mathrm{F}}+2U-i\gamma)t]}{\left(\Delta_L+\Delta_{\mathrm{F}}-i\frac{\gamma}{2}\right)\left(\Delta_L+\Delta_{\mathrm{F}}+2U-i\frac{\gamma}{2}\right)},
\end{aligned}$$

$$
\begin{aligned}
C_3(t) = &-\sqrt{6}\xi^3 \frac{\left\{1-\exp\left[-i\left(3\Delta_L+3\Delta_{\mathrm{F}}+6U-i\frac{3\gamma}{2}\right)t\right]\right\}}{\left(\Delta_L+\Delta_{\mathrm{F}}-i\frac{\gamma}{2}\right)\left(2\Delta_L+2\Delta_{\mathrm{F}}+2U-i\gamma\right)\left(3\Delta_L+3\Delta_{\mathrm{F}}+6U-i\frac{3\gamma}{2}\right)} \\
&+\sqrt{6}\xi^3 \frac{\left\{\exp[-i(2\Delta_L+2\Delta_{\mathrm{F}}+2U-i\gamma)t]-\exp\left[-i\left(3\Delta_L+3\Delta_{\mathrm{F}}+6U-i\frac{3\gamma}{2}\right)t\right]\right\}}{\left(\Delta_L+\Delta_{\mathrm{F}}-i\frac{\gamma}{2}\right)\left(2\Delta_L+2\Delta_{\mathrm{F}}+2U-i\gamma\right)(\Delta_L+\Delta_{\mathrm{F}}+4U-i\frac{\gamma}{2})} \\
&+\sqrt{6}\xi^3 \frac{\left\{\exp\left[-i\left(\Delta_L+\Delta_{\mathrm{F}}-i\frac{\gamma}{2}\right)t\right]-\exp\left[-i\left(3\Delta_L+3\Delta_{\mathrm{F}}+6U-i\frac{3\gamma}{2}\right)t\right]\right\}}{\left(\Delta_L+\Delta_{\mathrm{F}}-i\frac{\gamma}{2}\right)\left(\Delta_L+\Delta_{\mathrm{F}}+2U-i\frac{\gamma}{2}\right)(2\Delta_L+2\Delta_{\mathrm{F}}+6U-i\gamma)} \\
&-\sqrt{6}\xi^3 \frac{\left\{\exp[-i(2\Delta_L+2\Delta_{\mathrm{F}}+2U-i\gamma)t]-\exp\left[-i\left(3\Delta_L+3\Delta_{\mathrm{F}}+6U-i\frac{3\gamma}{2}\right)t\right]\right\}}{\left(\Delta_L+\Delta_{\mathrm{F}}-i\frac{\gamma}{2}\right)\left(\Delta_L+\Delta_{\mathrm{F}}+2U-i\frac{\gamma}{2}\right)(\Delta_L+\Delta_{\mathrm{F}}+4U-i\frac{\gamma}{2})},
\end{aligned}
$$

and for the infinite-time limit $\exp(-At)\to 0$ $(t\to\infty)$, we have:

$$
\begin{aligned}
C_0(\infty) &\equiv C_0 = 1, \\
C_1(\infty) &\equiv C_1 = \frac{-\xi}{\left(\Delta_L+\Delta_{\mathrm{F}}-i\frac{\gamma}{2}\right)}, \\
C_2(\infty) &\equiv C_2 = \frac{-\sqrt{2}\xi C_1}{(2\Delta_L+2\Delta_{\mathrm{F}}+2U-i\gamma)}, \\
C_3(\infty) &\equiv C_3 = \frac{-\sqrt{3}\xi C_2}{\left(3\Delta_L+3\Delta_{\mathrm{F}}+6U-i\frac{3\gamma}{2}\right)}.
\end{aligned} \tag{S88}
$$

For the state given in Eq. (S65), the infinite-time state (steady state) of the system reads as

$$
\begin{aligned}
|\varphi(t\to\infty)\rangle = |0\rangle &+ \frac{-\xi}{\left(\Delta_L+\Delta_{\mathrm{F}}-i\frac{\gamma}{2}\right)}|1\rangle + \frac{\sqrt{2}\xi^2}{\left(\Delta_L+\Delta_{\mathrm{F}}-i\frac{\gamma}{2}\right)\left(2\Delta_L+2\Delta_{\mathrm{F}}+2U-i\gamma\right)}|2\rangle \\
&+ \frac{-\sqrt{6}\xi^3}{\left(\Delta_L+\Delta_{\mathrm{F}}-i\frac{\gamma}{2}\right)\left(2\Delta_L+2\Delta_{\mathrm{F}}+2U-i\gamma\right)\left(3\Delta_L+3\Delta_{\mathrm{F}}+6U-i\frac{3\gamma}{2}\right)}|3\rangle,
\end{aligned} \tag{S89}
$$

and the normalization constant of the state is given by

$$
N = 1+|C_1|^2+|C_2|^2+|C_3|^2, \tag{S90}
$$

where:

$$
|C_1|^2 = \left|\frac{\xi}{\left(\Delta_L+\Delta_{\mathrm{F}}-i\frac{\gamma}{2}\right)}\right|^2 = \frac{\xi^2}{\left(\Delta_L+\Delta_{\mathrm{F}}-i\frac{\gamma}{2}\right)\left(\Delta_L+\Delta_{\mathrm{F}}+i\frac{\gamma}{2}\right)} = \frac{\xi^2}{\left[(\Delta_L+\Delta_{\mathrm{F}})^2+\frac{\gamma^2}{4}\right]}, \tag{S91}
$$

$$
\begin{aligned}
|C_2|^2 &= \left|\frac{\sqrt{2}\xi^2}{\left(\Delta_L+\Delta_{\mathrm{F}}-i\frac{\gamma}{2}\right)\left(2\Delta_L+2\Delta_{\mathrm{F}}+2U-i\gamma\right)}\right|^2 \\
&= \frac{2\xi^4}{\left(\Delta_L+\Delta_{\mathrm{F}}-i\frac{\gamma}{2}\right)\left(\Delta_L+\Delta_{\mathrm{F}}+i\frac{\gamma}{2}\right)(2\Delta_L+2\Delta_{\mathrm{F}}+2U-i\gamma)(2\Delta_L+2\Delta_{\mathrm{F}}+2U+i\gamma)} \\
&= \frac{2\xi^4}{\left[(\Delta_L+\Delta_{\mathrm{F}})^2+\frac{\gamma^2}{4}\right]\left[4(\Delta_L+\Delta_{\mathrm{F}}+U)^2+\gamma^2\right]},
\end{aligned} \tag{S92}
$$

$$
\begin{aligned}
|C_3|^2 &= \left|\frac{-\sqrt{6}\xi^3}{\left(\Delta_L+\Delta_{\mathrm{F}}-i\frac{\gamma}{2}\right)\left(2\Delta_L+2\Delta_{\mathrm{F}}+2U-i\gamma\right)\left(3\Delta_L+3\Delta_{\mathrm{F}}+6U-i\frac{3\gamma}{2}\right)}\right|^2 \\
&= \frac{6\xi^6}{\left|\Delta_L+\Delta_{\mathrm{F}}-i\frac{\gamma}{2}\right|^2\left|(2\Delta_L+2\Delta_{\mathrm{F}}+2U-i\gamma)\right|^2\left|3\Delta_L+3\Delta_{\mathrm{F}}+6U-i\frac{3\gamma}{2}\right|^2} \\
&= \frac{6\xi^6}{\left[(\Delta_L+\Delta_{\mathrm{F}})^2+\frac{\gamma^2}{4}\right]\left[4(\Delta_L+\Delta_{\mathrm{F}}+U)^2+\gamma^2\right]\left[9(\Delta_L+\Delta_{\mathrm{F}}+2U)^2+\frac{9\gamma^2}{4}\right]}.
\end{aligned} \tag{S93}
$$

The probabilities of finding single, two and three photons in the cavity are, respectively, given by:

$$P_1 = \frac{|C_1|^2}{N}, \tag{S94}$$

$$P_2 = \frac{|C_2|^2}{N}, \tag{S95}$$

$$P_3 = \frac{|C_3|^2}{N}. \tag{S96}$$

As mentioned in Sec. S2 B, the equal-time third-order correlation function can be written as

$$g^{(3)}(0,0) \equiv g^{(3)}(0) \equiv \frac{\langle a^{\dagger 3} a^3 \rangle}{\langle \hat{a}^\dagger \hat{a} \rangle^3} = \frac{\langle \hat{a}^\dagger \hat{a}(\hat{a}^\dagger \hat{a} - 1)(\hat{a}^\dagger \hat{a} - 2) \rangle}{\langle \hat{a}^\dagger \hat{a} \rangle^3} = \frac{\langle (\hat{a}^\dagger \hat{a})^3 - 3(\hat{a}^\dagger \hat{a})^2 + 2\hat{a}^\dagger \hat{a} \rangle}{\langle \hat{a}^\dagger \hat{a} \rangle^3}$$

When the cavity field is in the state (S65), we have

$$\begin{aligned} g^{(3)}(0) &= \frac{\sum_{n,n'=0}^{3} C_{n'}^* C_n \langle n' | (\hat{a}^\dagger \hat{a})^3 | n \rangle - 3 \sum_{n,n'=0}^{3} C_{n'}^* C_n \langle n' | (\hat{a}^\dagger \hat{a})^2 | n \rangle + 2 \sum_{n,n'=0}^{3} C_{n'}^* C_n \langle n' | \hat{a}^\dagger \hat{a} | n \rangle}{(\sum_{n,n'=0}^{3} C_{n'}^* C_n \langle n' | \hat{a}^\dagger \hat{a} | n \rangle)^3} \\ &= \frac{|C_1|^2 + 8|C_2|^2 + 27|C_3|^2 - 3(|C_1|^2 + 4|C_2|^2 + 9|C_3|^2) + 2(|C_1|^2 + 2|C_2|^2 + 3|C_3|^2)}{(|C_1|^2 + 2|C_2|^2 + 3|C_3|^2)^3} \\ &= \frac{N(P_1 + 8P_2 + 27P_3 - 3P_1 - 12P_2 - 27P_3 + 2P_1 + 4P_2 + 6P_3)}{N^2(P_1 + 2P_2 + 3P_3)^3} \\ &= \frac{6P_3}{N(P_1 + 2P_2 + 3P_3)^3} \end{aligned}$$

In the weak-driving regime, we have the following approximate amplitudes: $C_0 \sim 1$, $C_1 \sim \xi/\gamma$, $C_2 \sim \xi^2/\gamma^2$, and $C_3 \sim \xi^3/\gamma^3$, i.e., $N \sim 1$ with $|C_3|^2 \ll |C_2|^2 \ll |C_1|^2 \ll 1$. Hence, the third-order correlation function can be written as

$$g^{(3)}(0) \approx \frac{6P_3}{P_1^3}. \tag{S97}$$

Substituting Eqs. (S94) and (S96) into Eq. (S97), we can easily obtain

$$\begin{aligned} g^{(3)}(0) &\approx \frac{36\xi^6}{\left[(\Delta_L + \Delta_F)^2 + \frac{\gamma^2}{4}\right] [4(\Delta_L + \Delta_F + U)^2 + \gamma^2] \left[9(\Delta_L + \Delta_F + 2U)^2 + \frac{9\gamma^2}{4}\right]} \cdot \frac{\left[(\Delta_L + \Delta_F)^2 + \frac{\gamma^2}{4}\right]^3}{\xi^6} \\ &= \frac{\left[(\Delta_L + \Delta_F)^2 + \frac{\gamma^2}{4}\right]^2}{[(\Delta_L + \Delta_F + U)^2 + \frac{\gamma^2}{4}] \left[(\Delta_L + \Delta_F + 2U)^2 + \frac{\gamma^2}{4}\right]}, \end{aligned} \tag{S98}$$

where $\Delta_F > 0$ ($\Delta_F < 0$) denotes the light propagating against (along) the direction of the spinning resonator.

Here, we focus on the non-spinning case ($\Delta_F = 0$), the rotating case is discussed in Sec. S4. For this case, the third-order correlation function becomes

$$g_0^{(3)}(0) = \frac{(\Delta_L^2 + \gamma^2/4)^2}{[(\Delta_L + U)^2 + \gamma^2/4][(\Delta_L + 2U)^2 + \gamma^2/4]}. \tag{S99}$$

Including the second-order correlation function, we can quantitatively compare our analytical results with numerical calculations [S21, S22]. We find an excellent agreement between the numerical calculations and the approximate analytical solutions, as shown in Fig. S6. Here, the solid curves are plotted using the numerical solution, while the curves with symbols are based on the analytical solution given in Eqs. (S62) and (S99). As for the $g_0^{(2)}(0) \approx 2P(2)/P(1)^2$, given in Eq. (S60), the dip $D^{(2)}$ and the peak $P^{(2)}$ in the light green curves correspond to the single- and two-photon resonant driving cases, respectively. In the single-photon resonant driving case ($k = 1$), a single

photon can be resonantly injected into the cavity, while the probability of finding two photons in the cavity is largely suppressed due to the energy restriction; this represents 1PB. We find that the analytical value of $g_0^{(2)}(0) \sim 0.0008$ at this dip $D^{(2)}$, which is well-matched with our numerical value $g_0^{(2)}(0) \sim 0.0009$. In the two-photon resonant driving case ($k = 2$), the probability for finding two photons inside the cavity is resonantly enhanced, and this corresponds to a peak in the curve of $g^{(2)}(0)$. We find that the analytical value of $g^{(2)}(0) \sim 974$ at this peak $P^{(2)}$ is above the numerical solution $g^{(2)}(0) \sim 673$, since we neglected the two-photon probability in the denominator of the analytical formula [this can be seen more clearly in Eqs. (S59) and (S62)]. As for the $g_0^{(3)}(0) \approx 6P(3)/P(1)^3$, given in Eq. (S97), the dip $D^{(3)}$ and the peaks $P_1^{(3)}$ and $P_2^{(3)}$ in the dark green curves correspond to the single-, two-, and three-photon resonant-driving cases, respectively. In the single-photon resonant-driving case ($k = 1$), $P(1) \gg P(2) \gg P(3)$, thus, there is a dip [i.e., $D^{(3)}$] in the $g_0^{(3)}(0)$ curve. For the two-photon resonant-driving case ($k = 2$), the single-photon probability is suppressed, which causes the occurrence of the peak $P_1^{(3)}$. However, the peak $P_1^{(3)}$ is lower than the peak $P_2^{(3)}$ at $k = 3$, since the three-photon probability is enhanced at $k = 3$ (i.e., three-photon resonant-driving case), but still suppressed at $k = 2$ (i.e., two-photon resonant-driving case).

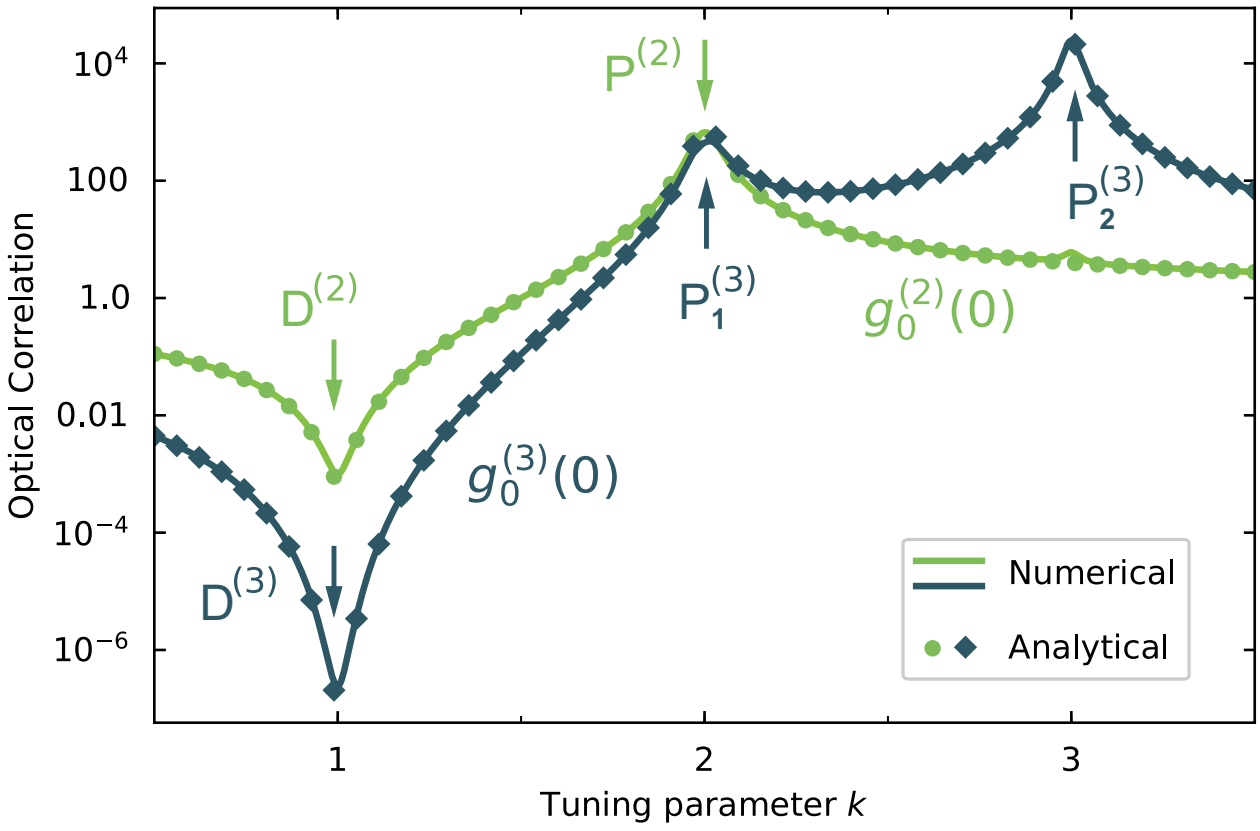


FIG. S6. The second- and third-order correlation functions versus the tuning parameter $k$ for the non-spinning resonator case. The symbols denote our approximate analytical results [$g_0^{(2)}(0)$ given in Eq. (S62), $g_0^{(3)}(0)$ given in Eq. (S99)], while the solid curves correspond to our numerical results. Here, $D^{(2)}$ [$D^{(3)}$] is the dip in the $g_0^{(2)}(0)$ [$g_0^{(3)}(0)$] curves; $P^{(2)}$ and $P^{(3)}$ are the peaks in the $g_0^{(2)}(0)$ and $g_0^{(3)}(0)$ curves, respectively. The parameters used here are the same as those in Fig. S4.

## S4. ROTATION-INDUCED QUANTUM NONRECIPROCITY

### A. Rotation-induced shifts

For the optical microtoroid resonator, an input-laser light applied from the left or right side of the cavity causes a clockwise (CW) circulating mode or a counterclockwise (CCW) circulating mode. When the microresonator is rotating, $\Delta_{\rm F} > 0$ and $\Delta_{\rm F} < 0$ denote the cases with the light propagating against and along the spinning direction of the resonator, respectively, i.e., for the CCW spinning resonator, $\Delta_{\rm F} > 0$ ($\Delta_{\rm F} < 0$) indicates an input-laser applied from the left (right) side; for the CW spinning resonator, $\Delta_{\rm F} > 0$ ($\Delta_{\rm F} < 0$) indicates an input-laser used from the right (left) side.

When the resonator is rotating, the second-order correlation function in Eq. (S61) can be written as

$$g_{\pm}^{(2)}(0) = \frac{(\Delta_L \pm |\Delta_{\rm F}|)^2 + \gamma^2/4}{(\Delta_L \pm |\Delta_{\rm F}| + U)^2 + \gamma^2/4}, \tag{S100}$$

where $g_{-}^{(2)}(0)$ [$g_{+}^{(2)}(0)$] denotes the equal-time second-order correlation function for $\Delta_{\rm F} < 0$ ($\Delta_{\rm F} > 0$).

For the $\Delta_{\rm F} < 0$ case, 1PB emerges at $\Delta_L = |\Delta_{\rm F}|$ with $g_{-}^{(2)}(0) = (\gamma^2/4)/(U^2 + \gamma^2/4) = [4(U/\gamma)^2 + 1]^{-1}$. This minimum value of $g_{-}^{(2)}(0)$ is independent of the angular speed $\Omega$; thus, the minimum value of $g_{-}^{(2)}(0)$ is a constant. Since $|\Delta_{\rm F}|$ is an amount proportional to the angular speed $\Omega$, the dip $D^{(2)}$ experiences linearly shifts with $\Omega$. Also, $D^{(2)}$ experiences linearly shifts to the opposite direction for the $\Delta_{\rm F} < 0$ case, since now 1PB emerges at $\Delta_L = -|\Delta_{\rm F}|$. The shifts of the curve can also be understood from an energy-level structure, where the rotation of the resonator causes upper or lower shifts of energy levels, as shown in Fig. S3.

Here, we plot the correlation function $g^{(2)}(0)$ as a function of $k$ when the angular speed $\Omega$ takes various values, as shown in Fig. S7. For the $\Delta_{\rm F} < 0$ case, a blue shift of the $g^{(2)}(0)$ curve can be clearly seen in Fig. S7(a). For the $\Delta_{\rm F} > 0$ case, a red shift can be seen in Fig. S7(b). This indicates a highly-tunable nonreciprocal PB device, i.e., *sub-Poissonian* light can be achieved by driving from one side; *super-Poissonian* light emerges by driving from the opposite side (see Fig. 2 in the main article).

For example, let us now fix the CCW rotation of the resonator; hence $\Delta_{\rm F} > 0$ ($\Delta_{\rm F} < 0$) corresponds to the situation of driving the resonator from its left (right) side, i.e., the CW (CCW) mode frequency is $\omega_{\circlearrowleft} \equiv \omega_0 + |\Delta_{\rm F}|$ ($\omega_{\circlearrowright} \equiv \omega_0 - |\Delta_{\rm F}|$), as aforementioned. When the optical resonator rotates with an angular velocity $\Omega = 6.6$ kHz [S6], we find $g_{\circlearrowleft}^{(2)}(0) \sim 0.39$ and $g_{\circlearrowright}^{(2)}(0) \sim 2.53$, i.e., *sub-Poissonian* light can be achieved by driving the device from its left side, while *super-Poissonian* light emerges by driving from the right side, as shown in Fig. S8.

The third-order correlation function Eq. (S98) in the rotating resonator becomes

$$g_{\pm}^{(3)}(0) = \frac{[(\Delta_L \pm |\Delta_{\rm F}|)^2 + \gamma^2/4]^2}{[(\Delta_L \pm |\Delta_{\rm F}| + U)^2 + \gamma^2/4][(\Delta_L \pm |\Delta_{\rm F}| + 2U)^2 + \gamma^2/4]}, \tag{S101}$$

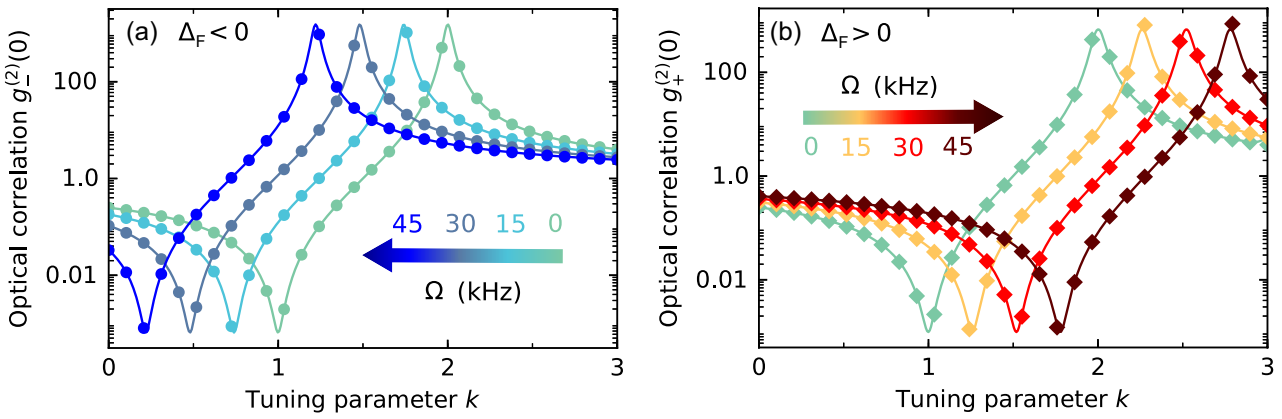


FIG. S7. Dependence of the equal-time second-order correlation functions $g_{\pm}^{(2)}(0)$ on the tuning parameter $k$ for various values of the angular speed $\Omega$. The symbols are our approximate analytical results given in Eq. (S100), while the solid curves are our numerical results. The other parameters used here are the same as those in Fig. S4.

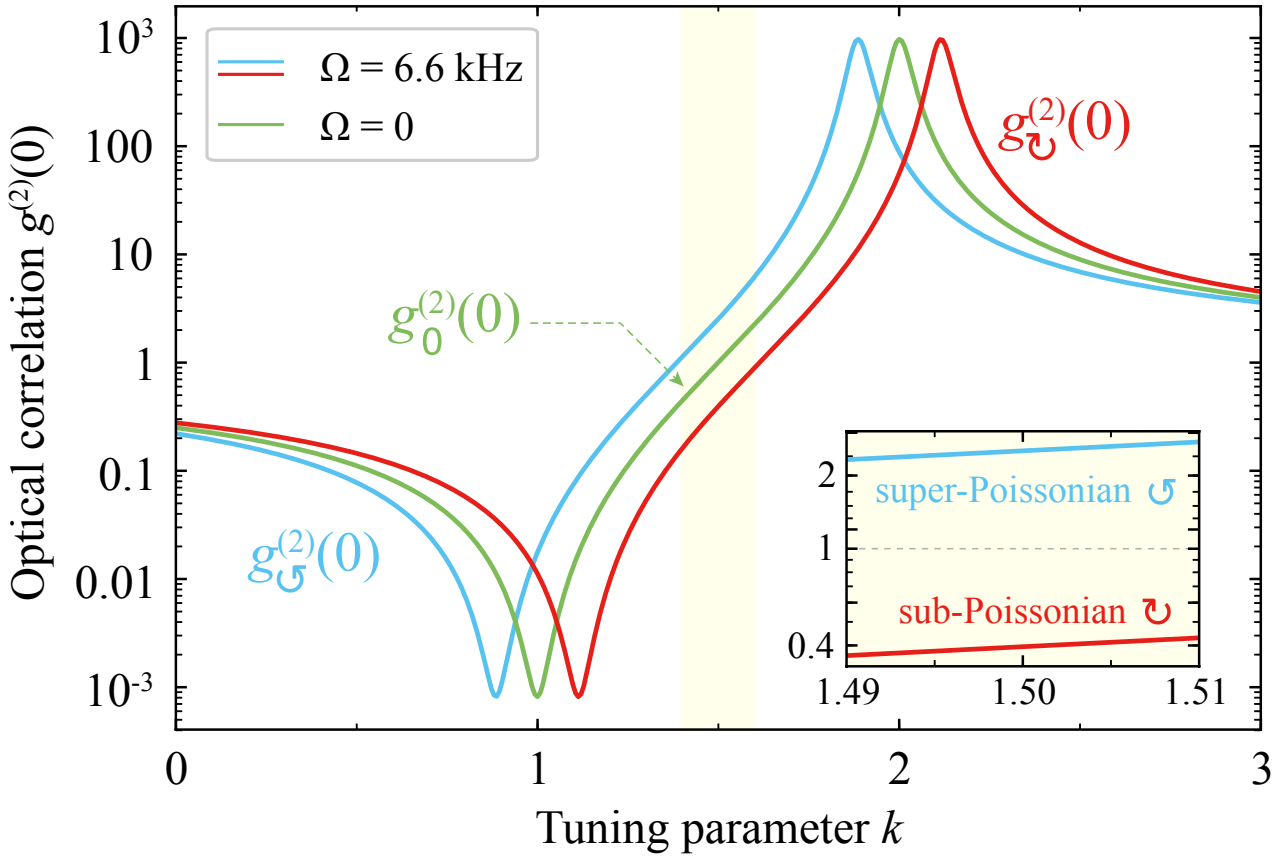


FIG. S8. Second-order correlation function $g^{(2)}(0)$ versus the tuning parameter $k$ for different input directions. At $k = 1.5$, sub- and super-Poissonian light can be achieved by driving the device from its left (red curve) and right (blue curve) sides, respectively. Here, we assume that the angular velocity is $\Omega = 6.6$ kHz [S6] ($\Omega = 0$) for the spinning (non-spinning) resonator. The other parameter values are the same as those in the main text.

where $g^{(3)}_{-}(0)$ ($g^{(3)}_{+}(0)$) denotes the third-order optical intensity correlation for the $\Delta_{\rm F} < 0$ ($\Delta_{\rm F} > 0$) case. Similarly, the curve of $g^{(3)}(0)$ also experiences opposite shifts for different driving directions.

### B. Nonreciprocal photon blockade

We have investigated PB effects (witnessing sub-Poissonian light) and photon-induced tunneling (PIT, corresponding to super-Poissonian light) for the non-spinning case in the former Sections. Note that PB and PIT always emerge at fixed locations of the tuning parameter $k$, no matter if the input-laser comes from the left or right side (see Figs. S4 and S5). However, the rotation of the resonator can lead to upper or lower shifts of energy levels for different driving directions, as discussed in Sec. S4 A. Therefore, using a spinning nonlinear optical resonator, under the same driving frequencies, PIT can emerge by driving from one side and 1PB/2PB can emerge by driving from the other direction, i.e., *unidirectional* 1PB/2PB. Furthermore, 1PB for driving from one side and 2PB for driving from the opposite direction can also be realized with this spinning device.

As shown in Figs. S9(a) and S9(b), when the angular speed of the resonator is $\Omega = 58$ kHz, we find (i) 1PB for $\Delta_{\rm F} > 0$ and PIT for $\Delta_{\rm F} < 0$, at $k = 2.0$; (ii) 2PB for $\Delta_{\rm F} > 0$ and PIT for $\Delta_{\rm F} < 0$, at $k = 3.0$. These nonreciprocal 1PB and 2PB can also be confirmed by comparing the photon-number distribution $P(n)$ with the Poissonian distribution $\mathcal{P}(n)$. Figure S9(b) shows that: (i) single-photon probability $P(1)$ is enhanced while two- and more-photon probabilities $P(m > 1)$ are suppressed for the $\Delta_{\rm F} > 0$ case, leading to 1PB; in contrast, $P(1)$ is suppressed while $P(m > 1)$ are enhanced for the $\Delta_{\rm F} < 0$ case, leading to PIT. (ii) only two-photon probability $P(2)$ is enhanced for $\Delta_{\rm F} > 0$, which corresponds to 2PB; in contrast, PIT emerges for $\Delta_{\rm F} < 0$. The unidirectional 2PB can also be achieved at

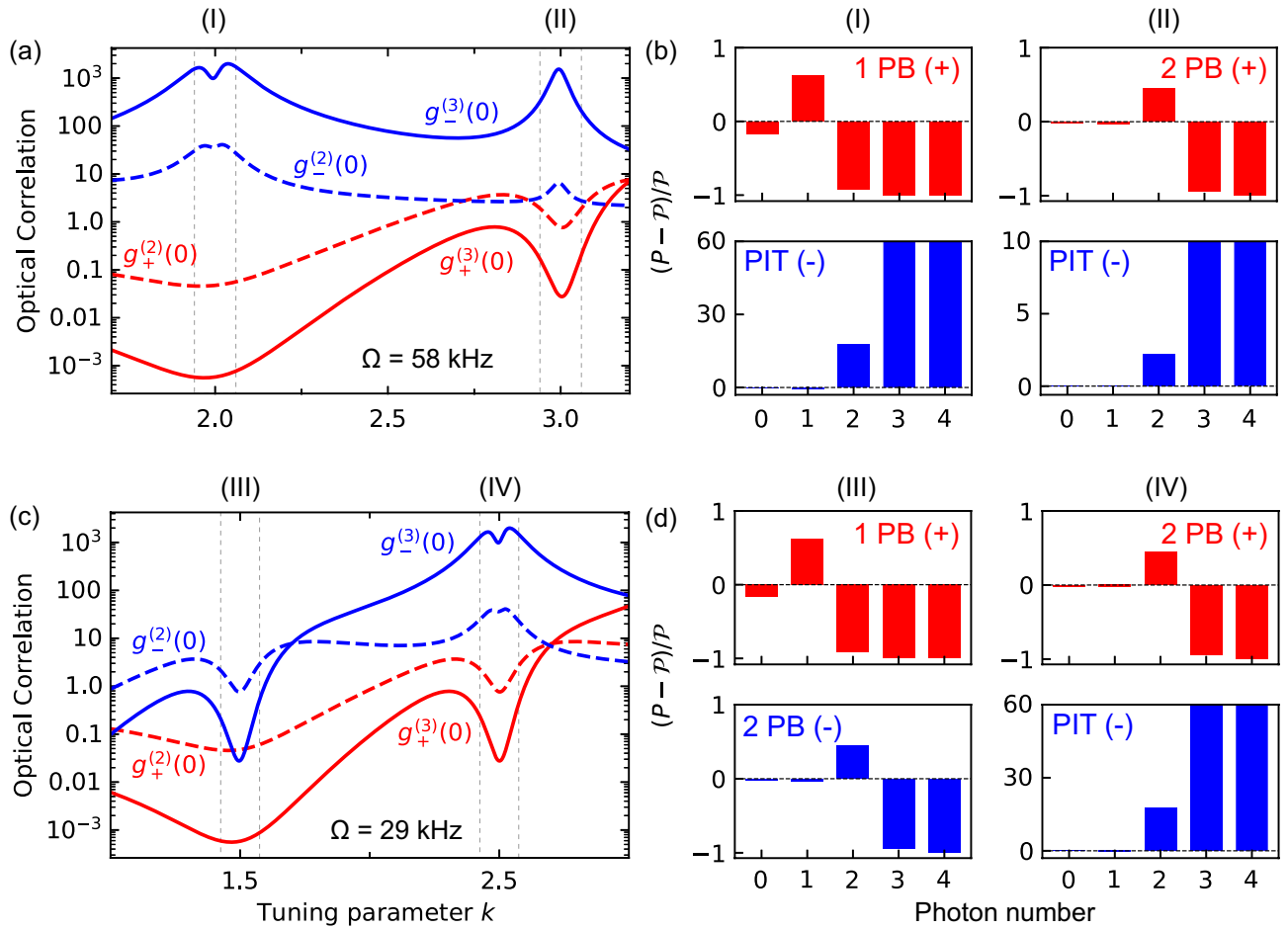


FIG. S9. Optical intensity correlation functions $g_{\pm}^{(2)}(0)$ (dashed curves) and $g_{\pm}^{(3)}(0)$ (solid curves) versus the tuning parameter $k$ for different driving directions. Different cases of nonreciprocal PB can be achieved for different angular speeds (a,b) $\Omega = 58\,\mathrm{kHz}$ and (c,d) $\Omega = 29\,\mathrm{kHz}$. These effects can also be recognized from (b,d) the deviations of the photon distribution to the standard Poissonian distribution with the same mean photon number [i.e., Eq. (S13)]. The panels (b) and (d) correspond to panels (a) and (b), respectively. Here, 'PIT' is photon-induced tunneling, and the other parameters used here are the same as those in Fig. S5.

$k = 2.5$ when $\Omega = 29\,\mathrm{kHz}$, as shown in Figs. S9(c) and S9(d). Such *quantum* nonreciprocities indicate one-way quantum devices at the few-photon level, and open up exciting prospects for applications in nonreciprocal quantum technologies, such as nonreciprocal quantum information processing or few-photon topological devices [S23–S25].

More interestingly, when the angular speed of the nonlinear optical resonator is $\Omega = 29$ kHz, 2PB emerges at $k = 1.5$ for $\Delta_{\mathrm{F}} < 0$, while 1PB emerges with the same driving strength for $\Delta_{\mathrm{F}} > 0$, as shown in Figs. S9(c) and S9(d). In contrast to the nonreciprocities of the former cases between the sub- and super-Poissonian states of light, this is a new kind of nonreciprocal PB between two sub-Poissonian states of light, indicating possible applications for few-photon nonreciprocal devices with direction-dependent counting-statics.

All of the cases of nonreciprocal PB can be intuitively understood by considering the energy-level structure of the system. As shown in Fig. S3(a), for the $\Delta_{\mathrm{F}} > 0$ case, when angular speed fulfills $|\Delta_{\mathrm{F}}| = U$ and the probe light with frequency $\omega_0 + |\Delta_{\mathrm{F}}|$ ($k = 2.0$), the light is resonantly coupled to the transition $|0\rangle \to |1\rangle$. The transition $|1\rangle \to |2\rangle$ is detuned by $2\hbar U$ and, thus, suppressed for $U > \gamma$, i.e., once, a photon is coupled into the resonator, it suppresses the probability of the second photon with the same frequency going into the resonator. In contrast, for the $\Delta_{\mathrm{F}} < 0$ case, there is a three-photon resonance with the transition $|0\rangle \to |3\rangle$, hence the absorption of the first photon favors also that of the second or subsequent photons, i.e., resulting in PIT. This is a clear signature of nonreciprocal 1PB, i.e., *sub-Poissonian* light emerges for $\Delta_{\mathrm{F}} > 0$, while *super-Poissonian* light can be observed for $\Delta_{\mathrm{F}} < 0$.

As shown in Figs. S3(c) [S3(e)], for the $\Delta_{\mathrm{F}} > 0$ case, by choosing $|\Delta_{\mathrm{F}}| = U$ ($|\Delta_{\mathrm{F}}| = U/2$) and $\Delta_L = -2U$ ($\Delta_L = -3U/2$), the transition $|0\rangle \to |2\rangle$ is resonantly driven by the input laser, but the transition $|2\rangle \to |3\rangle$ is

TABLE II. Different cases of nonreciprocal PB effects in a spinning resonator for $P_{\rm in} = 0.3\,$pw. Here, photon-induced tunneling (PIT) corresponds to an $n$-photon resonance ($n$ PR).

| No. | $\Delta_{\rm F} > 0$ | $\Delta_{\rm F} < 0$ | Conditions | Parameters |
|---|---|---|---|---|
| (1) | 1PB | PIT (3PR) | $\Delta_{\rm F} = \pm U$, $\Delta_L = -U$ | $\Omega = 58\,$kHz, $k = 2.0$ |
| (2) | PIT (3PR) | 1PB | prohibited | |
| (3) | 2PB | PIT (4PR) | $\Delta_{\rm F} = \pm U$, $\Delta_L = -2U$ | $\Omega = 58\,$kHz, $k = 3.0$ |
| (4) | PIT (4PR) | 2PB | prohibited | |
| (5) | 2PB | PIT (3PR) | $\Delta_{\rm F} = \pm U/2$, $\Delta_L = -3U/2$ | $\Omega = 29\,$kHz, $k = 2.5$ |
| (6) | PIT (3PR) | 2PB | prohibited | |
| (7) | 1PB | 2PB | $\Delta_{\rm F} = \pm U/2$, $\Delta_L = -U/2$ | $\Omega = 29\,$kHz, $k = 1.5$ |
| (8) | 2PB | 1PB | prohibited | |

detuned by $4\hbar U$, which features the 2PB effect; in contrast, for the $\Delta_{\rm F} < 0$ case, four-photon resonance (three-photon resonance) happens for the transition $|0\rangle \to |4\rangle$ ($|0\rangle \to |3\rangle$), leading to PIT. This is also a nonreciprocal PB.

As shown in Fig. S3(g), for the $\Delta_{\rm F} > 0$ case, when $|\Delta_{\rm F}| = U/2$ and $\Delta_L = -U/2$ ($k = 1.5$), the input light is resonantly coupled to the transition $|0\rangle \to |1\rangle$, and the transition $|1\rangle \to |2\rangle$ is detuned by $2\hbar U$, leading to 1PB. More interestingly, for the $\Delta_{\rm F} < 0$ case, the input light is just resonantly coupled to the transition $|0\rangle \to |2\rangle$, and the transition $|2\rangle \to |3\rangle$ is detuned by $4\hbar U$, i.e., resulting in 2PB. This 1PB-2PB nonreciprocity can suggest an application for a purely quantum device with *direction-dependent counting statistics*. This new nonreciprocal feature, which (to our knowledge) has not been revealed previously.

Table II shows different cases of nonreciprocal PB. Interestingly, both PB-PIT and 1PB-2PB nonreciprocities can only occur in an irreversible way. Unidirectional 1PB for $\Delta_{\rm F} > 0$, i.e., 1PB emerges for $\Delta_{\rm F} > 0$ and PIT emerges for $\Delta_{\rm F} < 0$, can occur with the same angular speeds ($\Delta_{\rm F} = \pm U$), and the same driving frequencies ($\Delta_L = -U$). However, the case of PIT for $\Delta_{\rm F} > 0$ and 1PB for $\Delta_{\rm F} < 0$ cannot be observed with the same angular speeds and driving frequencies, i.e., one-way 1PB is an irreversible quantum nonreciprocal effect. Also, 1PB-2PB nonreciprocity can only happen in the case of 1PB for $\Delta_{\rm F} > 0$ and 2PB for $\Delta_{\rm F} < 0$, but *not* vice versa.

Note that 1PB and 2PB correspond to the single- and two-photon resonances, respectively. PIT is also caused by a multi-photon resonance. The multi-photon resonance can be clearly seen in energy-level diagrams, thus, the origin of this irreversible feature can be understood from the energy-level diagrams for $\Delta_{\rm F} > 0$ and $\Delta_{\rm F} < 0$. Without the rotation, the energy-level diagrams for the $\Delta_{\rm F} > 0$ and $\Delta_{\rm F} < 0$ cases are symmetric. Due to the rotation, energy levels experience shifts to different directions for $\Delta_{\rm F} > 0$ and $\Delta_{\rm F} < 0$, leading to asymmetries of energy-level diagrams, as shown in Fig. S3. From Sec. S2 A, the energy levels of this spinning system are $E_n = n\hbar\Delta_L + n\hbar\Delta_{\rm F} + (n^2 - n)\hbar U$. Thus, we have

$$E_n/n = \hbar(\Delta_L + \Delta_{\rm F}) + (n-1)\hbar U. \tag{S102}$$

Then the driving frequency of an $n$-photon resonance for the $\Delta_{\rm F} > 0$ case is

$$\omega_L = \omega_0 + |\Delta_{\rm F}| + nU - U, \tag{S103}$$

and the driving frequency of an $m$-photon resonance for the $\Delta_{\rm F} < 0$ case is

$$\omega_L' = \omega_0 - |\Delta_{\rm F}| + mU - U. \tag{S104}$$

Under the same driving frequency, we have

$$\begin{aligned} \omega_0 + |\Delta_{\rm F}| + nU - U &= \omega_0 - |\Delta_{\rm F}| + mU - U \\ |\Delta_{\rm F}| + nU &= -|\Delta_{\rm F}| + mU \\ 2|\Delta_{\rm F}| &= (m-n)U. \end{aligned} \tag{S105}$$

Because $|\Delta_{\rm F}| > 0$ (i.e., $\Omega \neq 0$) and $U > 0$, we have the following condition for the allowed cases of nonreciprocal PB

$$n < m. \tag{S106}$$

When the driving frequencies for $\Delta_F > 0$ and $\Delta_F < 0$ are the same, an $n$-photon resonance for $\Delta_F > 0$ and an $m$-photon resonance for $\Delta_F < 0$ can only happen under the condition $n < m$. In contrast to this, the cases of $n > m$ are prohibited, as shown in Figs. S3(b), S3(d), S3(f), and S3(h).

*Corresponding author.
jinghui73@foxmail.com

[S1] G. J. Milburn, "Quantum and classical Liouville dynamics of the anharmonic oscillator," Phys. Rev. A **33**, 674 (1986).
[S2] W. Leoński and R. Tanaś, "Possibility of producing the one-photon state in a kicked cavity with a nonlinear Kerr medium," Phys. Rev. A **49**, R20 (1994).
[S3] A. Imamoğlu, H. Schmidt, G. Woods, and M. Deutsch, "Strongly interacting photons in a nonlinear cavity," Phys. Rev. Lett. **79**, 1467 (1997).
[S4] A. Miranowicz, M. Paprzycka, Y.-x. Liu, J. Bajer, and F. Nori, "Two-photon and three-photon blockades in driven nonlinear systems," Phys. Rev. A **87**, 023809 (2013).
[S5] G. B. Malykin, "The Sagnac effect: correct and incorrect explanations," Phys. Usp. **43**, 1229 (2000).
[S6] S. Maayani, R. Dahan, Y. Kligerman, E. Moses, A. U. Hassan, H. Jing, F. Nori, D. N. Christodoulides, and T. Carmon, "Flying couplers above spinning resonators generate irreversible refraction," Nature (London) **558**, 569 (2018).
[S7] A. Majumdar, M. Bajcsy, and J. Vučković, "Probing the ladder of dressed states and nonclassical light generation in quantum-dot–cavity QED," Phys. Rev. A **85**, 041801 (2012).
[S8] S. S. Shamailov, A. S. Parkins, M. J. Collett, and H. J. Carmichael, "Multi-photon blockade and dressing of the dressed states," Opt. Commun. **283**, 766 (2010).
[S9] A. Miranowicz, J. Bajer, M. Paprzycka, Y.-x. Liu, A. M. Zagoskin, and F. Nori, "State-dependent photon blockade via quantum-reservoir engineering," Phys. Rev. A **90**, 033831 (2014).
[S10] H. J. Carmichael, "Breakdown of photon blockade: a dissipative quantum phase transition in zero dimensions," Phys. Rev. X **5**, 031028 (2015).
[S11] C. J. Zhu, Y. P. Yang, and G. S. Agarwal, "Collective multiphoton blockade in cavity quantum electrodynamics," Phys. Rev. A **95** (2017).
[S12] C. Hamsen, K. N. Tolazzi, T. Wilk, and G. Rempe, "Two-photon blockade in an atom-driven cavity QED system," Phys. Rev. Lett. **118**, 133604 (2017).
[S13] A. Faraon, I. Fushman, D. Englund, N. Stoltz, P. Petroff, and J. Vučković, "Coherent generation of non-classical light on a chip via photon-induced tunnelling and blockade," Nat. Phys. **4**, 859 (2008).
[S14] A. Majumdar, M. Bajcsy, A. Rundquist, and J. Vučković, "Loss-enabled sub-Poissonian light generation in a bimodal nanocavity," Phys. Rev. Lett. **108** (2012).
[S15] X.-W. Xu, Y.-J. Li, and Y.-x. Liu, "Photon-induced tunneling in optomechanical systems," Phys. Rev. A **87**, 025803 (2013).
[S16] A. Rundquist, M. Bajcsy, A. Majumdar, T. Sarmiento, K. Fischer, K. G. Lagoudakis, S. Buckley, A. Y. Piggott, and J. Vučković, "Nonclassical higher-order photon correlations with a quantum dot strongly coupled to a photonic-crystal nanocavity," Phys. Rev. A **90** (2014).
[S17] K. M. Birnbaum, A. Boca, R. Miller, A. D. Boozer, T. E. Northup, and H. J. Kimble, "Photon blockade in an optical cavity with one trapped atom," Nature (London) **436**, 87 (2005).
[S18] R. J. Glayber, *Quantum Theory of Optical Coherence* (Wiley-VCH, Weinheim, 2007).
[S19] M. Wang, X.-Y. Lü, A. Miranowicz, T.-S. Yin, Y. Wu, and F. Nori, "Unconventional phonon blockade via atom-photon-phonon interaction in hybrid optomechanical systems," preprint arXiv:1806.03754 (2018).
[S20] M. B. Plenio and P. L. Knight, "The quantum-jump approach to dissipative dynamics in quantum optics," Rev. Mod. Phys. **70**, 101 (1998).
[S21] J. R. Johansson, P. D. Nation, and F. Nori, "Qutip: An open-source Python framework for the dynamics of open quantum systems," Comput. Phys. Commun. **183**, 1760 (2012).
[S22] J. R. Johansson, P. D. Nation, and F. Nori, "Qutip 2: A Python framework for the dynamics of open quantum systems," Comput. Phys. Commun. **184**, 1234 (2013).
[S23] C. H. Bennett and D. P. DiVincenzo, "Quantum information and computation," Nature (London) **404**, 247 (2000).
[S24] I. Buluta, S. Ashhab, and F. Nori, "Natural and artificial atoms for quantum computation," Rep. Prog. Phys. **74**, 104401 (2011).
[S25] P. Lodahl, S. Mahmoodian, S. Stobbe, A. Rauschenbeutel, P. Schneeweiss, J. Volz, H. Pichler, and P. Zoller, "Chiral quantum optics," Nature (London) **541**, 473 (2017).